UNIVERSITE DE BLIDA 1

Faculté de Technologie

Département d'Electronique

THESE DE DOCTORAT

Spécialité : Electronique

CONTRIBUTION DES SYSTEMES HYBRIDES DE SOURCE SOLAIRE-FOSSILE DANS LE RENFORCEMENT DE L'ELECTRIFICATION RURALE : CAS DE LA WILAYA DE TAMANRASSET

Par

Fadhela FODHIL

Devant le jury composé de :

HAMID Abdelkader	Prof.	Université de Blida 1	Président
KHELDOUN Aissa	Prof.	Université de Boumerdes	Examinateur
BRADAI Rafik	MC A	Université de Blida 1	Examinateur
HATTI Mustapha	DR.	UDES, Tipaza	Examinateur
HAMIDAT Abderrahmane	DR.	CDER, Alger	Directeur de thèse

Blida, Novembre 2019

RESUME

La Wilaya de Tamanrasset a bénéficié de plusieurs projets d'électrification rurale. Mais, la grande étendue de la Wilaya, la dépendance de la production électrique aux sources fossiles comme les groupes électrogènes et les turbines à gaz, le coût très élevé de l'extension du réseau électrique aux village éloignés, ont obligé le pouvoir publique de recourir à des solutions alternatives fiables et durables comme l'utilisation des systèmes hybrides fossiles/solaire. Ainsi, cette thèse propose une étude sur la faisabilité des systèmes hybrides de source solaire-fossile sur le renforcement de l'électrification rurale. Une étude de cas a été proposée pour la Wilaya de Tamanrasset. Ces systèmes sont constitués d'un groupe photovoltaïque, un groupe électrogène, des batteries de stockages électrochimiques et un onduleur. La technologie hybride solaire (PV)-fossile (Diesel) dans l'électrification rurale autonome demande des outils spécifiques pour son étude et son dimensionnement. Donc, ce travail a d'abord permis de cerner les enjeux techniques et économiques de l'hybridation tel que, la collection des données météorologiques, l'estimation de la consommation énergétique horaire et journalière des sites isolés à étudier. Ensuite, la modélisation des différents composants du système hybride (énergie photovoltaïque, groupe électrogène diesel, stockage électrochimique) a été réalisée. Enfin, le travail a abouti à la simulation du comportement avec l'optimisation du système hybride en utilisant deux approches l'approche heuristique, l'optimisation par les essaims de particule (OEP) et l'approche techno-économique. Avec une pénétration PV plus de 80%, et un capital initial entre 50% et 70% du coût total, le système hybride a permis de répondre à la demande énergétique grandissante des habitants ruraux sans déficits énergétiques. L'analyse des résultats énergétiques, économiques, et environnementaux a montré l'efficacité et la rentabilité du système hybride PV-diesel-batterie étudié.

ABSTRACT

The Wilaya of Tamanrasset has benefited from several rural electrification programs. The main features of the electrical network of the province are: the dependence of electricity production on fossil sources such as diesel generators and gas turbines, also, the high needed investment to extend the electricity grid to remote villages due to the large geographic area of Tamanrasset. Hence, reliable and sustainable alternative solutions should be proposed and integrated in the rural electrification plans such as the hybridization of renewable and fossil energy sources. Thus, this thesis studies the feasibility of hybrid solar - fossil systems on the enhancement of rural electrification, case study: Wilaya of Tamanrasset. These systems consist of a photovoltaic generator, a diesel generator, battery bank and a converter. The integration of the hybrid PV- diesel technology in rural electrification requires specific tools for its study and sizing. First, the technical and economic issues of hybridization, like the collection of meteorological data along with the estimation of the hourly and daily energy consumption of the isolated case studies have been identified. Subsequently, the modeling of the different components of the hybrid system (photovoltaic energy, diesel generators and electrochemical storage) has been performed. Ultimately, the simulation of the behavior and optimization of the hybrid system using two approaches, the heuristic particle swarm optimization (PSO) approach and the techno-economic approach have been achieved. With a PV penetration more than 80%, and a capital cost represents between 50% and 70% in the NPC of the system, the hybrid system supplies the load consumption in all villages without an unmet load. The analysis of the energetic, economic, and environmental results showed the efficiency and profitability of the hybrid PV-diesel-battery system.

مـلـخـص

لقد استفادت ولاية تمنراست من العديد من برامج كهربة الريف. غير أن السمات الرئيسية للشبكة الكهربائية للولاية هي: اعتماد إنتاج الكهرباء على المصادر الأحفورية مثل مولدات الديزل وتوربينات الغاز، بالإضافة الى ارتفاع تكلفة امداد القرى النائية بشبكة الكهرباء. ولهذا ينبغي اقتراح حلول بديلة موثوقة ومستدامة وإدماجها في خطط ومشاريع كهربة الريف مثل تهجين مصادر الطاقة المتجددة والأحفورية. وبالتالي، تهدف هذه الأطروحة الى دراسة جدوى النظام الهجين الأحفوري-الشمسي على تعزيز كهربة الريف، دراسة حالة: ولاية تمنراست. ويتكون هذه النظام من مولد كهروضوئي، مولد ديزل، نظام تخزين (البطاريات) ومحول كهربائي. يتطلب ادماج هذه التكنولوجيا الهجينة أدوات محددة لدراستها وتحجيمها. لذلك، قمنا أولا بالتطرق لمختلف الخصائص والميزات التقنية والاقتصادية للتهجين، مثل جمع بيانات الأرصاد الجوية جنبا إلى جنب مع تقدير استهلاك الطاقة الساعي واليومي للحالة المدروسة. كما تم القيام بنمذجة المكونات المختلفة للنظام الهجين (المولد الكهروضوئي، مولد الديزل، البطارية). في نهاية المطاف، تم تنفيذ محاكاة وتحسين للنظام الهجين باستخدام طريقتين، طريقة خوارزمية السرب وطريقة التحليل التقني الاقتصادي. بنسبة تفوق 80% من الطاقة الكهروضوئية ورأس مال أولي يمثل بين 50% و70% من التكلفة الكلية، تمكن النظام الهجين المدروس من تغطية الاستهلاك الكهربائي لمختلف الحالات المدروسة دون وجود عجز طاقوي. وأظهر تحليل النتائج الطاقوية، الاقتصادية، والبيئية كفاءة وربحية النظام الهجين المدروس.

ACKNOWLEDGEMENTS

I would like to express my sincere appreciation to my thesis supervisor, Director of Research Abderrahmane HAMIDAT, CDER - Algiers, for guidance, motivations, patience, ideas, valuable suggestions, comments, advice, constructive criticisms and encouragement throughout the work.

I also thank Professor Abdelkader HAMID, University of Blida 1, for accepting the chairmanship of the jury. I sincerely thank Professor Aissa KHELDOUN, University of Boumerdes, DR. HATTI Mustapha, UDES-Tipaza, and Dr. BRADAI Rafik, University of Blida 1, for agreeing to examine this work.

I am grateful to Dr. Omar NADJEMI for his valuable comments, discussions, encouragement and timely guidance along this thesis. I am highly grateful to Pr. Hassan SALHI for welcoming me into his laboratory (Laboratoire des systèmes Electriques et Télécommande, LABSET).

My gratitude also goes to the staff of SDC, Sonelgaz, Mrs. RAMDANI, Mrs. THABET and Mr. KOBBI, for the time, efforts and advices especially during the first and the last years of this thesis.

Last but not least, I am indebted to my family, I am sincerely grateful for their support and encouragement throughout my study. Thanks to my dear father and my deceased mother, who died last year, they have been an inexhaustible source of support and encouragement and have made an untold number of sacrifices for me and my sisters. Many thanks for my sisters for being supportive and helpful in many ways. Your encouragement, trust, and confidence in me have been highly important especially during difficult times when I was overwhelmed with self-doubts and anxiety. Finally, I am very thankful for all those who had directly or indirectly helped in my research work.

TABLE OF CONTENTS

LIST OF FIGURES

LIST OF TABLES

GENERAL INTRODUCTION

Access to electricity services is vital and crucial to the country's economic development and to provide healthcare, education, clean water, sanitation, lighting, cooking, transport and other important services, especially in an isolated countryside. In Algeria, the electricity is mainly generated (99%) from fossil fuel sources, the combined cycle (44.28%) and gas turbine (31.46%) are the dominants sources of electricity production. Further, the electricity consumption in Algeria has been increased 42 % from 23.61 TWh in 2005 to 33.68 TWh in 2014, the growth in electricity consumption has been accompanied by significant growth in the production from 33.6 TWh in 2005 to 68.5 TWh in 2015, up to 76.4 TWh in 2018 [1], this growth reflects the economic expansion and the rapid population growth. According to the International Energy Agency (IEA), the consumption of electricity in Algeria per individual (kWh/capita) in 2014 is about 1362 kWh which was less than the worlds average of 3144 kWh [2], these indicators can be explained by the fact that 30% of Algeria's population was considered to be part of the rural population [3]. Also, the largest part of Algeria (80 %) is desert land (Sahara). Nevertheless, the electrification of rural and Saharan regions is covered by three networks:

- The northern interconnected network (RIN: Le réseau interconnecté du nord) which spreads over the north of the country and covers the regions of Bechar, Hassi Messaoud, Hassi R'Mel and Ghardaïa.
- The Pole In-Salah – Adrar –Timimoune (PIAT), the network extends from In-Salah to Timimoun via Aoulef and Adrar.
- The Southern Isolated Networks (RIS: Les Réseaux Isolés du Sud), There are 26 sites in the south mainly in the province of Tamanrasset, fed by local networks through diesel gensets or gas turbine.

Despite all this, according to the Ministry of Energy, there are over 260,000 rural, small and scattered households not connected to the general electricity network [4] because it is technically very difficult, if not impossible, to be electrified by traditional means of extending transmission networks. Thus, rural, communities use engine generators to cover their basic need in electricity.

With the growth in electric demand, and the high solar potential specially in the Sahara region, if 1/20 of Saharan surface is covered with solar panels, it can supply electricity for the entire planet [5], the Algerian government realized that the renewable energy projects mainly solar energy could contribute significantly in the rural electrification strategy and sustainable development of rural communities. Algeria installed around 268 MW of solar photovoltaic (PV) capacity in 2015, especially in the highlands and Saharan regions, small scale PV stand-alone systems were installed in some rural villages in the southern of the country mostly in the provinces of Adrar, Illizi, Tindouf and Tamanrasset.

However, conventional diesel gensets or photovoltaic stand-alone system have their own limitations and advantages, diesel generators have low initial investment but suffer from increasing fuel prices, added cost for both fuel transportation and for operation and maintenance in remote areas. Moreover, solar energy is an intermittent energy resource, which requires storage (battery bank) and implies a high investment cost but low operating costs. Striking the right balance between delivering a reliable and sustainable electricity service based on renewable energies such as photovoltaics, and, fulfilling the electrical comfort is always a challenge in rural and Saharan regions. The concept requires an efficient and cost effective electrification solutions [6]. So, the hybridization of both technologies PV and diesel in the electrification process to create synergy in their combination can tackle and balance these constraints to sustain the socio-economic growth in rural areas.

The subject of this thesis is to study the potential and the energetic, economic and environmental feasibility of hybrid PV-Diesel-battery system as an electrification solution for rural, remote and Saharan villages in the province of Tamanrasset (Sahara region).

To achieve this goal, the accomplishment of the below objectives is required:

- The collection of the local meteorological data and studying the potential of the local solar resources.
- Estimating the daily load demand of rural villages.
- Overview of component characteristics and hybrid system configurations.
- Modeling and simulation of the hybrid PV-diesel- battery system.

- Optimization and sensitivity analysis of the hybrid system using two approaches: the first approach is the particle swarm optimization (PSO) approach with Matlab. The second is techno-economic analysis with HOMER software.
- Energetic, economic, and environmental evaluation of the hybrid PV-diesel-battery system.

To reach our goal, this thesis is structured in four chapters. The first chapter review the solar resource availability, its characteristics and highlight the most critical factors to be considered in PV based applications. The second chapter gives a brief overview of the PV technology and the types of solar PV systems. Then, it summarized the modeling of the components, the energy flow, and the control strategies of the hybrid PV-diesel-battery system. The third chapter discusses the optimization techniques of the hybrid system and presents the optimal sizing of PV-diesel-battery system using two approaches: the PSO approach and the techno-economic analysis. The fourth chapter provides an interpretation of the results achieved from the different case study, then the chapter discusses the energetic, economic and environmental impacts of the hybrid PV-diesel-battery system in the enhancement of the rural electrification in the province of Tamanrasset. Finally, general conclusion and recommendations are presented.

CHAPTER 1

SOLAR RADIATION

1.1. Introduction

Solar resource availability and its characteristics are the most critical factors to be considered in photovoltaic based applications, whether these applications are stand-alone systems or integrated into buildings. The solar resource is highly variable, both in time and in location, this chapter focuses on how we can obtain the best possible knowledge about this variability so that photovoltaic systems can be designed and deployed optimally regardless of the load consumption. For this reason, we will devote this chapter to summarize the characteristics, the possibilities and best practices addressing the influence of the solar resource on PV applications.

1.2. Sun and Earth

For billions of years, the Sun has been producing energy via nuclear fusion, which converts hydrogen nuclei into helium nuclei. This process releases energy, in accordance with the equation $E = m.c^2$. The mass of the helium nuclei that are stemmed from the hydrogen nuclei is lower than that of the hydrogen nuclei. The output of this tremendous nuclear reactor amounts to roughly $3.85.10^{26}$ W or $3.85.10^{17}$ GW, or Almost 1017 more than the thermal output of a 1200 MW nuclear power plant. Hence solar energy is in fact nuclear energy in the truest sense of the term. But fortunately the nuclear reactor we call the Sun is a very great and reassuringly safe distance from the Earth [7]. The Sun-Earth distance varies between 147.106 million kilometers (3rd January) and 153.106 million km (3rd July): its average value is 150.106 Million km.

1.2.1. Solar Constant

Figure 1.1 shows the Sun–Earth system more or less to scale. The distance between the two space bodies is approximately 150 million km and other dimensions can be taken from table 1.1. The Sun continuously radiates an amount

of P_{Sun} = 3.845 x 10^{26} W in all directions of which the Earth only receives a small fraction. In order to calculate this value, we assume there is a sphere around the Sun that has a radius of r = r_{SE}. At this distance the amount of radiation from the Sun has already spread over the whole area of the sphere. Thus at the position of the Earth we get the following power density or irradiance [8].

$$E_S = \frac{\text{Radiation power}}{\text{Area of sphere}} = \frac{P_{sun}}{4\pi r_{SE}^2} = 1367\ \text{W}/m^2 \qquad (1.1)$$

The result of 1367 W/m^2 is called the solar constant.

The solar constant is 1367 W/m^2. It denotes the irradiance outside the Earth's atmosphere.

Table 1.1: Characteristics of the Sun and the Earth [8].

Properties	**Sun**	**Earth**
Diameter	d_{Sun} = 1392520 km	d_{Earth} = 12756 km
Surface temperature	T_{Sun}= 5778 °K	T_{Earth}= 288 °K
Temperature at center	15000000 °K	6700 °K
Radiated power	P_{Sun}= 3.845 x 10^{26} W	-
Distance Sun-Earth	149.6 Mio km	-

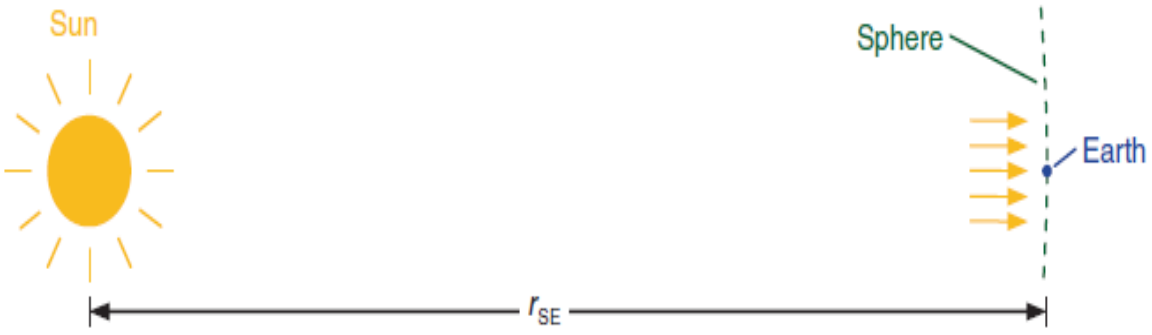

Figure 1.1: Determination of the solar constant [8]

1.2.2. Earth Movement

Earth's orbital movement around the Sun affects the climate, solar radiation, and temporal variations [9]. The Earth rotates around the Sun once a year and at

the same time rotates around its own axis once a day. The Earth's axis is at an angle of 23.45º relative to the plane of the Earth's path around the Sun, this is known as the ecliptic. Because of the Earth's rotation, the Earth's axis retains its orientation in space all year round which means that over the course of any given year the Sun's rays come from varying directions relative to the equatorial plane. During the summer, the Earth's axis is inclined towards the Sun, and in the winter it is inclined away from the Sun. This phenomenon is known as the solar declination δ, which is defined as the angle between the direction of the Sun and the equatorial plane, or the angle at which the Earth's axis is inclined towards the Sun (see figure 1.2). Hence at a northern hemisphere location at latitude Φ, the highest elevation of the Sun at noon is not constant throughout the year, but is instead h_{Smax}= 90º-Φ+δ. In the northern hemisphere, δ >0 in summer, but δ <0 during winter. The amount of solar radiation over the course of a given year is primarily determined by latitude φ and solar declination δ. Also, the speed of the Earth in its orbit around the Sun is not a uniform movement. It is larger in winter than in summer [7]. Because of that, the duration of spring and summer is longer than the duration of the autumn and winter (duration of summer is 93.6 days, the spring 92.8 days, autumn is 89.8 days and winter, 89.0 days). The combination of movements of the Earth on its axis and around the Sun allows us to determine the position of the Sun, according to the site (latitude and longitude) and time (day of the year and time) on the one hand and day length on the other hand.

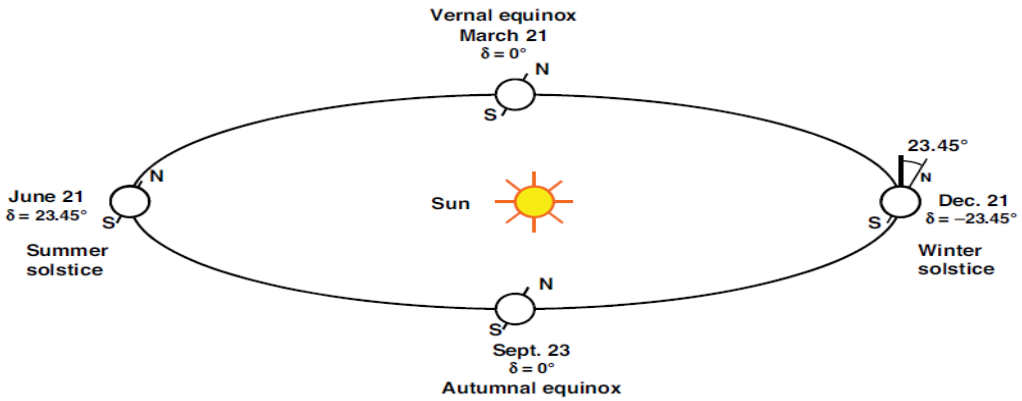

Figure 1.2: The Earth's orbit around the Sun and the position of the Earth's axis over the course of a year [7].

1.2.3. Geographic parameters

Earth is separated by the equator into two hemispheres, the northern hemisphere located on the side of the North Pole and the southern hemisphere, which is situated adjacent to the south Pole. On the other hand, it is divided from west to east by the meridian passing through Greenwich town (near London in England).

1.2.3.1. Latitude

In geography, latitude (ϕ) is a geographic coordinate that specifies the north-south position of a point on the Earth's surface. Latitude is an angle which ranges from 0° at the equator to 90° (North or South) at the poles, it is counted positively (0 to 90 °) to the north and negatively (0 to -90°) to the south.

1.2.3.2. Longitude

Longitude is a geographic coordinate that specifies the east-west position of a point on the Earth's surface. It is an angular measurement, usually expressed in degrees and denoted by (φ). The angle extent of 360° with respect to a meridian reference, with a range of +180° t o -180° or 180° east to 180° west.

1.2.3.3. Altitude

Altitude or height is a distance measurement, usually in the vertical or up direction, between a reference datum and a point or object. Altitude is commonly used to mean the difference between a point and a mean level, usually the sea level (or level 0) of a location. Geographic coordinates of a location (45°N 45°W) are illustrated in figure 1.3.

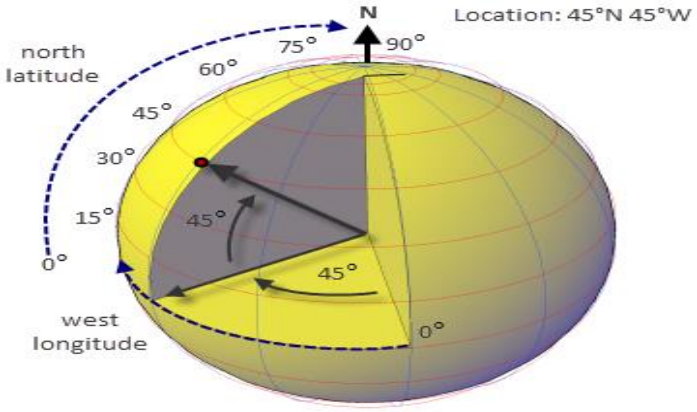

Figure 1.3: Geographic coordinates of a location.

1.2.4. Astronomical parameters

1.2.4.1. Sun position

Solar radiation and energy calculations require some geometric and time quantities concerning the Sun position relative to the Earth and any point on the Earth. The Sun's position is marked at every moment of the day and year by two different coordinate systems (equatorial and horizontal), see figure 1.4.

1.2.4.1.1. Equatorial coordinates

The Sun movement is marked with respect to the equatorial plane of the Earth using two angles; the declination δ and hour angle ω.

- Solar declination

The solar declination is the angle of the direction of the Sun with its projection on the equatorial plane. It varies between 23°45 ' at the summer solstice (June 21) and -23°45' at the winter solstice (December 21) [10]. This variation produces the seasons. The solar declination is expressed by the following equation [11]:

$$\delta = (0.006918 - 0.399912\cos\Gamma + 0.07257\sin\Gamma - 0.006758\cos 2\Gamma + 0.000907\sin\Gamma - 0.002697\cos 3\Gamma + 0.00148\sin 3\Gamma)\,(180/\pi) \quad (1.2)$$

Γ is the day angle expressed in radians given by

$$\Gamma = \frac{2\pi(N_d - 1)}{365} \tag{1.3}$$

Expressing all angles in degrees, then eq. (1.2) will be expressed as follows.

$$\delta = 23{,}45^{o}.\sin\left[\frac{360}{365}(N_d + 284)\right] \tag{1.4}$$

N_d is the day number of the year, ranging from 1 to 365. (For 1st January N_d = 1, and 31st December N_d = 365).

- Hour angle

The hour angle, ω, is the angular distance required for the Earth to rotate once a day, which is equal to 15° multiplied by the number of hours (15×24 = 360°) from local solar noon. It can be defined in degree by:

$$\omega = 15(12 - TST) \tag{1.5}$$

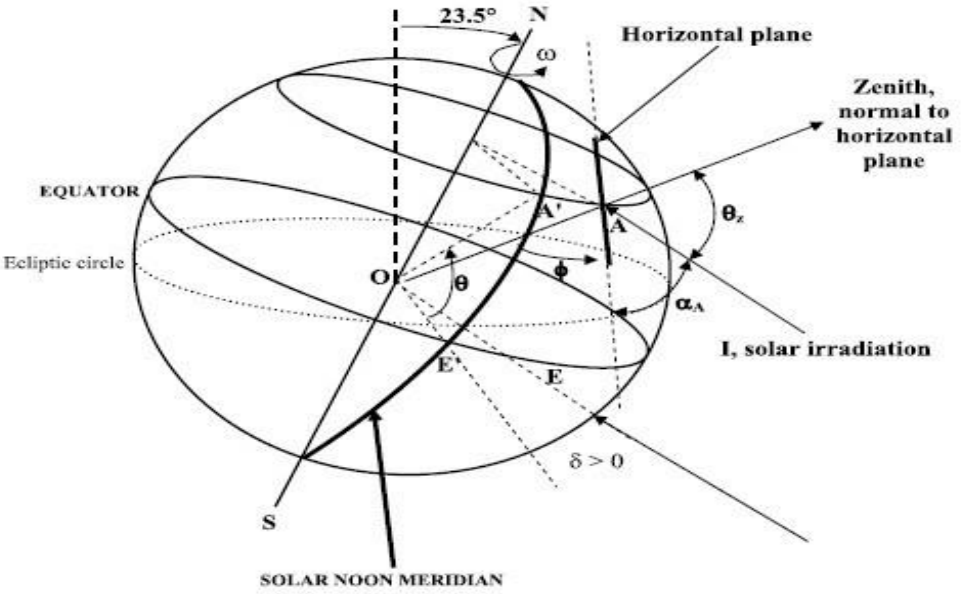

Figure 1.4: Useful angles [9].

TST is the true solar time. The hour angle is measured from solar noon, it is positive if it is before noon and negative if it is afternoon (ω is 0° at noon, -90° at 6 PM and 90° in 6 AM).

1.2.4.1.2. Horizontal coordinates

The horizontal coordinate system is formed by the plane of the astronomical horizon and vertical location, the coordinates are the Sun height, h, and the azimuth, θ_z [11, 12].

- Sun height

The height of the Sun is the angle formed by the direction of the Sun and its projection on the horizontal plane. It is particularly equal to 0 ° at sunrise and sunset in true solar time. Its value is maximum at noon. It expresses by:

$$\sin(h) = \cos(\delta)\cos(\phi)\cos(\omega) + \sin(\phi)\sin(\delta) \tag{1.6}$$

- Azimuth of the Sun

The azimuth of the Sun is the angle between the projection of the Sun direction in the horizontal plane and the South direction.

$$\sin(\theta_z) = \frac{\cos(\delta)\sin(\omega)}{\cos(h)} \tag{1.7}$$

It equals to zero at true solar time noon and it is maximum at sunrise and sunset.

1.2.4.2. Time zones

Geometrical division of time across the world is 24 longitudinal divisions. Time zones are determined by dividing the Earth into 24 lines with 15 degrees of longitude in width. The prime meridian is the Greenwich, which defines the Universal Time. Each country uses the nearest longitude time as principal time.

1.2.4.2.1. Solar time

For applications of solar energy, it is necessary to introduce the solar time, which is calculated taking into account the difference between the mean solar time and local time.

- Mean solar time (MST)

The rotation of the Earth around itself introduces the concept of using MST. It is the average time between two successive passages of the meridian of the place, a full rotation of the Earth around itself takes 24 hours.

- Universal Time (UT)

Universal Time is a time standard based on the rotation of the Earth. It is a modern continuation of Greenwich Mean Time (GMT). GMT is sometimes used loosely as a synonym for UTC (Universal time Coordinated). The difference between mean solar time and universal time is called the longitude correction. The relation between universal time and mean solar time is defined by:

$$MST = UT \pm \left(\varphi / 15 \right) \tag{1.8}$$

(+) for eastern longitude, and (-) for western longitude.

- Legal Time

Standard time (or local) is the official time of the state. It differs from the global Greenwich time by a shift in hours.

$$LT = UT + \Delta H \tag{1.9}$$

ΔH is the time difference between states (ΔH =1 for Algeria).

- True solar time (TST)

Solar time is a reckoning of the passage of time based on the Sun's position in the sky. The fundamental unit of solar time is the day. True solar time and mean solar time differs. This difference is called the equation of time varies depending on the day [11]:

$$TST = MST + ET \tag{1.10}$$

ET is the equation of time.

1.2.4.2.2. Equation of time (ET)

This is an equation which takes into account the rotation speed variation of the Earth, it is given in minutes by [13]:

$$ET = 9.87 \sin(2\beta_0) - 7.53 \cos(\beta_0) \tag{1.11}$$

β_0 is a function defined in degree by:

$$\beta_0 = \frac{360}{365}(N_d - 81) \quad (1.12)$$

- Transition from the standard time to the true solar time

In general, to convert the standard local time LT to true solar time TST, the following expression is used:

$$TST = LT - \Delta H + \left(\frac{ET + 4\phi}{60}\right) \quad (1.13)$$

1.2.4.3. Surface Orientation

Any surface is defined by two angles (α_z, γ):

α_z: the surface azimuth, is the angle between the projection of the normal to the horizontal surface and south direction.

γ: surface height, is the angle between the normal of the surface and its projection on the horizontal plane.

1.2.4.4. Angle of incidence

The angle of incidence i for a plane of an inclination β' is the angle formed by the directional vector of the solar beam and the outgoing normal to the plane.

For a south oriented plane.

$$\cos(i) = \cos(\delta)\cos(\omega)\cos(\phi - \beta') + \sin(\delta)\sin(\phi - \beta') \quad (1.14)$$

For a north-oriented plane

$$\cos(i) = \cos(\delta)\cos(\omega)\cos(\phi - \beta') + \sin(\delta)\sin(\phi + \beta') \quad (1.15)$$

For a horizontal plane

$$(\beta - 0 = 0), \cos(i) = \sin(i) \quad (1.16)$$

1.3. Spectrum of the Sun

The solar radiation is an electromagnetic wave emitted by the Sun. We are talking about electromagnetic radiation (EMR) when the radiation behaves like a force field that affects the electrical and magnetic properties of matter. Light is the

visible part of EMR [9]. Every hot body gives off radiation to its surroundings. According to Planck's Law of Radiation the surface temperature determines the spectrum of the radiation. In the case of the Sun, the surface temperature is 5778 K, which leads to the idealized Black Body Spectrum shown in figure 1.5 (dashed line). The actual spectrum measured outside the Earth's atmosphere (AM 0) approximately follows this idealized line. The term AM 0 stands for Air Mass 0 and means that this light has not passed through the atmosphere. If the individual amounts of this spectrum are added together in figure 1.5, then the result is an irradiance of 1367 W/m^2, which is the already mentioned solar constant. However, the spectrum changes when sunlight passes through the atmosphere. There are various reasons for this [8]:

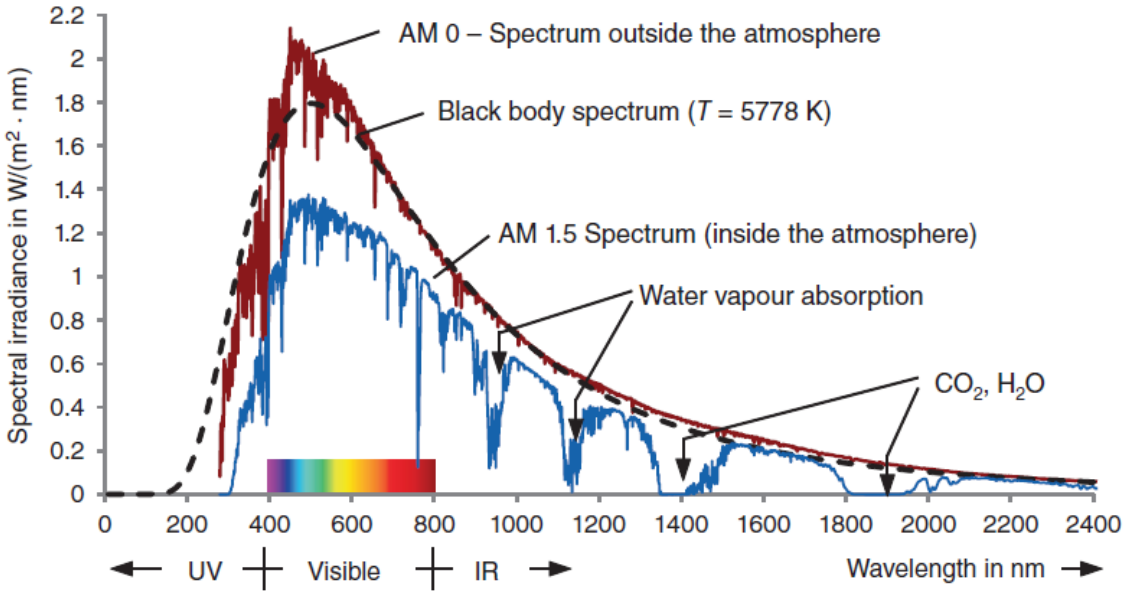

Figure 1.5: Spectrum outside and inside the atmosphere [8]

- Reflection of light: Sunlight is reflected in the atmosphere and this reduces the radiation reaching the Earth.

- Absorption of light: Molecules (O_2, O_3, H_2O, CO_2 . . .) are excited at certain wavelengths and absorb a part of the radiation causing "gaps" in the spectrum especially in the infrared region (see figure 1.5 at λ=1400 nm).

- Rayleigh scattering: If light falls on particles that are smaller than the wavelength, then Raleigh scattering occurs. This is strongly dependent on wavelength ($\sim 1/\lambda^4$) so shorter wavelengths are scattered particularly strongly.

- Scattering of aerosols and dust particles: This concerns particles larger than the wavelength of light. In this case one speaks of Mie scattering. The strength of Mie scattering depends greatly on the location; it is greatest in industrial and densely populated areas.

1.3.1. Air Mass

As we have seen, the spectrum changes when passing through the atmosphere. The effect is greater, the longer the path of the light. For this reason, one designates the different spectra according to the path of the rays through the atmosphere. Figure 1.6 shows the principle: the term AM1.5 means for example that the light has travelled 1.5 times the distance in comparison to the vertical path through the atmosphere. At a known sun height angle γ of the sun, the AM value x gives:

$$x = \frac{1}{\sin \gamma_S} \tag{1.17}$$

The sun has different heights depending on the time of day and year. Figure 1.6 shows on which days the respective AM values are reached (always a noon sun position).

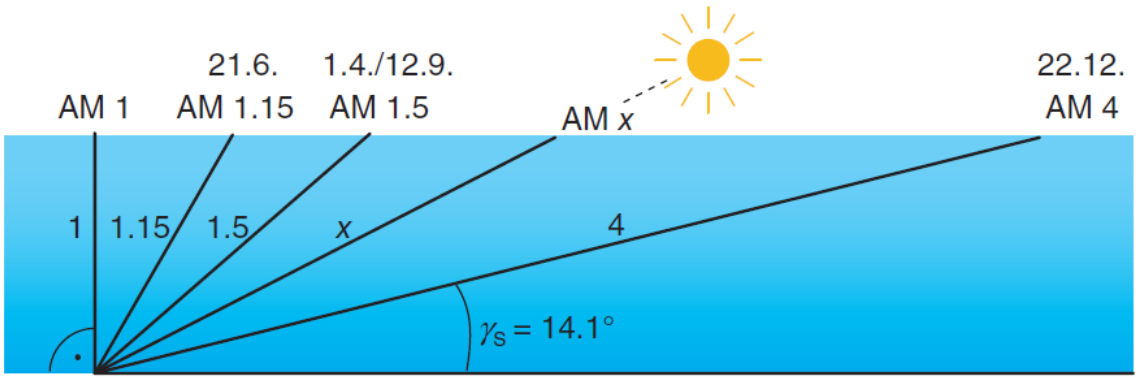

Figure 1.6: Explanation of the term Air Mass: The number x represents the extension of the path compared to the vertical distance through the atmosphere [14].

The standard spectrum for measuring solar modules has established itself at the AM 1.5 spectrum as it arrives in spring and autumn and can be viewed as an average year's spectrum [8].

1.3.2. Global radiation

1.3.2.1. Origin of Global radiation

The various effects such as scattering and absorption cause a weakening of the AM 0 spectrum from Space. In the summation of the AM1.5 spectrum in figure 1.6, we receive only 835 W/m^2. Thus, of the originally available 1367 W/m^2, the Earth receives just 61% as so-called direct radiation. However, due to the scattering of light in the atmosphere there exists a further portion: the diffuse radiation (see figure 1.7). Weak radiation portions arrive from all directions of the sky and are added to diffuse radiation. The sum of both types of radiation is called global radiation.

$$E_G = E_{Direct} + E_{Diffuse} \tag{1.18}$$

On a nice, clear summer's day it is possible to measure on a surface vertical to the radiation of the sun a global radiation value of E_G=E_{STC}=1000 W/m^2. This is the reason why, in the definition of the standard test conditions for solar modules, one uses an enhanced AM 1.5 spectrum by the factor 1000/835=1.198. This has a total irradiance of exactly E_{STC}=1000 W/m^2 and is thus suitable for determining the peak power of a solar module.

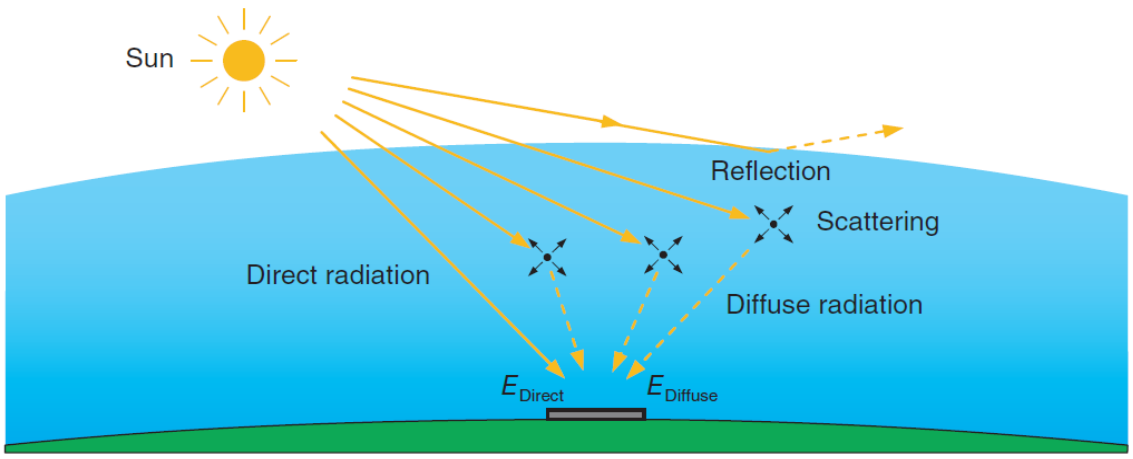

Figure1.7: Origin of global radiation [8].

1.3.2.2. Global radiation maps

In order to be able to estimate the yield of a photovoltaic module already in the planning stage, it is necessary to obtain the data of the global radiation at the

planned site. Nowadays global radiation maps are available in high resolution. The basis of these maps is many years of measurements by a dense network of measuring stations, satellite pictures and simulation tools [8]. Figure 1.8 shows this type of map for Algeria.

1.3.3. Radiation on tilted surfaces

Most of the solar energy systems are predominately installed on tilted collected surfaces or roofs in order to achieve a higher annual yield. Therefore, it is necessary to have knowledge about the availability of solar radiation on tilted surfaces.

1.3.3.1. Radiation calculation with the three-component model

Figure 1.9 shows the radiation relationships in the case of a suitable solar module surface (or more generally, a solar generator). Besides the direct and diffuse radiation there is still a further radiation component: the radiation reflected from the ground. These add themselves to an overall radiation E_{Gen} on the tilted generator [8].

$$E_{Gen} = E_{Direct\_Gen} + E_{Diffuse\_Gen} + E_{\mathrm{Re}\,fl\_Gen} \tag{1.19}$$

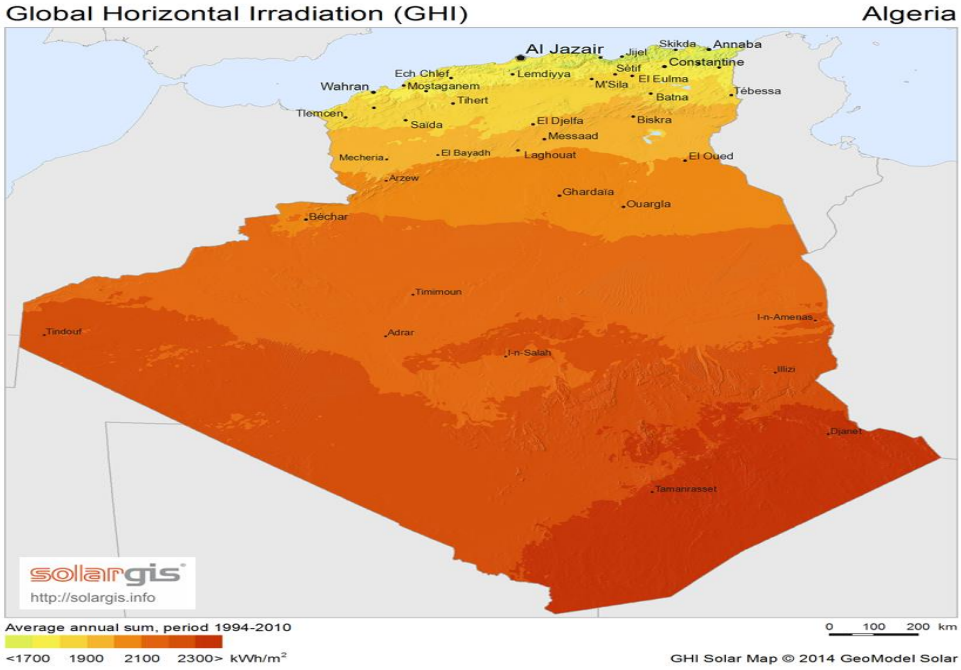

Figure 1.8: Global horizontal irradiation map for Algeria [15].

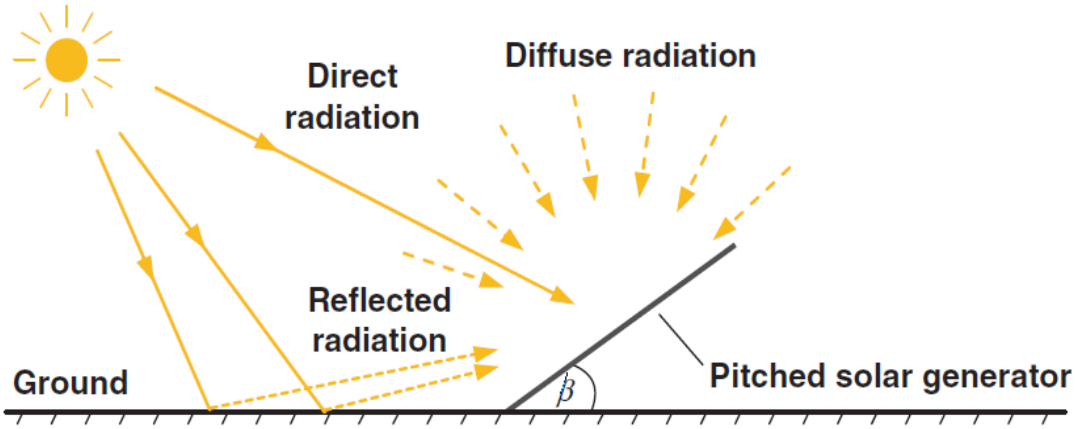

Figure 1.9: Radiation situation with tilted surfaces: The radiation is made up of the direct, diffused and reflected radiation [8].

1.3.3.2. Direct radiation

Let us consider the case that direct sunlight shines on a tilted solar module. For this case the left sketch of figure 1.10 shows how solar radiation impinges on a horizontal surface AH. The optical power P_{Opt} of the impinging radiation is [8]:

$$P_{Opt} = E_{Direct\_H} . A_H \tag{1.20}$$

If a solar generator were arranged exactly vertically to the solar radiation, it would be possible to take up the same power on a smaller surface $A_{Vertical}$:

$$P_{Opt} = E_{Direct\_H} . A_H = E_{Direct\_Vertical} . A_{Vertical} \tag{1.21}$$

The strength of the radiation $E_{Direct\_Vertical}$ is therefore increased by the factor $A_H/A_{Vertical}$ compared to the horizontal strength of radiation. This increase can be seen in figure 1.10 in that the light rays are closer together on the vertical surface in comparison to the horizontal surface.

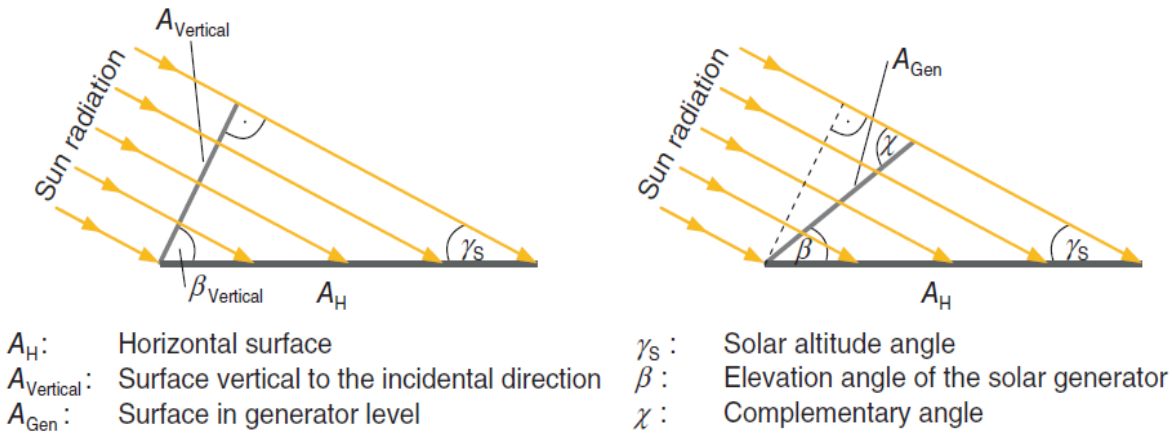

Figure 1.10: Influence of the solar generator tilt on direct radiation [8].

The right-hand sketch in figure 1.10 shows the general case: a solar generator tilted by the angle β. A pair of trigonometric equations are used to determine the strength of the radiation in the generator level [8]:

$$A_{Verical} = A_H . \sin \gamma_S \tag{1.22}$$

$$A_{Verical} = A_{Gen} \sin \chi \tag{1.23}$$

The complementary angle χ can be calculated by the sum of the angles in the triangle and as subsidiary angle:

$$\chi = \gamma_S + \beta \tag{1.24}$$

Using the equation (1.21 and 1.24) we can derive:

$$E_{Direct\_Gen} = E_{Direct\_H} \cdot \frac{\sin(y_S + \beta)}{\sin y_S} \tag{1.25}$$

It must be noted that this equation applies only for direct radiation.

1.3.3.3. Diffuse radiation

The calculation of the diffuse radiation of tilted surface can be much simplified. For this purpose, we make a simple assumption that the diffuse radiation from the whole sky is approximately of the same strength (the isotropic assumption: Figure 1.11, left). Thus the strength of radiation of a solar generator at an angle β is calculated as [8]:

$$E_{Diffus\_Gen} = E_{Diffus\_H} \cdot \frac{1}{2} \cdot (1 + \cos\beta) \quad (1.26)$$

Starting with a horizontal generator (β=0º) the radiation is reduced until at (β=90º) it is:

$$E_{Diffus\_Gen} = \frac{E_{Diffus\_H}}{2} \quad (1.27)$$

In this case, the solar generator is vertical so that only the left hand side of the sky can be used (figure 1.11, right). The isotropic assumption is only to be understood as a coarse approximation. Thus, the sky around the sun is mostly brighter than in the region of the horizon. More refined models are used in modern simulation programs in order to achieve greater degrees of accuracy.

1.3.3.4. Reflected radiation

As shown in figure 1.9, a part of the global radiation is reflected from the ground and can act as an additional radiation contribution to the solar generator. In the calculation of this portion the main problem is that every ground material reflects (or more exactly: scatters) differently. The so called albedo value (ALB) describes the resulting reflection factor. Table 1.2 lists the albedo value of some types of ground.

The large range of the given values shows that the simulation of the reflected radiation is accompanied by large uncertainties. If the ground is not known, then the standard value of ALB = 0.20 is often used [8].

Table 1.2: Albedo value of different types of ground [16].

Material	**Albedo (ALB)**	**Material**	**Albedo (ALB)**
Grass (July, August)	0.25	Asphalt	0.15
Lawn	0.18 . . . 0.23	Concrete, clean	0.30
Unmown fields	0.26	Concrete, weathered	0.20
Woods	0.05 . . . 0.18	Snow cover, new	0.80 . . .0.90
Heath surfaces	0.10 . . . 0.25	Snow cover, old	0.45 . . .0.70

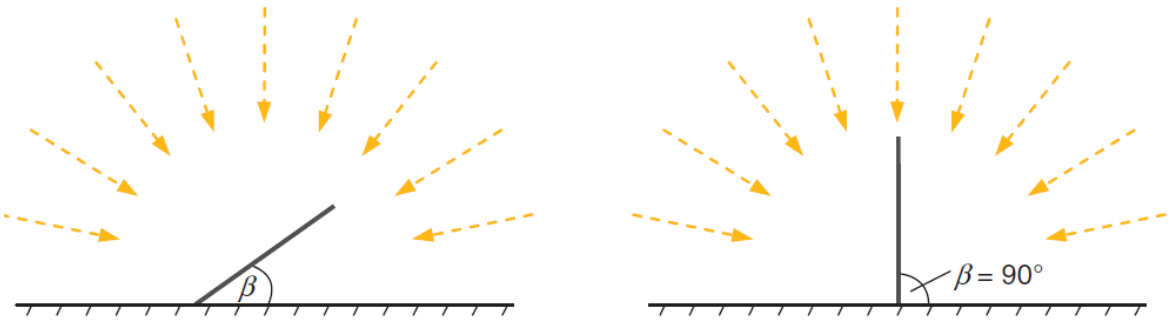

Figure 1.11: Isotropic assumption for diffuse radiation on a tilted surface [8].

An isotropic assumption is again made for the calculation of the reflected radiation on the tilted generator.

$$E_{\mathrm{Re}\,fl} = E_G \cdot \frac{1}{2} \cdot (1 - \cos\beta) \tag{1.28}$$

Figure 1.12 shows the results for the case of ground covered with lawn and fresh snow. In the case of flat solar modules (β =0) the portion of the radiation reflected by the ground is zero and then rises continuously by rising the angle β. At β =90° half the available reflective radiation reaches the solar generator. This is the case of façade plants where solar modules are fixed to the vertical house walls. If one goes beyond 90° then the part of the reflection radiation continues to rise but the top face of the solar module now faces down, which obviously is not the optimum for overall radiation [8].

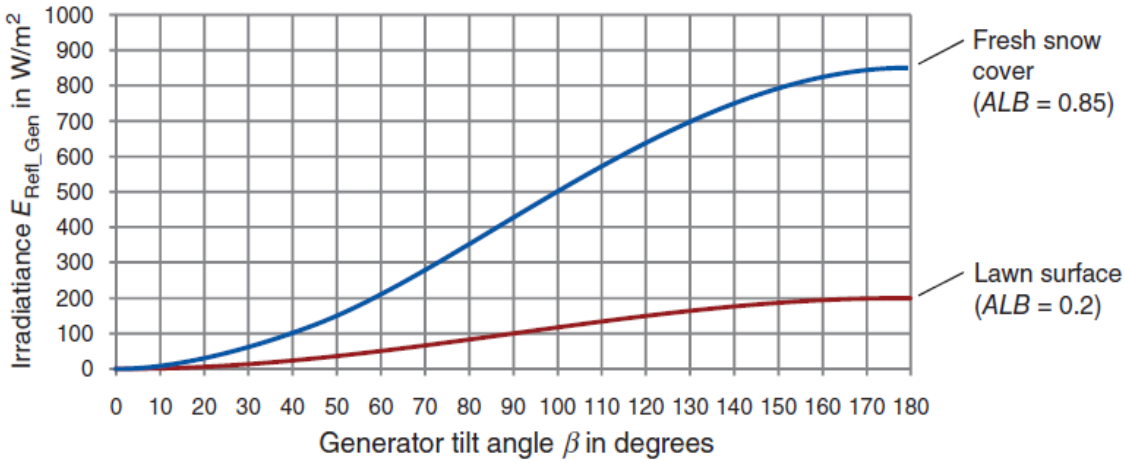

Figure 1.12: Reflected radiation as an example of lawn and fresh snow for various degrees of tilt of the solar module (E_G=1000 W/m^2) [8].

1.3.4. Radiation availability and world energy consumption

1.3.4.1. The Solar radiation energy cube

The sun shines continuously on the earth with a power density of 1367 W/m^2. Approximately 1000 W/m^2 of this arrives inside the atmosphere. We can simply calculate the energy arriving on Earth W_{Earth}. For this, we calculate the cross sectional area A_{Earth} of the Earth's sphere as shown in figure 1.13. The total optical power P_{Earth} radiated by the Sun on the Earth is then [8]:

$$P_{Earth} = E_{STC}.A_{Earth} = E_{STC}.\frac{\pi.d_{Earth}^2}{4} = 1.278.10^{17} W \tag{1.29}$$

Over the year the Earth receives radiation energy of:

$$W_{Earth} = P_{Earth}.t = 1.278.10^{17} W.8760h = 1.119.10^{18} kWh \tag{1.30}$$

This number only tells us something if, for instance, we use it in relationship to the current yearly world energy consumption approximately 12.5 billion tons of oil equivalent. After conversion into kWh we get:

$$\frac{W_{Earth}}{W_{World}} = \frac{1.119 \cdot 10^{18} kWh}{1.454 \cdot 10^{14} kWh} = 7969 \tag{1.31}$$

The Sun sends us more than 7000 times the energy than we use in a year.

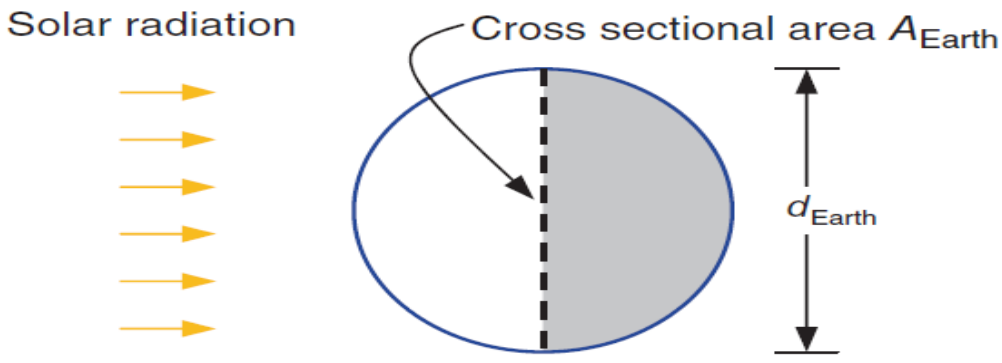

Figure 1.13: Cross sectional area of Earth for determining the total incidental radiation energy [8].

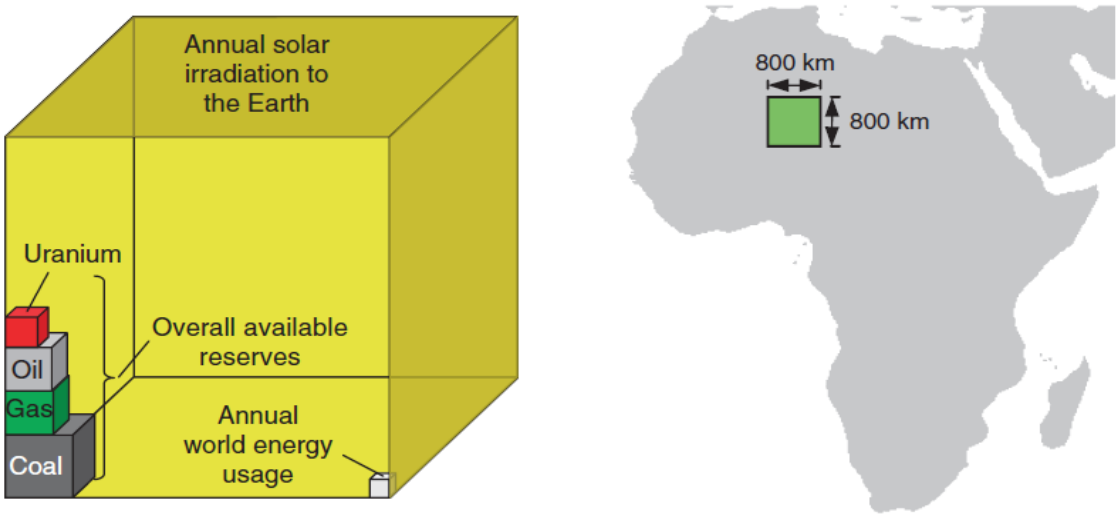

Figure 1.14: Energy cube and the “Sahara Miracle” [14].

This relationship is clearly seen in the energy cube as depicted in the left side of figure 1.14. The yearly solar incidental radiation is represented by the large cube, the small blocks of world energy usage at the bottom-right look tiny compared with the large solar cube. It must be mentioned here that with these cubes at the bottom-left, the reserves still available are included whereas the large solar radiation cube is available again every new year [8].

1.3.4.2. The Sahara Miracle

Now we will not be able to make use of all the energy radiating on to the Earth. Therefore, we will look at the case from another point of view and ask ourselves: What area would be necessary in order to supply the whole primary consumption of the world with photovoltaics?

To find a solution, let us assume that the solar modules would be erected in the Sahara. The best solar modules available on the market have an efficiency of 20%. As a precautionary measure, we will take a total system efficiency of η_{Total}=10%. In this way the losses from cables, inverters, transmission lines as well as the distance between module rows are more than covered.

The Sahara annually supplies approximately 2500 kWh/m^2 radiation energy [17]. With an efficiency of 10% it is possible to obtain electrical energy of approximately 250 kWh/m^2. For covering the worldwide primary energy consumption World, we would thus need an area of:

$$A = \frac{W_{World}}{250kWh/m^2} = \frac{1.454.10^{14}kWh}{250kWh/m^2} = 5.816 \cdot 10^5 km^2 \quad (1.32)$$

In order to estimate the size, the right side of figure 1.14 shows a square of 800 km X 800 km, which is about 7% of the size of the Sahara's surface. Thus, this area is sufficient to cover the Earth's primary energy consumption with photovoltaics. So, we could really speak about a "Sahara Miracle".

1.4. Solar resource measurement and estimation techniques

Studying of solar radiation is essential to estimate its amount at ground level. In practice, there are two sources of solar data, the first consists of the measured ground data available in meteorological networks and radiometric solar stations. And, the other consists of modeling or estimating the solar resource using data sources such as imagery of cloud characteristics observed from weather satellites, ground-based cloud cover observations, numerical weather prediction models, or sunshine duration records. This section provides an overview of these approaches.

1.4.1. Classification of the radiometric models

Radiometric models are based on the exploitation of some ground measured parameters to calculate the various components of solar radiation, particularly in areas where there are no radiometric stations. Generally, these models are based on the main meteorological parameters, such as ambient temperature, relative humidity, sunshine duration and some astronomical parameters such as declination of the Sun, the astronomical day length, solar constant, variation of the distance between Earth and Sun and extraterrestrial radiation calculated on a horizontal plane at the top of the atmosphere. Generally, we can classify the radiometric models in four families: spectral models, semi-empirical models, meteorological models and physical models (table 1.3 reviewed some examples of different types of these models).

1.4.1.1. Spectral models

Spectral models are essentially the calculation of the spectral components of solar radiation on the ground. They are based on the determination of transmission coefficients. They depend on the knowing of the characteristics of certain

atmospheric elements such as aerosols and clouds.

1.4.1.2. Semi-empirical

Semi-empirical models have a local character and used to calculate the direct, diffuse and global components. They use meteorological and geographical parameters as inputs. The limit of these models is the fact that they are applicable only in situations of clear sky [18].

1.4.1.3. Meteorological models

Meteorological models calculate global radiation whatever the sky condition using directly the solar data collected at ground stations. They have the advantage of generating solar radiation data for different inclined surfaces [18].

1.4.1.4. Physical models

Physical models consist of exploiting and processing satellite imagery. These models have proven their efficiency to reconstruct hourly and daily cycles of solar radiation. They depend on the data extracted from satellite images (clearness index, sky cases, cloud cover and thickness. . . etc.) and global solar radiation received at the ground under clear sky [18].

Table 1.3: Radiometric models

Models	Examples	Characteristics of the model
Semi-empirical models	Lacis and Hansen,1974 [19]	The model estimated the global horizontal solar radiation.
	Bird and Hulstrom model 1981 [20]	This model is based on empirical representations of radiate transfer equations and attempts to take into account the cumulative effects of aerosols, water vapor, ozone and other gases, and Rayleigh (molecular) scattering upon sunlight reaching the Earth's surface.
	Davies and Hay model 1980 [21]	In the Hay–Davies model, diffuse radiation from the sky is composed of an isotropic and circumsolar component and horizon brightening is not taken into account.
	Liu and Jordan model 1960 [22]	The proposed model estimated the amount of solar radiation at ground level basing on the day number, the latitude and the high of the Sun.
	Temps and Coulson 1977 [23]	this model is based on the Lui and Jordan (1960) model, Temps and Coulson (1977) developed a new model taking into consideration the non-isotropic characters of the reflected radiation from the ground, including maximum intensities near the Sun and the horizons, minimum intensities in the direction normal to that of the Sun.
Meteorological models	Angstrom model 1924 [24]	This Model proposed a linear expression to estimate of the daily , monthly and annual global solar radiation from the sunshine records.
	Garg model 1983 [25]	The model estimated the average monthly solar radiation using a correlation between relative humidity HR , ambient temperature T and sunshine fraction.
	Hussain model 1984 [26]	This model estimated the global solar radiation on horizontal surface using average monthly humidity and sunshine fraction
	Frutos model 1985) [27]	These models estimated the average monthly diffuse solar radiation models.
	Page model 1967 [28]	
Physical models	GISTEL model [29]	GISTEL is a satellite methodology based on a simple physical model. It is used to estimate global solar irradiance from METEOSAT data.
	Yang et al 2001 [30]	suggested a new form hybrid model which considered the spectral and temporal physical processes and still preserved the simplicity of Angstr¨om correlation.

1.4.2. Solar forecasting

Because of the limitation of solar models, which they take a lot of calculation time (for each hour we need to resolve equations). Different uses of PV forecasts require different types of forecasts. Forecasts may apply to a single PV system, or refer to the aggregation of large numbers of systems spread over an extended geographic area. Forecasts may focus on the output power of systems or on its rate of change (also known as the ramp rate). Accordingly, different forecasting methods are used. Forecasting methods also depend on the tools and information available to forecasters, such as data from weather stations and satellites, PV system data and outputs from numerical weather prediction (NWP) models. Forecasting methods can be broadly characterized as physical or statistical. The physical approach uses solar and PV models to generate PV forecasts, whereas the statistical approach relies primarily on past data to “train” models, with little or no reliance on solar and PV models [31].

1.4.2.1. Forecasting methods for different forecast horizons

1.4.2.1.1. Solar and PV forecasting 0 to 6 hours ahead (Intra-day forecasts)

Intra-day forecasts are an important component of the integration of variable renewable resources into the electric grid [32]. For example, in California (the state with by far the largest amount of installed solar power in the US, the independent system operator CAISO uses the following forecasts:

- The day ahead (DA) forecast is submitted at 05:30 on the day before the operating day, which begins at midnight on the day of submission and covers (on an hourly basis) each of the 24 hours of that operating day. Therefore, the day ahead forecast is provided 18.5 to 42.5 hours prior to the forecasted operating day. The vast majority of conventional generation is scheduled in the DA market.
- The hour ahead (HA) forecast is submitted 105 minutes prior to each operating hour. It also provides an advisory forecast for the 7 hours after the operating hour. Note that the CAISO HA forecast is really a 1.75 to 8.75 hour ahead forecast. CAISO also is considering the implementation of intra-hour forecasts on 5 minute intervals; a similar intra-hour forecast is already implemented by

the Midwest Independent System Operator (ISO). The US Federal Energy Regulatory Commission (FERC) has issued a Notice of Proposed Rulemaking requiring public utility transmission providers to offer all customers the opportunity to schedule transmission service every 15 minutes, and requiring providers with variable renewables on their systems to use power production forecasting. Similar day-ahead schedules are applicable throughout the different power exchange markets in Europe. In summary, intra-day forecasts are currently of smaller economic value than DA forecasts but with increasing solar penetration and the expected accuracy improvement of intra-day compared to DA forecasts substantial market opportunities will likely materialize [31].

For solar forecasting, very different methodologies are preferred, depending on the forecast horizon (table 1.4). Some of these techniques are summarized below [33]:

- Stochastic learning techniques identify patterns in data both within one variable (e.g. auto-regression) and between variables or even images. The underlying assumption is that future irradiation can be predicted by training the algorithms with historical patterns. The simplest stochastic learning technique is the persistence forecast which is based on current or recent PV power plant or radiometer output and extrapolated to account for changing sun angles. Persistence forecast accuracy decreases strongly with forecast duration as cloudiness changes from the current state.
- Total sky imagery can be used to forecast from real time (nowcast) up to 10-30 minutes ahead by applying image processing and cloud tracking techniques to sky photographs. The published methods assume persistence in the opacity, direction, and velocity of movement of the clouds [34]. Irradiance is predicted for the current cloud shadow and then the cloud shadow is moved forward in time based on cloud velocity and direction.
- For satellite imagery, similar methods as in total sky imagery are applied. Clouds reflect light into the satellite leading to detection and the ability to calculate the amount of light transmitted through the cloud (transmissivity = 1 – reflectivity – absorptivity). The lower spatial and temporal resolution probably causes satellite forecasts to be less accurate than sky imagery on intra-hour

time scales, but extensive comparisons or combinations of the two approaches have not been conducted. Satellite imagery is commonly considered the best forecasting technique up to 5 hour forecast range [35].

Table 1.4: Characteristics of solar forecasting techniques.

Technique	**Sampling rate**	**Spatial resolution**	**Spatial extent**	**Maximum Suitable Forecast horizon**	**Application**
Persistence	High	One point	One Point	Minutes	Baseline
Whole Sky Imagery	30 sec	10 to 100 meters	3-8 km radius	10s of minutes	Ramps, regulation
Geostationary satellite imagery	15 min	1 km	65°S – 65°N	5 hours	Load following
Numerical weather prediction (NWP)	1 hour	2 - 50 km	Worldwide	10 days	Unit commitment regional power prediction

1.4.2.1.2. Solar and PV forecasting 6 hours to days ahead

One of the key uses of solar and PV forecasting is « day-ahead » forecasting of the hourly output power that will be generated by PV systems within an area managed by an electricity system operator or utility. These day-ahead forecasts are typically required by about noon for each hour of the next day, which implies that day-ahead forecasts must in fact extend at least 36 hours ahead to a few days ahead, depending on the timing of electricity markets and of weather forecasts. weather forecasts from numerical weather prediction (NWP) models are the key inputs for day ahead forecasting [31].

Numerical weather prediction models are based on dynamical equations that predict the evolution of the atmosphere up to several days ahead from initial conditions. The NWP models that underlie all others are global models covering the whole Earth. The model equations and inputs are discretized on a three-dimensional grid extending vertically from the surface of the Earth. Since global models are computationally and otherwise intensive, there are only 14 of these currently in operation worldwide [36].

Model runs are typically initiated two to four times per day, for example at 0, 6, 12 and 18 UTC. Their initial conditions are derived from satellite, radar, radiosonde and ground station measurements that are processed and interpolated to the 3D grid. In order to limit computational requirements, the resolution of global NWP models is relatively coarse, with grid spacing of the order of 40 km to 90 km [36]. Mesoscale or limited area models are NWP models that cover a limited geographical area with higher resolution, and that attempt to account for local terrain and weather phenomena in more detail than global models. Initial conditions for these models are extracted from the global models.

The best day-ahead solar and PV forecasts combine NWP forecasts with post-processing of these forecasts in order to improve them or to generate forecasts that are not included in the direct model outputs of the NWP, such as PV forecasts or direct normal irradiance forecasts [31].

1.4.2.2. Forecast accuracy

The solar and the PV production forecasting accuracy are mainly influenced by the variability of the meteorological and climatological conditions. Accuracy is affected by uncertainties related to the different modelling steps that are needed to make energy forecasts out of irradiation forecasts. The maximum achievable accuracy is determined mainly by the following factors [31]:

- Local climate and weather conditions
- Single-site or regional forecast
- Forecast horizon
- Accuracy metric used

1.4.2.2.1. Accuracy metrics and confidence intervals

Whatever the intended use of forecasts, standardizing performance measures or metrics help facilitate forecast evaluations and benchmarking. Beyer et al [37] have attempted to standardize solar forecast benchmarking and accuracy metrics, while Madsen et al [38] have proposed standardized measures of wind forecast accuracy. Common metrics proposed by these authors include mean bias error (MBE, or bias), mean square error (MSE) and root mean square error (RMSE), mean absolute error

(MAE) and standard deviation (SDE or σ). These are defined as follows:

$$RMSE = (MSE)^{1/2} = \left(\frac{1}{N} \sum_{i=1}^{N} e_i^2 \right)^{1/2} \quad (1.33)$$

$$SDE = \sigma = \left(\frac{1}{N-1} \sum_{i=1}^{N} \left(e_i - \overline{e_i} \right)^2 \right)^{1/2} \quad (1.34)$$

$$MAE = \frac{1}{N} \sum_{i=1}^{N} |e_i| \quad (1.35)$$

$$MBE = \frac{1}{N} \sum_{i=1}^{N} e_i \quad (1.36)$$

$$e_i = y_{i,\text{forecast}} - y_{i,\text{observed}} \quad (1.37)$$

Where $y_{i,forecast}$ and $y_{i,observed}$ are the i^{th} forecast and observation, respectively, and e_i is the i^{th} error, with i=1,…,N running through all forecast-observation pairs in the test dataset.

The bias or MBE is the average forecast error, and encapsulates the systematic tendency of a forecast model to under or over-forecast. Model output statistics approaches can be used to significantly reduce the bias when past observations are available. MAE gives the average magnitude of forecast errors, while RMSE (and MSE) give more weight to the largest errors. Madsen et al [38] argue that large errors are disproportionately costly, so that RMSE better reflects the costs of forecast errors to system operators than the MAE. MSE, SDE and bias are related as follows:

$$\text{RMSE}^2 = \text{MSE} = \text{MBE}^2 + \text{SDE}^2 \quad (1.38)$$

In other words, the standard deviation captures the part of the RMSE that is not due to systematic error, and provides an indication of the RMSE that can be achieved once the bias is essentially eliminated.

1.4.3. Solar resource measurement techniques

Although efforts to measure the solar resource quantitatively have been around for nearly two centuries (such as recording the number of hours of direct sunshine or the use of bimetallic strip recorders), at the beginning of the twentieth century,

methods that convert the incoming solar radiation to an electrical output were developed, and today this is the most common approach for developing precise measurements of the solar resource. Instruments using this approach fall into two broad categories: those using thermopile-type detectors and those using silicon photodiode- type detectors) [39]. Examples of commercially available solar monitoring devices are illustrated in figure 1.15.

1.4.3.1. Thermopile-type detectors

A thermopile detector works on the principle of the thermoelectric effect, where a voltage is generated from the temperature difference between two dissimilar metals. Today's precision solar monitoring devices make use of this effect by deploying two different metals under a glass dome (or double-glass dome) and monitoring the voltage output of the incoming solar radiation, either from the total sun and sky (pyranometers) or directly from the solar disk (pyrheliometers) [39].

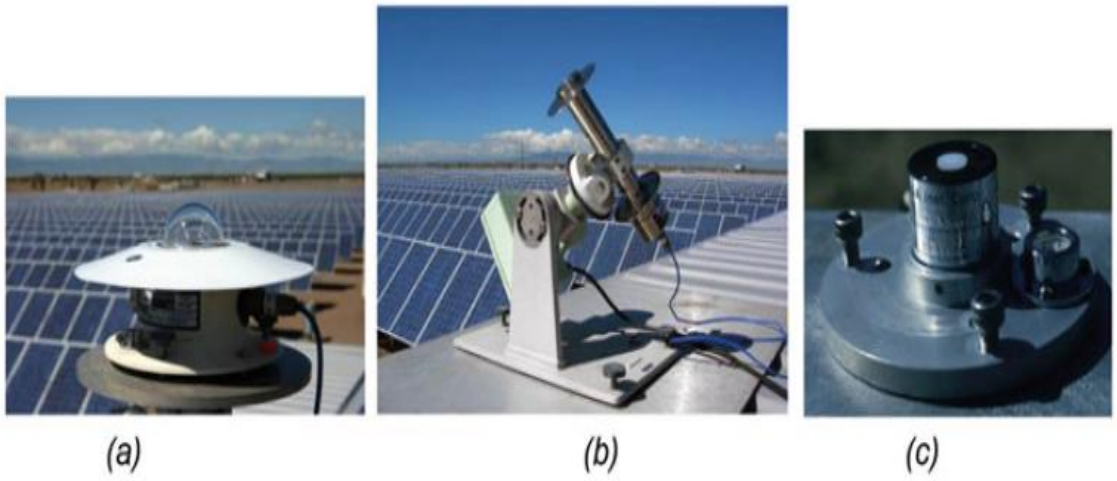

Figure 1.15: Examples of commercially available solar monitoring devices: (a) Eppley pyranometer, (b) Eppley pyrheliometer mounted on a tracker, and (c) LiCor silicon photodiode sensor (source: NREL Image Gallery # 15537, 15554, and 15483)

1.4.3.1.1. Pyranometer

Pyranometer measured the global hemispherical solar radiation (direct + diffuse) with a 360° field of view. The pyranometer is represented in figure 1.16. It consists of

a white disk that limits the acceptance angle to 180° and two domes made of glass to protect the sensor from the weather threat (rain, wind and dust). A cartridge of silica gel inside the dome absorbs water vapor. The diffuse solar radiation can be measured by eliminating the direct beam radiation, a small shading disk can be mounted on an automated solar tracker that ensures that the pyranometer is continuously shaded. However, because the variation of the Sun elevation angle from day to another, the shadow ring must be oriented to ensuring the shadow during the day. In addition, the shadow ring may intercept a part of the diffuse radiation. The percentage of diffuse radiation intercepted by the shadow ring varies during the year with its position and atmospheric conditions for that its value must be corrected [40].

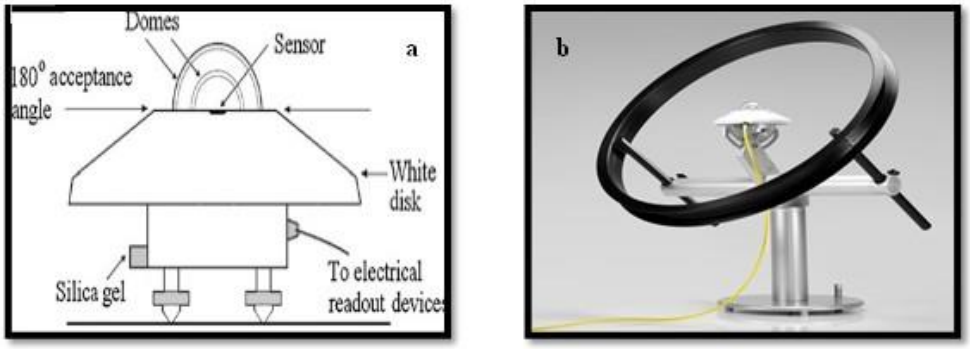

Figure 1.16: a) Schematic of a pyranometer. b) pyranometer equipped with shadow ring.

1.4.3.1.2. Pyrheliometer

Pyrheliometer is an instrument that measures the direct solar radiation. It should be always oriented toward the Sun. Hence, a two-axis sun tracking mechanism was used for this purpose. Figure 1.17 shows a pyrheliometer that consists of a detector (multi-junction thermopile) placed at the bottom of a collimating tube provided with a quartz window to protect the instrument. The detector is coated with optical black paint (to act as full absorber of solar energy in the wavelengths range 0.280 - 3 µm). The radiation received from the Sun is limited to a circumsolar region (with an acceptance angle of 5°), the other diffuse radiation from the sky is excluded. At the end of the tube, an electrical readout device is used to give the instantaneous values of direct solar radiation in W/m^2 [40].

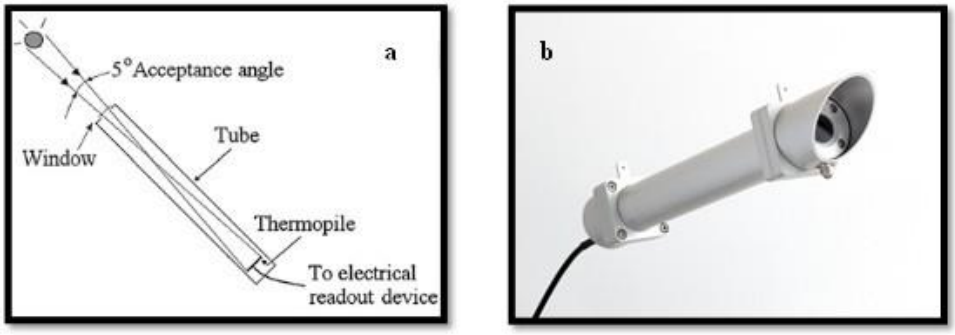

Figure 1.17: a) Schematic of a pyrheliometer. b) Photo of Hukseflux DR01 first class pyrheliometer [41]

1.4.3.1.3. Sunshine duration measurement

Sunshine duration is the sum of the time intervals for which the direct solar radiation exceeds the threshold of 120 W/m^2 [42]. Two methods are used in practice for measuring sunshine duration, the burning card method and pyranometric method. Burning card method is based on the Campbell-stokes (CS) sunshine recorder developed by John Francis Campbell in 1853 and later modified in 1879 by Sir George Gabriel Stokes. It consists of a glass sphere filled with water mounted in a spherical bowl that holds the recording card as shown in figure 1.18. The glass sphere focuses the beam radiation onto the card, burning a trace whenever the Sun is shining. The position and length of the trace indicate the starting and the duration of the sunshine interval. The Campbell-stokes recorder is still manufactured and used today. However, it presents an error depends on the burning card temperature, humidity and clouds [43].

The pyranometric method consists of determining the sunshine duration during a time interval Δt by multiplying the mean sunshine number (mean of ξ) during Δt. Sunshine number is a Boolean variable stating whether the Sun is covered or not by clouds. It is calculated from the subtraction of the global and diffuse solar radiation. Then, direct radiation obtained is compared with the WMO threshold as illustrated in equation 1.32 where θ_z is the Sun zenith angle [44]. The disadvantage of this method that is depends strongly on the accurate measuring of the global and diffuse radiation.

$$x = \begin{cases} 1 & \text{if } \left(G - G_d\right)/\cos\left(\theta_z\right) > 120\ \text{W/m}^2 \\ 0 & \text{otherwise} \end{cases} \tag{1.39}$$

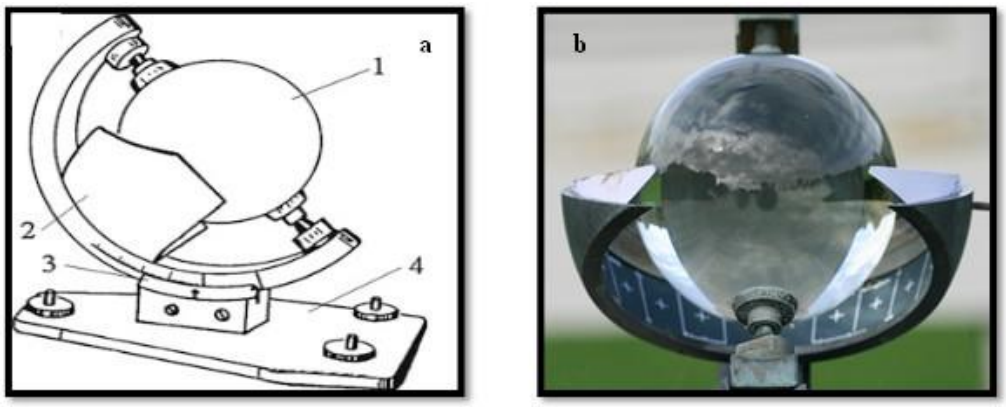

Figure 1.18: a) Schematic of Campbell-Stokes sunshine recorder (1. glass sphere, 2. burning card, 3. Spherical bowl, 4. Sphere and Card holder). b) Photo of a typical Campbell- Stokes sunshine recorder.

Modern instruments such as electronic sunshine recorders (using photodiodes) are used to determine the patent of sunshine. These devices have much time resolution and more precise results that improve the reliability, and the accuracy of the measurements comparing with the CS instruments.

1.4.3.2. Silicon photodiode- type detectors

Silicon photodiodes are made from crystalline silicon that has been transformed into a semiconductor, similar to the principles of a crystalline silicon PV cell. Instruments using this technology have the advantage of much lower cost and much faster response time than a thermopile-based instrument, their main disadvantage is their limited spectral response characteristics (they do not respond at all to wavelengths above 1100 nm). This disadvantage results in a slightly higher uncertainty than instruments using thermopile detectors.

1.4.3.3. The choice of instruments

The use of thermopile radiometers became common beginning in the mid-1920s due to the innovative work of companies such as Kipp & Zonen and, later, Eppley Laboratories and EKO Instruments, which continue to develop and refine improved thermopile instruments for a variety of scientific purposes. Other companies such as Hukseflux and Yankee Environmental Systems have entered the market more recently

with thermopile-based products. Instruments based on silicon photodiode technology are also very common, due to their low cost.

The choice of instruments used in a solar resource measurement campaign depends on the uncertainty goals established for the project. Currently, the World Meteorological Organization (WMO) and International Organization for Standardization (ISO) 9060 categorize pyranometers and pyrheliometers according to their accuracy and uncertainty. Examples of a thermopile-based pyranometer and pyrheliometer currently on the market are shown in figure 1.15 a, b, an example of a silicon photodiode pyranometer currently on the market is shown in figure 1.15 c.

1.4.3.4. Surface solar radiation networks

The knowledge of the solar energy available at any location depends not only on the total measured values, but also on its temporal repartition, spectral distribution and its nature (global, direct or diffuse). In most areas of the world, measuring solar radiation stations are installed. However, their investment and maintenance cost is considered high. Hence, the national networks consist of a small number of stations even in industrialized countries. In addition, measurements are varying from station to another. The global solar radiation and sunshine duration are available in mean daily or monthly basis. The diffuse, direct and cloud cover data on hourly bases are rarely recorded. Nowadays, some databases are created in the world that based on the interpolation and extrapolation of the available data for estimating solar radiation at each point in the world. However, the error of estimating radiation increases with the distance from the closest station. Moreover, the databases store various format and units using various time idioms. Thus, sometimes even data access and correct interpretation is a difficult task. In following, some surface networks as the World Radiation Data Center (WRDC) and Baseline Surface Radiation Network (BSRN), Photovoltaic Geographical Information System (PVGIS) and METEONORM (METEONORM) are summarized.

1.4.3.4.1. World Radiation Data Center

World Radiation Data Center [45] is located at the Main Geophysical Observatory in St. Petersburg, Russia and serves as a central depository for solar radiation data collected at over 1000 measurement sites throughout the world. Using

the data measured from the WMO (World Meteorological Organization), the WRDC archive contains mainly measurements of global solar radiation, diffuse solar radiation and sunshine duration in the format of daily sums and monthly mean. Data collected from 1964 to 1993 are accessible online on the site of the US Department of Energy's, National Renewable Energy Laboratory and data collected from 1994 to present are accessible on the site of the Main Geophysical Observatory, St. Petersburg, Russia [40].

1.4.3.4.2. Baseline Surface Radiation Network

BSRN is a project of the Radiation Panel from the Global Energy and Water Cycle Experiment [46] as part of the World Climate Research Programme [47]. It contains about 40 stations located on the world between latitude 80° N and 90° S. BSRN is used for detecting important changes in the Earth's radiation, which related to the climate changes. It measures solar and atmospheric radiation with instruments of the highest available accuracy and high time resolution (1–3 min) [40].

1.4.3.4.3. Photovoltaic Geographical Information System

PVGIS is a server [48], operated by the Joint Research Centre of the European Commission that offers a map of solar radiation, temperature and other data for Europe and Northern Africa. In Europe, the database is based on interpolation of ground station measurements (1 km grid, period 1981–1990). For Mediterranean Basin and Africa, the maps are developed by processing the HelioClim-1 database (2 km grid resolution, period 1985–2004) [40].

1.4.3.4.4. Meteonorm

Meteonorm [17] is a database for solar energy application contains a large database of ground station measurements collected from various sources (more than 8300 are listed for the version 7). It offers two periods of measurements: (1) from 1961 to 1990 and 1996 to 2005 for temperature, humidity, precipitation, and wind speed, and (2) 1961–1990 and 1981–2000 for radiation parameters. The METEONORM outputs are climatology averages and derived products for any point on Earth, estimated by interpolation at very high resolution (0.1–1 km) [40].

1.4.4. Online available databases

Online solar radiation databases are the data derived from satellite data provided by web based systems. The data are saved on servers in some websites, among them:

1.4.4.1. Satel-Light (European Database of Daylight and Solar Radiation)

Satel-Light [49] was one of the first websites to provide solar radiation data. It's based on the Heliosat model (images produced by the Meteosat satellite every half hour) and covers Europe and a small region of the North Africa. It provides monthly means of hourly and daily values from the period 1996 to 2000 [40] .

1.4.4.2. SoDa

The project Solar Data [50] is a web service that offers long-term monthly, daily and hourly solar radiation data and other information such as temperature measurements at any place in the world. The SoDa database [51] is processed by MINES ParisTech—ARMINES [40].

1.4.4.3. NASA Surface Meteorology and Solar Energy

It is a large archive that covers the entire globe using over 200 satellite-derived meteorological and solar radiation parameters. Data can be retrieved from the SMSE server [52], where they can be used in various solar applications, e.g., sizing and pointing solar modules, solar cooking, tilted solar modules and cloud information [40].

1.4.5. Meteorological network of Algeria

Algeria has a considered sunny area with mean annual sunshine varies between 2600 h/year in the North and 3500 h/year in the South. It has the most important solar potential of the Mediterranean basin (169440 TWh/year). The average of the received solar energy in coastal regions is 1700 kWh/m²/year while it is 1900 kWh/m²/year on highlands and 2650 kWh/m²/year in the Sahara [53]. It has been proved that alone, the solar potential of the Sahara could cover all the needs of energy in the world [8] if we put the necessary amount of investments in this field.

However, the number of meteorological stations (56 stations) is low comparing with the total surface of Algeria (more than 2 million km^2). Figure 1.19 shows the

localization of stations on the Algeria map. It is clearly shown that the most of stations are situated in the north and High Plateaus. However, their number is negligible in the south (Sahara region) where there are high solar radiation values.

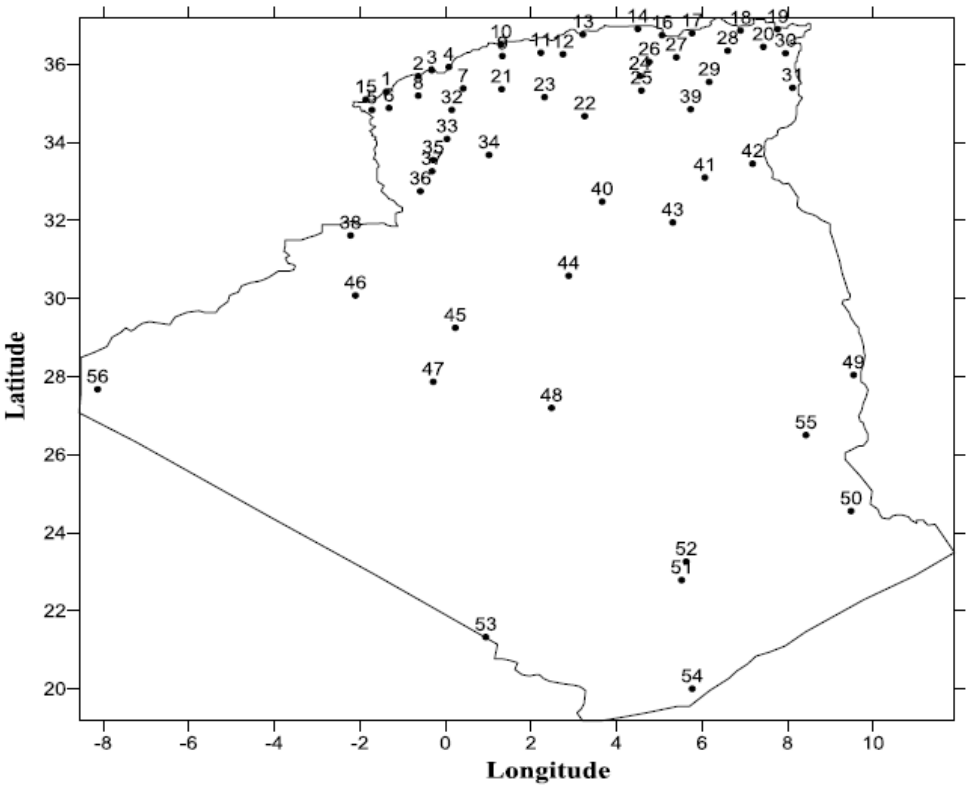

Figure 1.19: Meteorological stations over Algeria [18].

From the spatial distribution of the 56 meteorological stations showed in figure 1.19, we can note that Algeria has considerable territory, which cannot be reflect the reality of solar zones in Algeria.

We can see from the monthly average sunshine maps of Algeria as shown in figure. 1.20 that the average sunshine map is well constructed in the north of Algeria that contains many meteorological stations with small distance between them compared to the Sahara region that needs more installation of this meteorological stations.

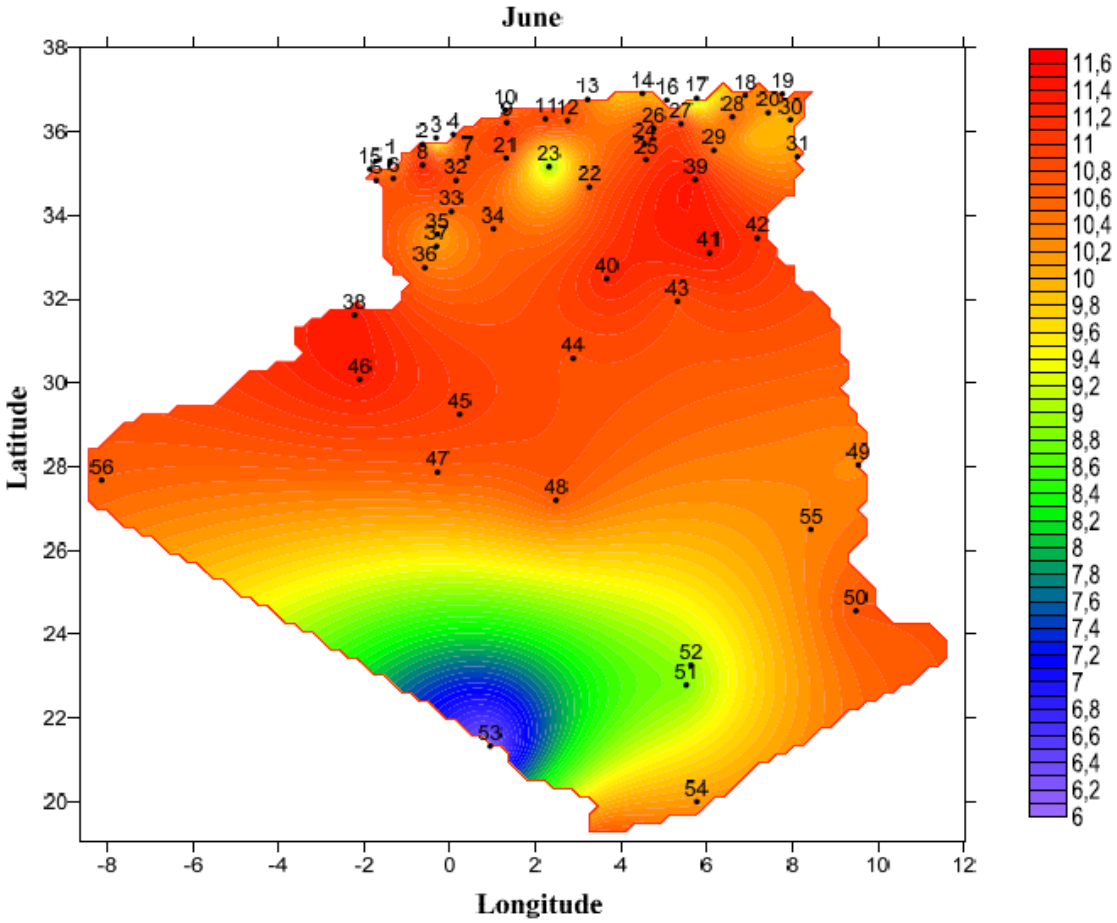

Figure 1.20: Monthly average sunshine maps of Algeria (June) [18].

1.5. Conclusion

This chapter introduced the basic characteristics (astronomical, geographical and meteorological) and possibilities of solar radiation. The most important radiometric models with different methods and resources used in solar measurement are presented. an overview of solar and photovoltaic forecasting is summarized. Also The meteorological network and the solar potential in Algeria are discussed. This chapter focused on how we can obtain the best possible knowledge about this variability so that photovoltaic systems can be designed and deployed optimally regardless of the load they are being used to meet.

CHAPTER 2

HYBRID PV-DIESEL-BATTERY SYSTEM

2.1. Introduction

As we already discussed in chapter 1 the different characteristics and perspectives of the solar energy, this chapter gives an overview of the PV technology and the types of solar PV systems. Then, it summarized the modeling of the components, the energy flow, and the control strategies of the hybrid PV-diesel-battery system.

2.2. A brief history of solar cells

In the seventh century BCE, humans were already using magnifying glasses to concentrate sunlight and hence to make fire. Later, the ancient Greeks and Romans used concentrating mirrors for the same purpose. In the 18th century the Swiss physicist Horace-Bénédict de Saussure built heat traps, which are a kind of miniature greenhouse. He constructed hot boxes, consisting of a glass box within another bigger glass box, with a total number of up to five boxes. When exposed to direct solar irradiation, the temperature in the innermost box could rise up to 108°C; warm enough to boil water and cook food. These boxes can be considered as the World's first solar collectors [54]. In 1839, the French physicist Alexandre-Edmond Becquerel discovered the photovoltaic effect at the age of only 19 years. He observed this effect in an electrolytic cell, which was made out of two platinum electrodes, placed in an electrolyte. An electrolyte is an electrically conducting solution, Becquerel used silver chloride dissolved in an acidic solution. He observed that the current of the cell was enhanced when his setup was irradiated with sunlight.

In 1887, the German physicist Heinrich Hertz discovered the photoelectric effect. In this effect, electrons are emitted from a material that has absorbed light with a frequency exceeding a material-dependent threshold frequency. Photovoltaics is inextricably linked with the development of quantum mechanics [55]. In 1905 Albert Einstein published a paper in which he explained the photoelectric effect by assuming that light energy was being carried with quantized packages of energy [56], which we

nowadays call photons. In 1918 the Polish chemist Jan Czochralski invented a method to grow high quality crystalline materials. Nowadays this technique is very important for growing monocrystalline silicon used for high quality silicon solar cells. The development of the c-Si technology started in the second half of the 20th century. The real development of solar cells as we know them today, started at the Bell Laboratories in the United States. In 1954, their scientists Daryl M. Chapin, Calvin S. Fuller, and Gerald L. Pearson, made a silicon-based solar cell with an efficiency of about 6% [57]. In the same year, D. C. Reynolds et al. reported on the photovoltaic effect for cadmium sulphide (CdS), a II-VI semiconductor [58]. In the mid and late 1950s several companies and laboratories started to develop silicon-based solar cells in order to power satellites orbiting the Earth. In the late 1970s and 1980s many companies started to develop PV modules and systems for terrestrial applications. Solar cells are still very important for space applications as seen in figure 2.1, which shows a solar panel array on the International Space Station (ISS).

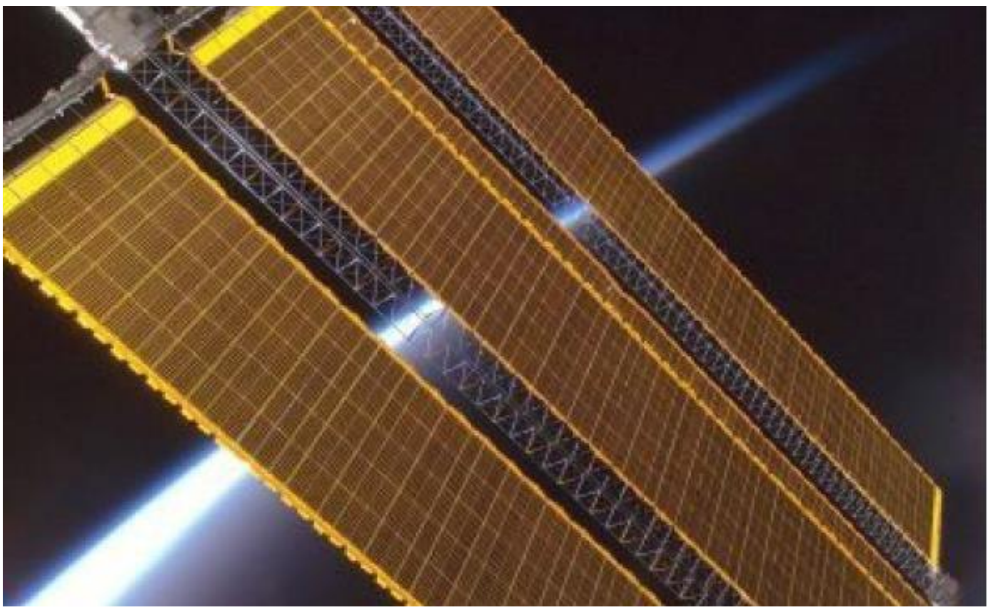

Figure 2.1: A solar panel array on the International Space Station (ISS) [59].

In 1980 the first thin-film solar cells based on a copper-sulphide/cadmium-sulphide junction were demonstrated with a conversion efficiency above 10% at the University of Delaware. From 1984 through 1991 the world's largest solar thermal energy generating facility in the world was built in the Mojave Desert in California. It

consists of nine plants with a combined capacity of 354 megawatts. In 1991 the first high efficiency dye-sensitized solar cell was published by the École polytechnique fédérale de Lausanne in Switzerland by Michael Grätzel and co-workers. The dye-sensitized solar cell is a kind of photo electrochemical system, in which a semiconductor material based on molecular sensitizers is placed between a photo-anode and an electrolyte. In 1994, the US National Renewable Energy Laboratory in Golden, Colorado, demonstrated a concentrator solar cell based on III-V semiconductor materials. Their cell, based on an indium-gallium-phosphide/gallium-arsenide tandem junction, exceeded the 30% conversion limit. In 1999, the total global installed photovoltaic power passed 1 GWp. Starting from about 2000, environmental and economic issues started to become more and more important in the public discussion, which renewed the public interest in solar energy. Since 2000, the PV market therefore transformed from a regional market to a global market [54]. Germany took the lead with a progressive feed-in tariff policy, leading to a large national solar market and industry [60]. Since about 2008, the Chinese government has been heavily investing in their PV industry. As a result, China has been the dominant PV module manufacturer for several years now. In 2012 the worldwide solar energy capacity surpassed the magic barrier of 100 GWp [61]. Between 1999 and 2012, the installed PV capacity has hence grown by a factor of 100. In other words, during these last 13 years, the average annual growth of the installed PV capacity was about 40% [54].

2.3. Photovoltaic Materials

Solar cells are made from semiconductors (see the periodic table in figure 2.2). the most important one being silicon, the figure 2.3 shows the silicon crystal. Semiconductors have special electronic properties which allow them to be conducting or insulating depending on their composition, semiconductor acts as insulators at low temperatures, but as conductors when energy or heat is available. At present, most solar cells are silicon-based, since this is the most mature technology. However, other materials are under active investigation and may supersede silicon in the long term. The electrical properties of semiconductors can be explained using two models, the bond and the band models. These models are described briefly below.

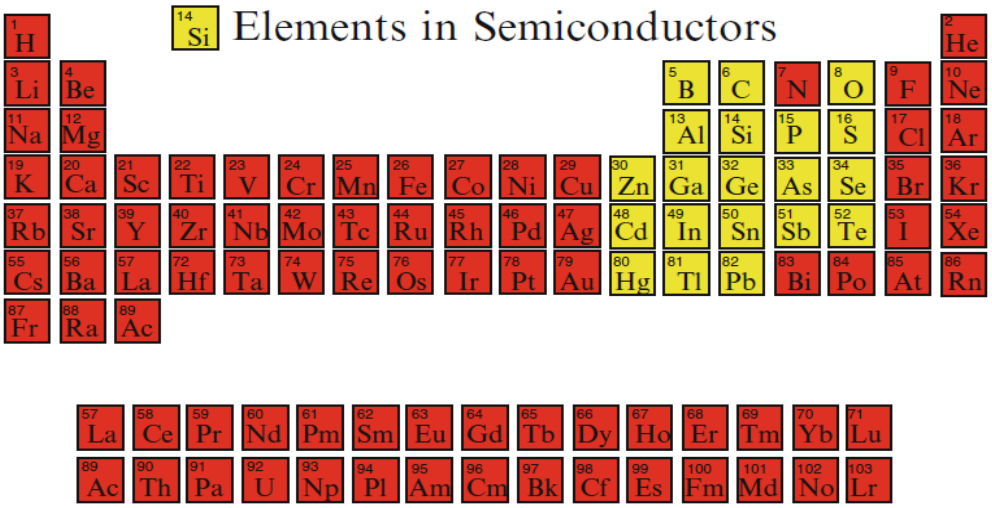

Figure 2.2: The periodic table.

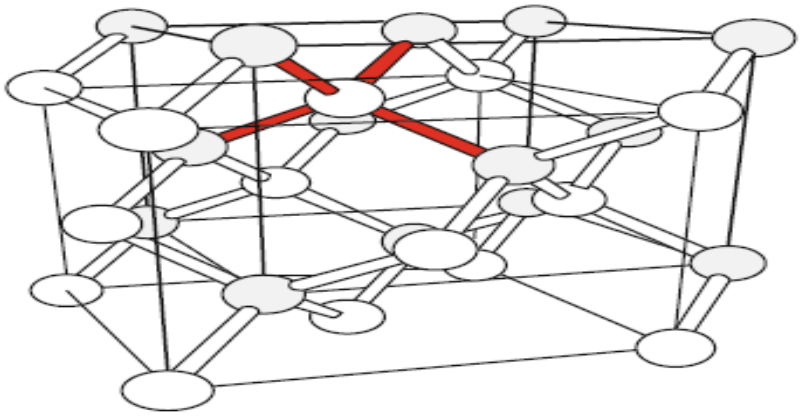

Figure 2.3: Silicon crystal.

2.3.1. The Bond model

The bond model uses the covalent bonds joining the silicon atoms to describe semiconductor behavior. Figure 2.4 illustrates the bonding and the movement of electrons in a silicon crystal lattice.

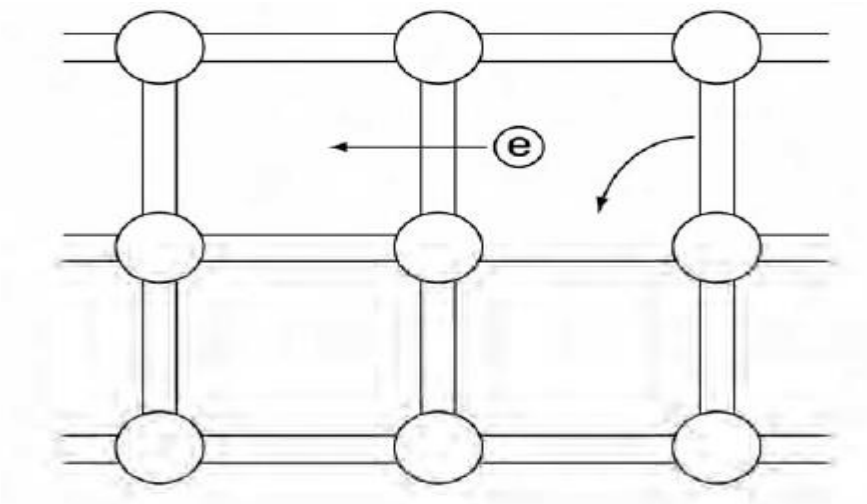

Figure 2.4: Schematic representation of covalent bonds in a silicon crystal lattice [55].

At low temperatures, the bonds are intact and the silicon behaves as an insulator. At high temperatures, some bonds are broken and conduction can occur by two processes [55]:

1. Electrons from broken bonds are free to move.
2. Electrons from neighboring bonds can also move into the 'hole' created in the broken bond, allowing the broken bond or hole to propagate as if it had a positive charge.

The concept of a moving hole is analogous to that of a bubble in a liquid. Although it is actually the liquid that moves, it is easier to describe the motion of the bubble going in the opposite direction [55].

2.3.2. The band model

In band theory, there are three types of materials which are differentiated by their electronic structure: insulators, conductors, and semiconductors. The band model describes semiconductor behaviour in terms of the energy levels between valence and conduction bands [55]. For the semiconductor, there is a gap between the valence and conduction bands, this is known as the bandgap and is denoted as E_g (energy of the gap). The Fermi energy (E_f) is also shown for the insulator and semiconductor. The Fermi energy is the level (if there is one) where half of the states are occupied with electrons.

2.3.3. Doping

It is possible to shift the balance of electrons and holes in a silicon crystal lattice by ‘doping’ it with other atoms. Atoms with one more valence electron than the semiconductor are used to produce ‘n-type’ material. Atoms with one less valence electron result in ‘p-type’ material. There are three types of semiconductors as shown in figure 2.5, Intrinsic, n-type, p-type. The semiconductors that conduct electricity are types 2 and 3.

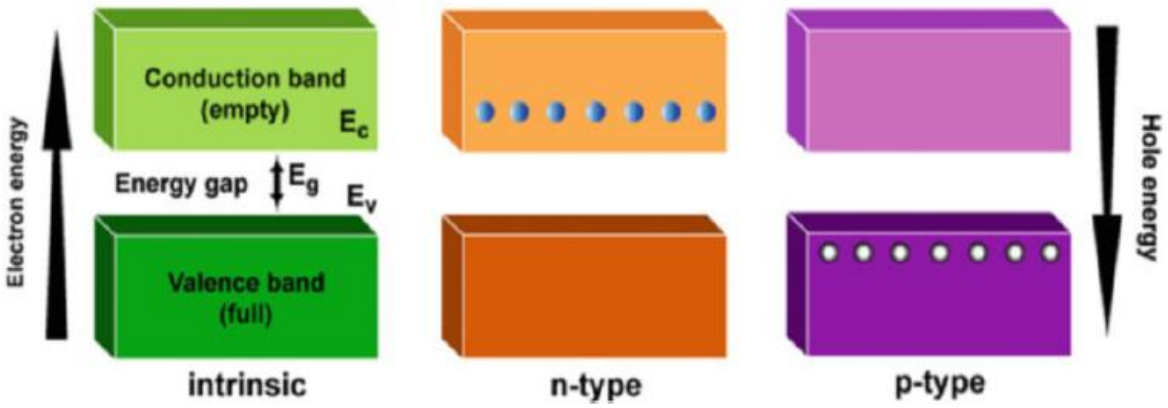

Figure 2.5: Intrinsic, n-type, and p-type semiconductor [39].

2.3.4. Semiconductor junctions

When it comes to understanding the main operating principle of solar cells, it suffices to investigate what is known as a homogeneous junction, i.e. the junction between p- and n-conducting semiconductors made of the same base material. A homogeneous junction automatically engenders a space charge zone and thus a strong electric field, which can be used to separate the electron–hole pair resulting from the internal photoelectric effect, as can of course the space charge zones and electric fields associated with the p–n junction between different base materials. In this scenario, known as a heterogeneous junction, the p- and n-doped parts are composed of chemically heterogeneous materials, or a Schottky junction can occur, i.e. a junction between a semiconductor and a metal. Figure 2.6 illustrates such a p–n junction without an external voltage source. Here, electrons are diffused into the p-zone from the n-zone, where they fill holes. The positively charged donor atoms left behind engender a positive space charge in the n-zone, while the now negatively charged

acceptor atoms engender a negative space charge in the p-zone. These space charges create an electric field in the boundary layer that initially impedes further electron diffusion and ultimately brings it to a halt [7].

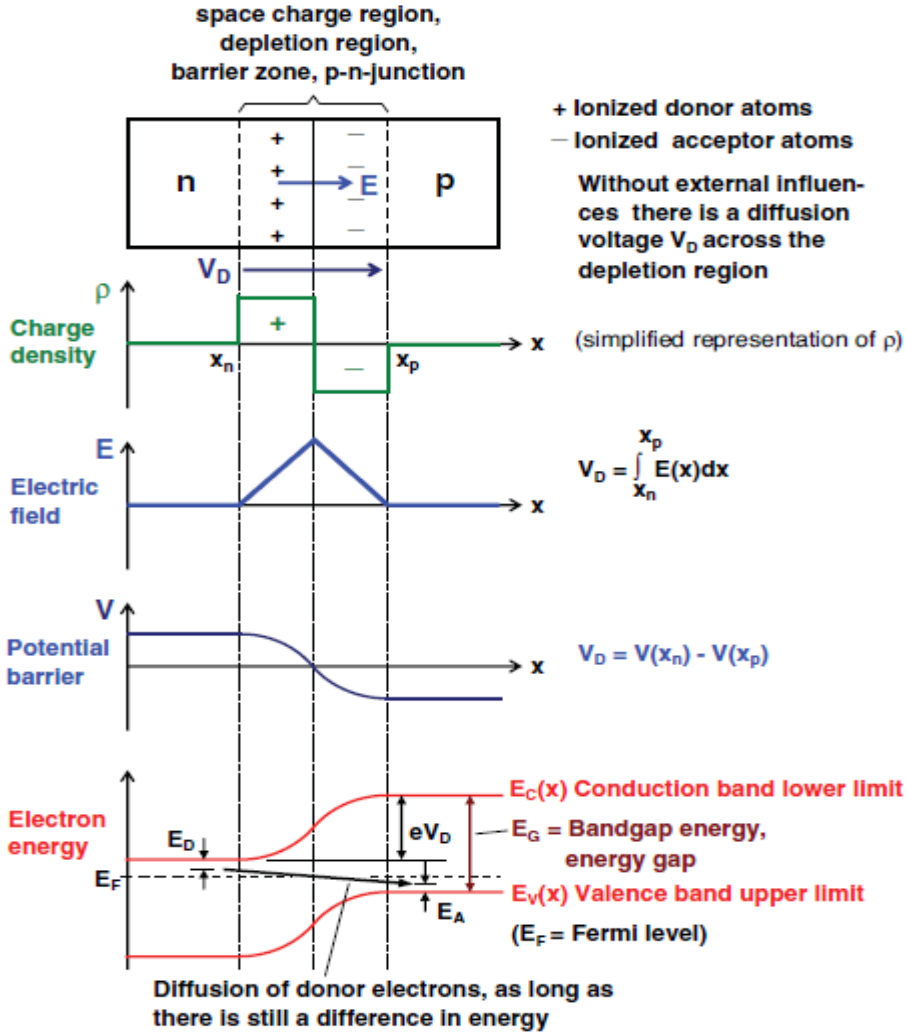

Figure 2.6: Simplified depiction of the scenario at a p–n junction without an external voltage source [7].

The barrier layer thus created at the boundary between the n- and p-material is now devoid of freely moving charge carriers. Diffusion voltage V_D is created via the diffusion zone, thus also engendering a potential difference.

Although what we have said thus far accounts for the creation of a diffusion voltage V_D, we are still in the dark as to its level, which is a key factor for solar cells as it determines the maximum possible open circuit voltage V_{OC}. In all solar cells, V_{OC} is lower than V_D.

When the effects of electron diffusion from the n-zone to the p-zone in the band model are taken into consideration, it becomes clear that the consequent lower potential V on the p-side induces an increase in the p-side energy bands (the electrons have more energy on account of their negative charge resulting from lower potential). The electrons diffused from the n-zone to the p-zone can gain energy until the lower valence band edge in the p-zone increases to the point where there is no longer a substantial difference between the energy level of the donor electrons on the n-side and that of the acceptor holes on the p-side.

Inasmuch as the energy of the donor electrons is E_D lower than the bottom conduction band edge, and the energy of the acceptor holes is E_A higher than the upper valence band edge, eV_D must be somewhat lower than band gap energy E_G.

The following equation applies to homogeneous p–n junctions at ambient temperature:

$$Diffusion\ \text{voltage}\ \ \mathrm{V_D} \approx E_G/e - (0.35 - 0.5)V \tag{2.1}$$

Hence the diffusion voltage is roughly 0.35–0.5 V lower than the so-called theoretical photovoltage V_{Ph} (see equation 2.2), which is determined by dividing the band gap energy E_G by the electron charge (e = 1.602 x 10^{-19} Coulomb).

$$V_{ph} = \frac{E_G}{e} \tag{2.2}$$

If a metal contact is integrated into the n-zone and p-zone, a semiconductor diode results. If such a diode is briefly short-circuited, despite the diffusion voltage at the p–n junction the flow of current is still blocked. In such a case, space and contact charges are immediately created at the contact points between the metal and semiconductor, and this exactly compensates for the diffusion voltage [7].

2.3.5. Semiconductor types

The basic element of a photovoltaic system (PV) is solar cells which convert the sunlight energy directly to direct current. A typical solar cell consists of a PN junction formed in a semi-conductor material similar to a diode. Semi-conductor material most widely used in solar cells is silicon. Each material gives different efficiency and has different cost. There are several types of solar material cells [62]:

2.3.5.1. monocrystalline silicon (c-Si)

It is the widely available cell material. Its efficiency is limited due to several factors. The highest efficiency of silicon solar cell is around 23%, by some other semi-conductor materials up to 30%, which is dependent on wavelength and semiconductor material.

2.3.5.2. polycrystalline cells

It is also called polysilicon. In this case, the molten silicon is cast into ingots. Then it forms multiple crystals. These cells have slightly lower conversion efficiency compared to the single crystal cells. Monocrystalline and polycrystalline silicon modules are highly reliable for outdoor power applications.

2.3.5.3. Thin films

Thin-film solar cell (TFSC), also called a thin-film photovoltaic cell (TFPV), is a solar cell made by thin film materials. Thin film solar cells usually used are [63, 64]:

- Amorphous silicon (a-Si) and other thin-film silicon (TF-Si). The efficiency of amorphous solar cells is typically between 10 and 14%. Their lifetime is shorter than the lifetime of crystalline cells.
- Cadmium Telluride (CdTe) which is a crystalline compound formed from cadmium and tellurium and its efficiency is around 22.1%.
- Copper indium gallium selenide (CIS or CIGS) is composed of copper, indium, gallium and selenium. Its efficiency is around 23.4%.
- Dye-sensitized solar cell (DSC) belongs to emerging PV technology, it is formed by a photo-sensitized anode and an electrolyte. Its efficiency is around 11.9%.
- Thin-film cells cost less than crystalline cells.

2.3.5.4. Other new technologies

There are other new technologies used in solar cells fabrication such as:

- Organic solar cells (OSC) are made of thin layers of organic materials. Three different types of organic solar cells are known: the organic semiconducting material can either be comprised of so-called small molecules (SM solar cells)

or polymers (polymer solar cells). The third type of organic solar cells is called dye-sensitized solar cell (or Grätzel cell) [65].

- Tandem or stacked cells: in this case, different semi-conductor materials, which are suited for different spectral ranges, will be arranged one on top of the other.
- Concentrator cells use mirror and lens devices. This system uses only direct radiation and needs an additional mechanism for tracking the sun. Its efficiency is around 47.1% of direct radiation [63].
- Metal-Insulator-Semiconductor (MIS) Inversion Layer cells: the inner electrical field is produced by the junction of a thin oxide layer to a semiconductor.

2.3.6. Photovoltaic cells and Photovoltaic modules models

2.3.6.1. Equivalent circuit of a Solar cell

A non-irradiated solar cell is a standard semiconductor diode that allows forward current to flow from the p-side to the n-side if the voltage is directed from p to n via the diode. When the diode is exposed to light, photocurrent I_{Ph} is also generated that is proportional to irradiance G and flows from the n-side to the p-side. This arrangement can be readily represented using an equivalent circuit from an ideal current source I_{Ph} and a diode, if necessary with an added series resistance R_S and parallel resistance R_P (see figure 2.7).

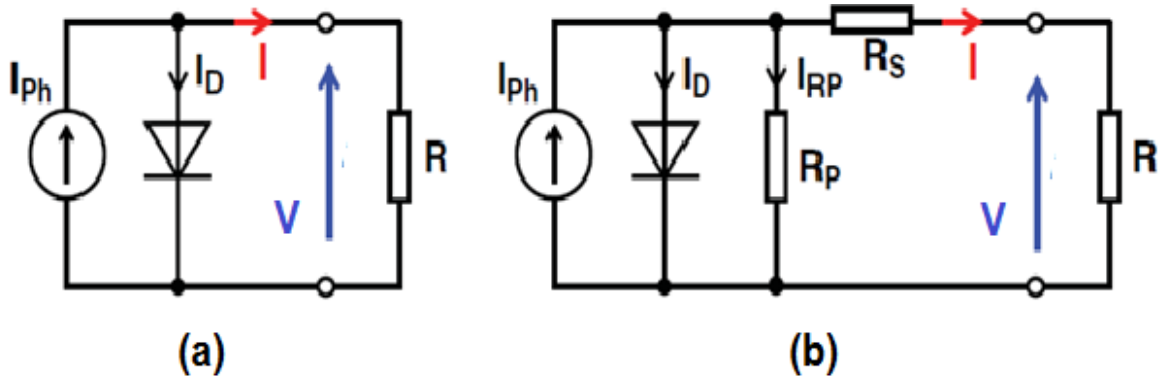

Figure 2.7: Simplified diagram of an equivalent circuit for a loaded solar cell (no-load, $R=\infty$; shorted, R=0). I_{Ph} is proportional to irradiance G and solar cell area A_Z

Under open-circuit conditions, an equalization current flows continuously in the solar cell's equivalent circuit, and thus the following occurs: the photocurrent I_{Ph} from the n-side to the p-side resumes flowing (under the influence of the open-circuit voltage V_{OC} thus engendered) through the diode from the p-side to n-side as current I_D.
The following equation applies to the output current I in the simplified equivalent circuit (without R_S or R_P) as a function of voltage V:

$$I = I_{Ph} - I_D = I_{Ph} - I_S\left(e^{eV/nkT} - 1\right) = I_{Ph} - I_S\left(e^{V/V_T} - 1\right) \quad (2.3)$$

Where:
I_{Ph}: photocurrent (~G) = solar cell short-circuit current I_{SC} (in the simplified circuit)
I_S: saturation current in the reverse direction, which increases roughly exponentially as temperature rises (doubles at approximately 10 K intervals)
V: voltage applied at the diode (from p to n)
I_D: current conducted by the diode (I_D in the solar cell equivalent circuit shown in Figure 2.7).
e: elementary charge = 1.602 x 10^{-19} coulomb.
n: diode quality factor (1<n<2; this factor is close to 1 in most cases).
k: Boltzmann's constant=1.38 x 10^{-23} J/^{o}K
T: absolute temperature (in ^{o}K)
The following abbreviation is also useful:

$$\text{Thermal (diode) voltage} \quad V_T = nkT/e \quad (2.4)$$

The interrelationships are somewhat more complex for the complete equivalent circuit with R_S and R_P. Although I_{SC} is still approximately I_{Ph} and thus approximately proportional to G, I and V cannot be represented by a closed expression and thus an iteration is necessary. To calculate I as a function of V, a value such as V_i (a value near any desired V) at the inner diode is applied, and then the resulting current I is computed as follows:

$$I = I_{Ph} - I_S\left(e^{eV_i/nkT} - 1\right) - \frac{V_i}{R_P} \quad (2.5)$$

The effective output voltage at the solar cell terminals is then determined as follows:

$$V = V_i - R_S.I \tag{2.6}$$

this term can then be used in equation 2.5:

$$I = I_{Ph} - I_S\left(e^{e(V+R_s\cdot I)/nkT} - 1\right) - \frac{V + R_s \cdot I}{R_P} \tag{2.7}$$

In addition to the single-diode model discussed above, the two-diode model is also used. In this model, in lieu of only one diode where two separate diodes where $n_1 = 1$ and $n_2 = 2$, respectively are used. However, this method is more labour intensive on account of the additional parameter. The two-diode model is mainly suitable for highly precise simulations of solar cell characteristics using calculation software. A full basic understanding of the behaviour of solar cells and modules can be achieved via the single-diode model discussed above.

2.3.6.2. Characteristic curves of Solar cells

If a solar cell uses the same metering direction for both voltage and current like with standard diodes (load metering system), the characteristic curves shown in figure 2.8 for illuminated and non-illuminated solar cells are obtained; this constitutes the idealized case using diodes with good reverse properties. The characteristic curve of an irradiated solar cell exhibits the same form as that of a non-irradiated cell and is simply shifted by I_{SC} in the negative current direction by virtue of the fact that photocurrent and diode current flow in opposite directions (in comparing figures 2.6 and 2.7, note that I' = -I). The solar cell consumes power in quadrants 1 and 3, but it generates power when the cell is operated in quadrant 4. No problems arise when solar cells are wired to solar modules, so long as measures are taken to ensure that: (a) the load on a shaded solar cell in the forward direction does not exceed more than about I_{SC} (which the cell can tolerate without problems under open-circuit conditions); and (b) in the reverse direction it is not subjected to unduly high voltages, so as to avoid unduly high cell power loss. Unduly high stress can overheat solar cells and thus ruin an entire solar module [7].

For solar cells, the characteristic curves of power quadrant 4 are of overriding importance as this is where they generate power. Hence in most cases only this characteristic curve is indicated, whereby the metering directions for V and I shown in

figure 2.6 are used (generator metering system) so as to ensure that V and I are positive.

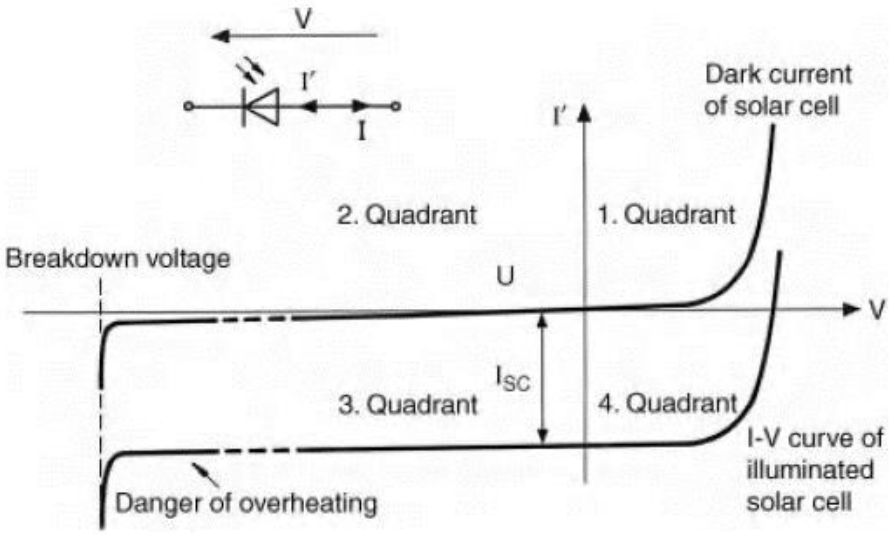

Figure 2.8: Idealized characteristic curve of a solar cell.

Figure 2.9 shows a characteristic curve I = f(V) for a solar cell. When used with low voltages, a solar cell is a virtually ideal source of current. But once voltages approaching open-circuit voltage V_{OC} are reached, the current drops off fairly sharply (the diode in the equivalent circuit as in Figure 2.6 begins to conduct current).

In addition to current, power is also a key parameter since solar cells are used to produce electrical energy. Power is determined by multiplying current by voltage. Determining the power for each point along the characteristic curve I=f(V) results in the curve P=f(V), which is likewise shown in figure 2.9. When a solar cell is in an open-circuit or short-circuit state, it produces no power. At a defined point known as the maximum power point (MPP), a solar cell reaches its maximum power and thus the value $P_{max} = P_{MPP}$. So V_{MPP} is calculated using the following equation:

$$V_{MPP} = V_{OC} - \frac{nkT}{e}\ln\left(1+\frac{eV_{MPP}}{nkT}\right) = V_{OC} - V_T \ln\left(1+\frac{V_{MPP}}{V_T}\right) \tag{2.8}$$

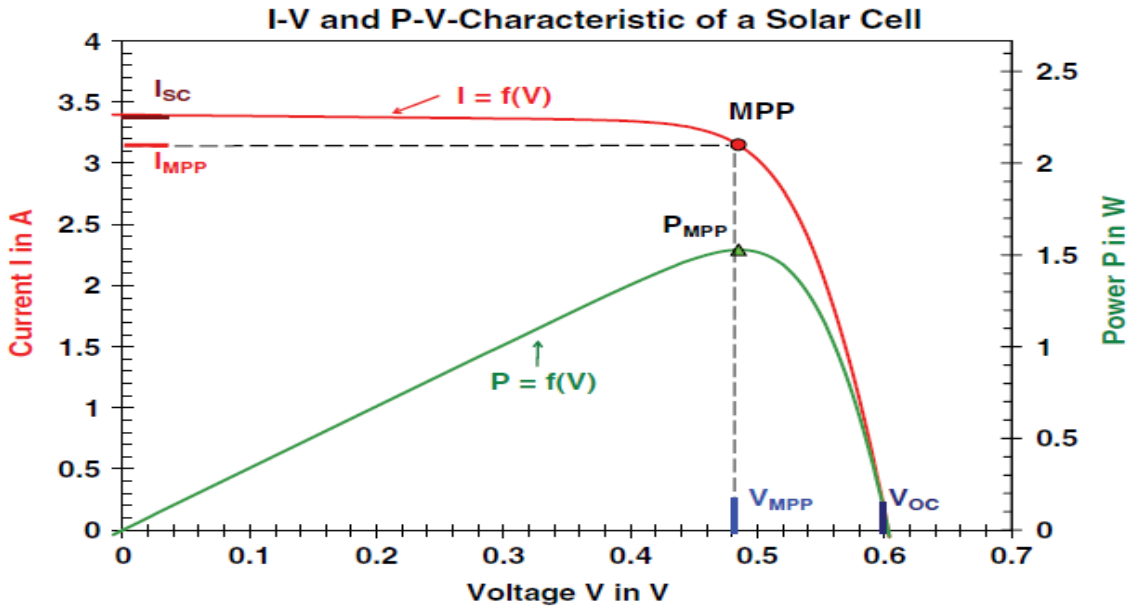

Figure 2.9: Characteristic curves I = f(V) and P = f(V) of a monocrystalline silicon solar cell.

In the interest of using solar cell power optimally, a connected consumer should be installed in such a way that it operates in as close proximity as possible to the MPP. since the MPP site is determined by irradiance, temperature, manufacturing tolerance and ageing. A device that ensures that a consumer is always operating at the MPP is known as a maximum power point tracker (MPPT) or maximum power tracker (MPT). The maximum power, $P_{max} = P_{MPP} = V_{MPP} * I_{MPP}$, that a solar cell can produce at the MPP is always lower than the value obtained by multiplying open-circuit voltage V_{OC} by short-circuit voltage I_{SC}. The ratio of P_{max} to $V_{oc} * I_{sc}$ is a key solar cell measurement value, along with efficiency. This ratio is known as the fill factor:

$$\text{Fill factor } FF = \frac{P_{max}}{V_{OC} \cdot I_{SC}} \tag{2.9}$$

The fill factor for commercially available solar cells ranges from around 60 to 80%, while this factor for lab cells can go as high as about 85% [7].

2.3.6.2.1. Irradiance Effect

Figure 2.10 shows the current–voltage characteristics I_{pv}-V_{pv} and MPP of the PV cell for different levels of radiation. We note that the current I_{sc} increases quasi linearly with irradiance and that the voltage V_{oc} increases slightly. Then, the maximum electric power P_{MPP} increases faster than the irradiance, i.e the efficiency is better for high irradiance. The reference conditions are generally chosen with an irradiance of 1000 W/m^2. In practice, the irradiance on PV without light concentration is lower, and thus the efficiency is lower than its rated value.

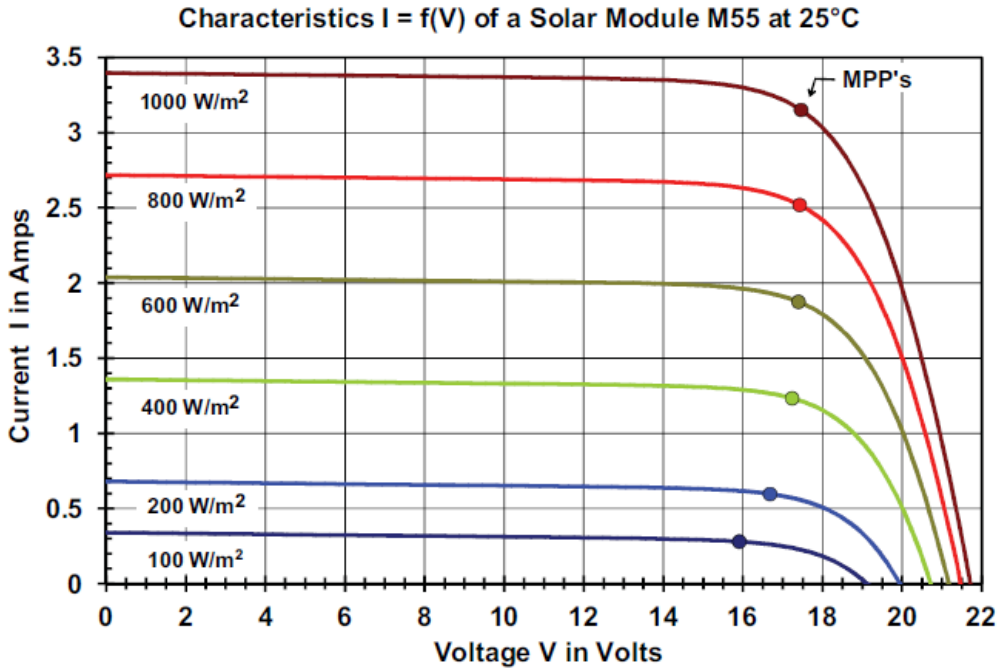

Figure 2.10: Characteristic I= f(V) curves for the M55 monocrystalline solar module, at various insolation levels and a cell temperature of 25 °C [7].

2.3.6.2.2. Temperature Effect

When the internal temperature T_j increases, the short circuit current I_{sc} increases slightly due to better absorption of light (as an effect of the gap energy decrease with temperature) but the open-circuit voltage strongly decreases with temperature. The maximum electric power also strongly decreases with temperature, see figure 2.11. The standard conditions are generally chosen for a value of internal temperature T_j equal to 25 °C. Under sunshine, the internal temperature is often higher and thus the efficiency lower. The short-circuit current I_{sc} can be calculated at a given temperature T_j, for small temperature variation by:

$$\Delta T = T_j - T_{jref} \tag{2.10}$$

$$I_{sc} = I_{sc-T_{jref}} \left(1 + \alpha_{sc} \cdot \Delta T\right) \tag{2.11}$$

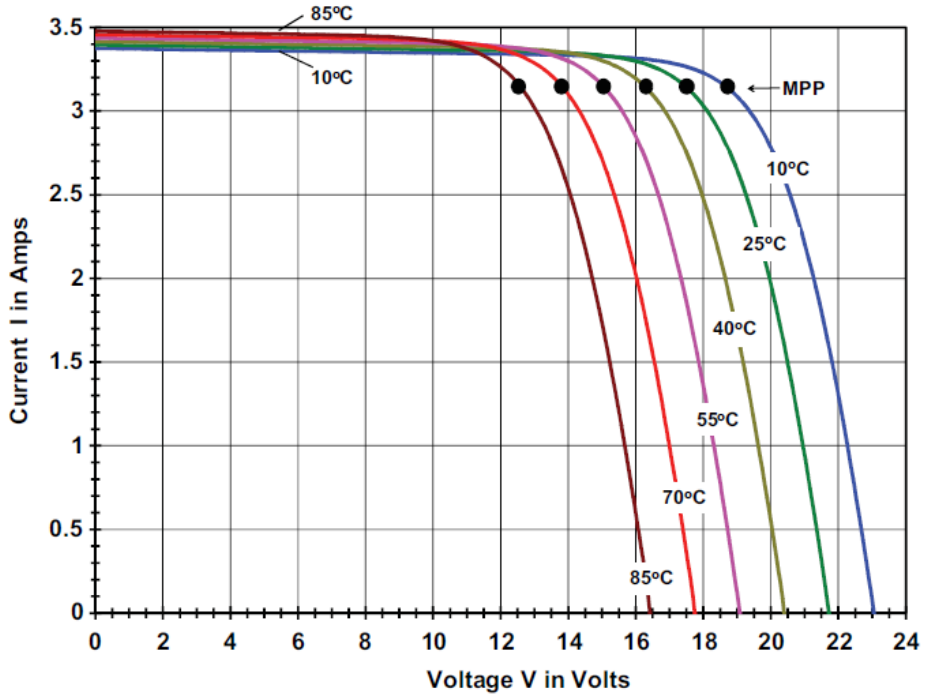

Figure 2.11: Characteristic I=f(V) curves for the M55 monocrystalline solar module, at various cell temperatures and 1 kW/m^2 insolation.

Where α_{sc} is the relative temperature coefficient of short-circuit current (/ºK) as found from the data sheet, T_{jref} is the reference temperature of the PV cell (ºK), $I_{sc\text{-}Tjref}$ is the short-circuit current at the reference temperature.

Similarly, the open-circuit voltage, for small temperature variations can be also expressed as:

$$V_{OC} = V_{OC-T_{jref}} \left(1 + \beta_{OC} \cdot \Delta T\right) \tag{2.12}$$

Where $V_{oc\text{-}Tjref}$ is the open-circuit voltage at the reference temperature and β_{oc} is the relative temperature coefficient of that voltage (/ºK) as found from the data sheet.

Often, datasheet also gives the temperature coefficient of P_{MPP}:

$$P_{MPP} = P_{MPP-T_{jref}} \left(1 + \gamma_{MPP} \cdot \Delta T\right) \tag{2.13}$$

Where $P_{MPP\text{-}Tjref}$ is the maximum power at the reference temperature, γ_{MPP} is the

relative maximum power temperature coefficient (/^{o}K) as found from the data sheet.

2.3.6.2.3. Spectral Effect

White light can be considered as a sum of radiations with different wave length (colors). The efficiency of PV generators is not the same for each wave length. For that reason, the standard conditions used for cells and modules rating include a constraint on the light spectrum. The standard spectrum commonly used is that one named AM 1.5. As a consequence, the PV cells and modules are sometimes optimized for that standard spectrum. In real condition, the light spectrum can be different, and that has also an effect on the PV efficiency.

The others models of the PV module will be discussed in section 2.5.1

2.4. Types of solar PV systems

PV systems are broadly classified into three distinct types:

- Grid-connected systems.
- Stand-alone systems.
- Solar PV hybrid system.

2.4.1. Grid-connected systems

Grid-connected PV systems have become increasingly popular for applications in the built environment. As illustrated in figure 2.12, they are connected to the grid via inverters, which convert the DC power into AC electricity. In small systems such as those installed in residential homes, the inverter is connected to the distribution board, from where the PV generated power is transferred into the electricity grid or to AC appliances in the house. In principle, these systems do not require batteries, since they are connected to the grid, which acts as a buffer into which an oversupply of PV electricity is transported. The grid also supplies the house with electricity in times of insufficient PV power generation. However, more and more grid-connected systems also contain batteries in order to increase self-consumption, i.e. the amount of PV-generated electricity that is consumed by the household [66]. Large PV fields act as power stations from which all the PV-generated electricity is directly transported to the electricity grid. They can reach peak powers of up to several hundreds of MW_p.

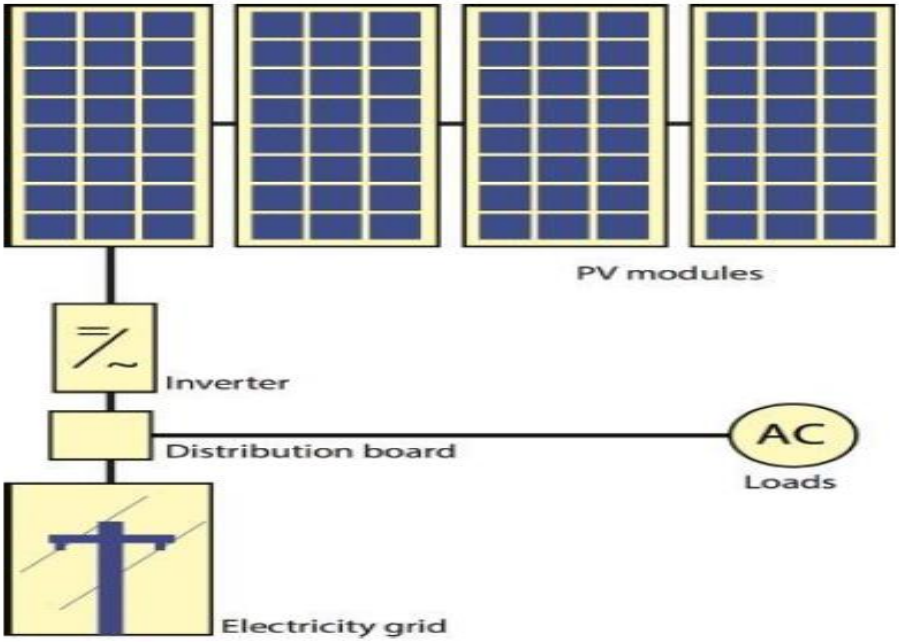

Figure 2.12: Schematic representation of a grid-connected PV system [54].

One of the important components of a grid-connected system is net metering with standard service meters like odometer-type and digital electric meters that make use of digital electronic technology.

Inverters are the main difference between a grid-connected system and a standalone system. Inverters must have line frequency synchronization capability to deliver the excess of power to the grid. Net meters have a capability to record consumed or generated power in an exclusive summation format. The recorded power registration is the net amount of power consumed minus the total power used minus the amount of power that is produced by the solar power cogeneration system. Net meters are supplied and installed by utility companies that provide grid-connection service systems. Net metered solar PV power plants are subject to specific contractual agreements and are subsidized by state and governmental agencies [67].

2.4.2. Stand-alone systems

A stand-alone system is an electricity installation that supplies one or more appliances with energy completely independently of a power grid. The possible output of such a system ranges from milliwatts to watts for power supplies for portable devices

(e.g. watches, calculators, small radio devices and so on) to tens of kilowatts (for transport infrastructure facilities, large buildings, radio transmitters and so on). Appliances that depend on a steady supply of electricity need an accumulator, usually a battery bank [7].

The solar PV array configuration, a DC load with battery backup, is essentially the same as the one without the battery except that there are a few additional components that are required to provide battery charge stability. PV panels are connected in series to obtain the desired increase in DC voltage, such as 12, 24, or 48 V. The charge controller regulates the current output and prevents the voltage level from exceeding the maximum value for charging the batteries. The output of the charge controller is connected to the battery bank [67]. Damage to the battery is prevented by means of a special deep-discharge protection in which the load is uncoupled in case the voltage falls below a critical level. DC loads, for instance, are energy saving lamps, radios or also water pumps. If, besides the direct current loads there are also AC loads then a special additional stand-alone inverter must be provided [8]. Figure 2.13 displays Schematic representation of a PV system including batteries, power conditioners, and both DC and AC loads

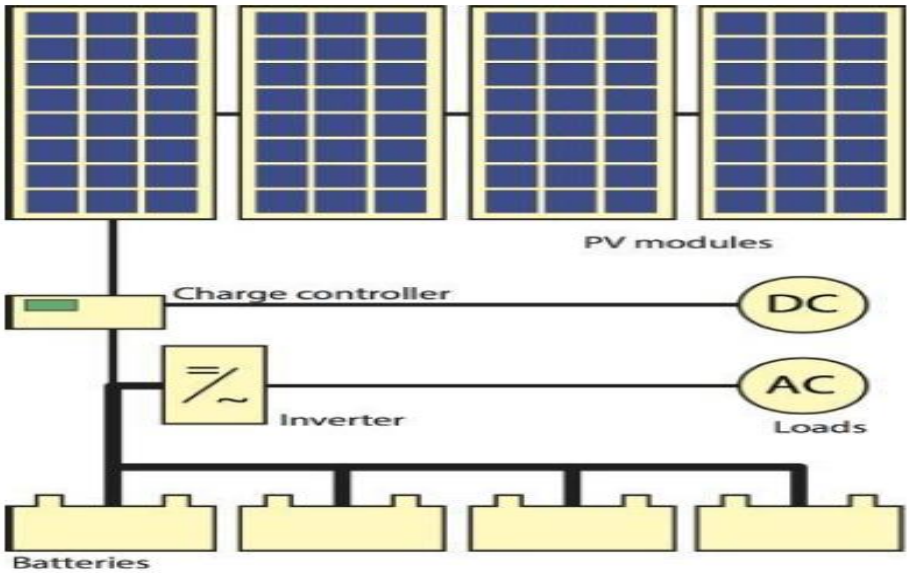

Figure 2.13: Schematic representation of a PV system including batteries, power conditioners, and both DC and AC loads [54].

2.4.3. Solar PV hybrid system

Hybrid systems generally refers to the combination of any two input sources. Solar PV can be integrated with diesel generator, Wind Turbines, Biomass or any other renewable or non-renewable energy sources. Solar PV systems will generally use battery bank to store energy output from the panels to accommodate a pre-defined period of insufficient sunshine, there may still be exceptional periods of poor weather when an alternative source is required to guarantee power production. PV hybrid systems combine a PV module with another power sources typically a diesel generator, but occasionally another renewable supply such as a wind turbine. The PV generator would usually be sized to meet the base load demand, with the alternate supply being called into action only when essential. This arrangement offers all the benefits of PV in respect of low operation and maintenance costs, but additionally ensures a secure supply. Hybrid systems can also be sensible approach in situations where occasional demand peaks are significantly higher than the base load demand. It makes little sense to size a system to be able to meet demand entirely with PV if, for example, the normal load is only 10 % of the peak demand. By the same token, a diesel generator set sized to meet the peak demand would be operating at inefficient part-load for most of the time. In such a situation a PV-diesel hybrid would be a good compromise [67]. Figure 2.14 shows the block diagram of Solar PV hybrid system that has a diesel generator as an alternative electricity source.

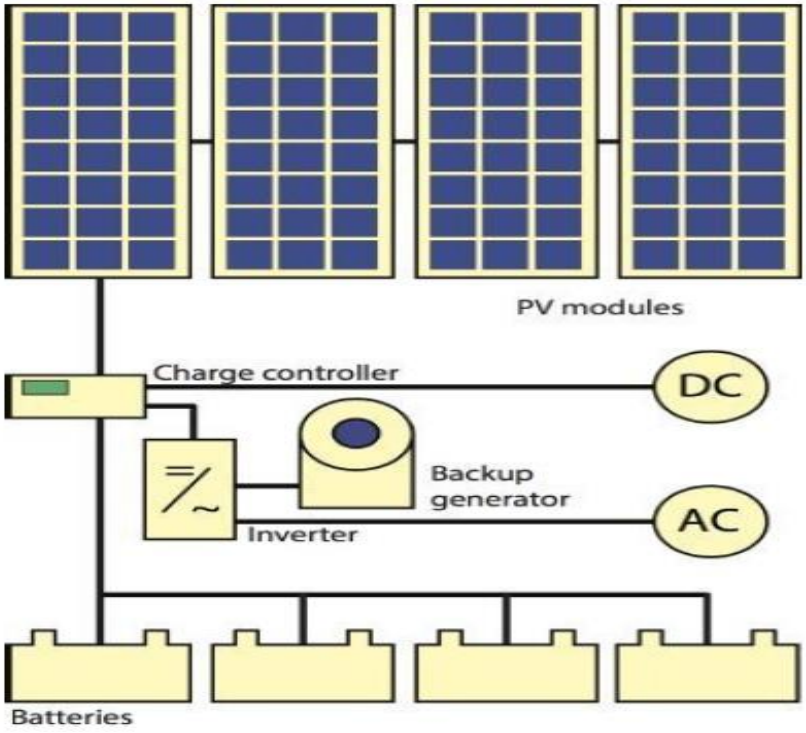

Figure 2.14: Schematic representation of a hybrid PV system that has a diesel generator as an alternative electricity source.

Our work addresses hybrid PV–diesel systems consisting of a PV subsystem, a diesel generator and a battery bank.

2.5. Stand-alone hybrid PV-diesel-battery system

A PV-Diesel system has greater reliability for electricity production than a PV-only system. This fact provides greater flexibility, higher efficiency and lower costs for the same energy quantity produced [68]. Also, PV-Diesel systems, compared with Diesel-only systems, provide a reduction of the operation costs and air pollutants emitted to the atmosphere [69]. For this reason, hybrid PV-diesel systems offer interesting opportunities and can be used productively within local minigrids [70] to electrify a rural and remote communities.

2.5.1. System components characteristics and modeling

2.5.1.1. PV module modeling

The ideal model, one diode and two diode models were discussed in section 2.3.6, in this section, we will present the power models.

2.5.1.1.1. Model No. 1

This model can give the same power of solar modules operating at MPP (Maximum Power Point). It is intended to polycrystalline silicon technology. The maximum power P_{pvmax} can be given by [71]:

$$P_{pv-\max} = K_1.\left(1+K_2\left(T_j - T_{jref}\right)\right)\cdot\left(K_3 + G\right) \tag{2.14}$$

where K_1, K_2, and K_3 are constants to be determined (data sheets).

2.5.1.1.2. Model No. 2

The following model can determine the maximum power provided by a PV module for given irradiance and temperature with only four constant parameters to determine a, b, c, and d. These parameters are obtained solving a simple equation system for a resulting set of measurement points sufficiently extended [72]. We have

$$P_{pv-\max} = \left(a\cdot G + b\right)\cdot T_j + c\cdot G + d \tag{2.15}$$

where $P_{pv\text{-}max}$ is the maximum power output and where a, b, c, and d are positive constants which can be obtained experimentally.

2.5.1.1.3. Model No. 3

The energy produced by a photovoltaic generator is estimated from the data of the global irradiation on inclined plane, the ambient temperature data manufacturer for the PV module used. The power output of PV array can be calculated from the following equation [73]:

$$P_{pv-\max} = \eta_{pv}\cdot A_{pv}\cdot N_m \cdot G \tag{2.16}$$

Where A_{pv} is the total area of the photovoltaic generator, N_m is the number of PV modules and η_{pv} the efficiency of the photovoltaic generator.

$$\eta_{pv} = \eta_r \cdot \eta_{pc}\cdot\left[1-\alpha_{sc}\left(T_j - T_{jref}\right)\right] \tag{2.17}$$

Where G is a solar radiation on tilted plane module, η_r is the reference efficiency of the photovoltaic generator, η_{pc} is the power conditioning efficiency which is equal to 1 if a perfect maximum power tracker (MPPT) is used, α_{sc} is the temperature coefficient of short-current (/^{o}K) as found on the datasheet, T_j is cell temperature and T_{jref} is the reference cell temperature.

2.5.1.1.4. Model No. 4

Jones and Underwood developed the following practical model in 2002 for the production of optimal output power of a photovoltaic module [72, 74]:

$$P_{pv-\max} = FF \cdot \left(I_{sc} \cdot \frac{G}{G_{ref}} \right) \cdot \left(V_{oc} \cdot \frac{\ln(P_1 \cdot G)}{\ln(P_1 \cdot G_{ref})} \cdot \frac{T_{jref}}{T_j} \right) \quad (2.18)$$

Where P_1 is a constant coefficient, which can be calculated by the following formula:

$$P_1 = \frac{I_{sc}}{G} \quad (2.19)$$

FF is the Filling factor.

2.5.1.2. Battery Bank model

In the market, there are many different types of batteries and most of them are subject to further research and development. In PV systems, several types of batteries can be used: nickel-cadmium (NiCd), Nickel-Zinc (Ni-Zn), Sodium-Sulfur (NaS), lead acid etc. Nevertheless, it must have some important properties as high charge-discharge efficiency, low self-discharge, and long life under cyclic charging and discharging [62]. This work considered only the lead acid batteries.

The lead acid batteries are the most used in PV applications especially in standalone power systems because its spill proof and the ease to transport [75]. However, when we use this battery type in PV systems, we can have excessive overcharges mode and loss of electrolyte. In this case, the charge controller must prevent overcharging. The lead acid battery consists of two electrodes immersed in sulfuric acid electrolyte. The negative one is attached to a grid with sponge metallic lead, and the positive one is attached to a porous grid with granules of metallic lead

dioxide. During discharge, the lead dioxide on the positive electrode is reduced to lead oxide, which reacts with sulfuric acid to form lead sulfate, and the sponge lead on the negative electrode is oxidized to lead ions that react with sulfuric acid to form lead sulfate. In this manner electricity is generated and during charging this reaction is reversed. There are two types of lead acid batteries [75, 76]:

- Flooded type: in the flooded type battery an aqueous sulfuric acid solution is used.
- Valve regulated lead acid batteries (VRLA): these batteries are closed with a pressure regulating valve to deal with the problem of overpressure risk when overcharging, so that they are sealed. In addition, the acid electrolyte is immobilized.

The active materials are:

- In the positive plate: lead dioxide (PbO_2),
- In the negative plate: sponge lead (Pb),
- In water as the electrolyte: a solution of sulfuric acid (H_2SO_4).

Different mathematical models exist to predict the performance of batteries like: electrochemical battery models, Peukert model, Shepherd model, Unnewehr universal model and equivalent circuit battery models. We will consider only the equivalent circuit battery models.

The factors that affect battery performance are [77, 78]:

- State of charge
- Battery storage capacity
- Rate of charge/discharge
- Environmental temperature
- Age/Shelf life.

2.5.1.2.1. Equivalent Circuit Battery Models

These models are modeling the batteries in the shape of electronic circuits [62]. There are many models proposed by different scientists.

2.5.1.2.1.1. Simple Battery Model

The simple model consists of an ideal voltage source of value E_b (equal to open circuit voltage) and an internal series resistance R_{batt}. Where U_{batt} is the terminal voltage of battery. This model is only suitable for applications where the state of charge is not important [79] (see figure 2.15).

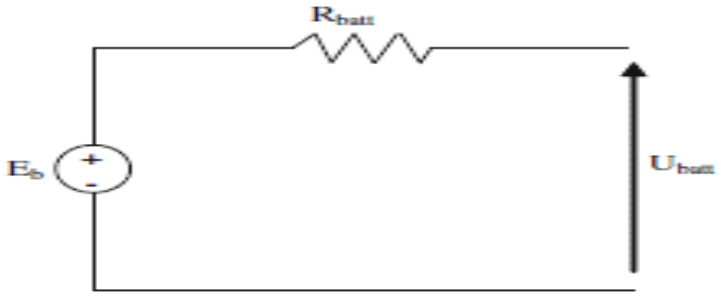

Figure 2.15: Simple battery model.

2.5.1.2.1.2. Improved Simple Model

Improved simple model varies the resistance of the battery. The resistance R_{batt} will be a function of the state of charge (SOC). We can write the resistance R_{batt} as [79]:

$$R_{batt} = \frac{R_0}{SOC^k} \tag{2.20}$$

With

$$SOC = 1 - \frac{I_{batt} \cdot t}{C_{10}} \tag{2.21}$$

Where SOC varies from 0 (for fully discharging) up to 1 (for fully charged), k is the capacity coefficient and takes the change in battery capacity under different discharge rates into account similar to the Peukert factor, R_0 is the initial resistance of the fully charged battery, t is the time of discharging and C_{10} is the 10-h capacity.

2.5.1.2.1.3. Modified Battery Model

Jean Paul Cun proposed an improved model based on the battery configuration given in figure 2.15. In this model the battery's state of charge is taken into account.

He considers that the voltage E_b and the resistance of the battery R_{batt} are no longer constant but vary in accordance with its state of charge [80]. We have:

$$E_b = E_0 - k_{E_b} \cdot SOC \tag{2.22}$$

$$R_{batt} = R_0 - k_R \cdot SOC \tag{2.23}$$

Where k_{Eb} and k_R are coefficients that can be calculated experimentally.

2.5.1.2.1.4. Thevenin Battery Model

Thevenin battery model is a basic model, and consists of an ideal no-load voltage (E_0), an internal resistance (R_{batt}), a capacitance C_0 and an overvoltage resistance R_{NL} [81] (figure 2.16). C_0 is the capacitance of the parallel plates and R_{NL} is the nonlinear resistance contributed by the contact resistance of plate to electrolyte. The disadvantage of this model is that all the parameters are assumed to be constant but in reality these parameters change with temperature and battery conditions.
A new approach to evaluate batteries is a modified Thevenin model .The electrical equivalent of the proposed model is shown in figure 2.17, where E-battery is a simple DC voltage source designating the voltage in the battery cells, E-polarization represents the polarization effects due to the availability of active materials in the battery, E-temperature represents the effect of temperature on the battery terminal voltage and R_{batt} is the battery internal impedance, the value of which depends primarily on the relation between cell voltage and state of charge (SOC) of the battery. Voltage–sensor–current is basically a voltage source with a value of 0 V. It is used to record the value of battery current. Thus, this model is comparatively more precise and can be extended for use with NiCd and Li-ion batteries [78]. Only a few modifications need to be carried out in order to vary the parameters, such as state of charge, current density and temperature.

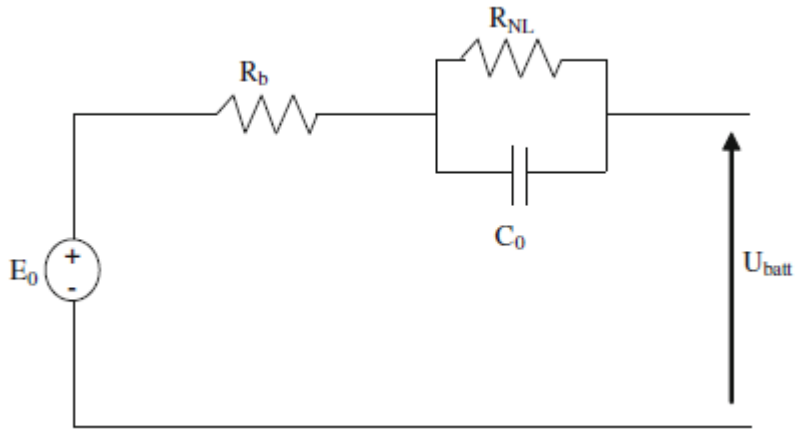

Figure 2.16: Thevenin battery model [81].

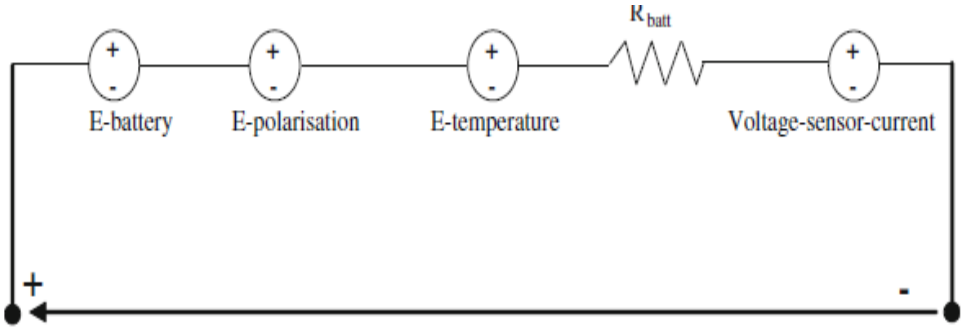

Figure 2.17: Modified Thevenin model [62].

2.5.1.2.1.5. Linear Dynamic Model

An improved variant of the Thevenin model is a linear electrical battery model [82]. It models the behavior of the battery during overvoltage and self-discharge of the battery. This model is more accurate than the Thevenin model but it still does not consider the change of the value of parameters according to different operating conditions (figure 2.18).

2.5.1.2.1.6. Nonlinear Dynamic Model

The nonlinear dynamic model takes into account the variation of different parameters with state of charge of the battery, temperature and discharge rate (figure 2.19). The circuit is composed of two sections:

- The battery open-circuit voltage which is represented by a controlled dc voltage source and its magnitude is changed by state of charge and temperature,

- Internal resistance which is modeled by R_c and R_d representing charging and discharging resistances, respectively. The value of these resistances is changed by the state of charge and temperature as well.

The model is nonlinear in the sense that the elements V_{oc}, R_d and R_c are not constants but are modeled as a function of state of charge and temperature. Only C_1 has been considered constant although it is changing with state of charge but its change is not significant [83, 84].

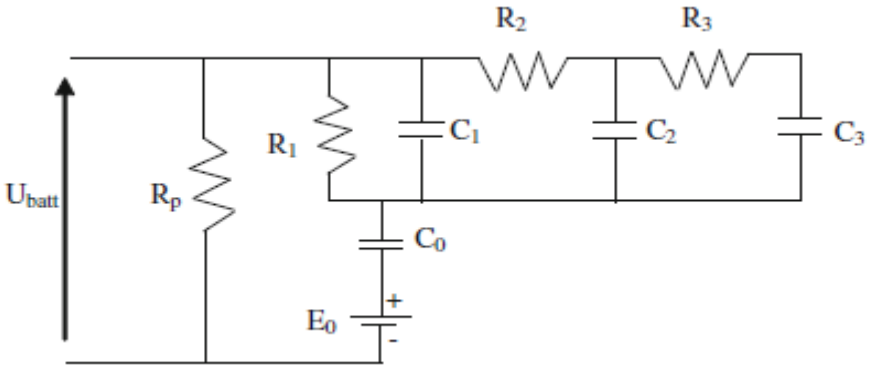

Figure 2.18: Linear dynamic model [81].

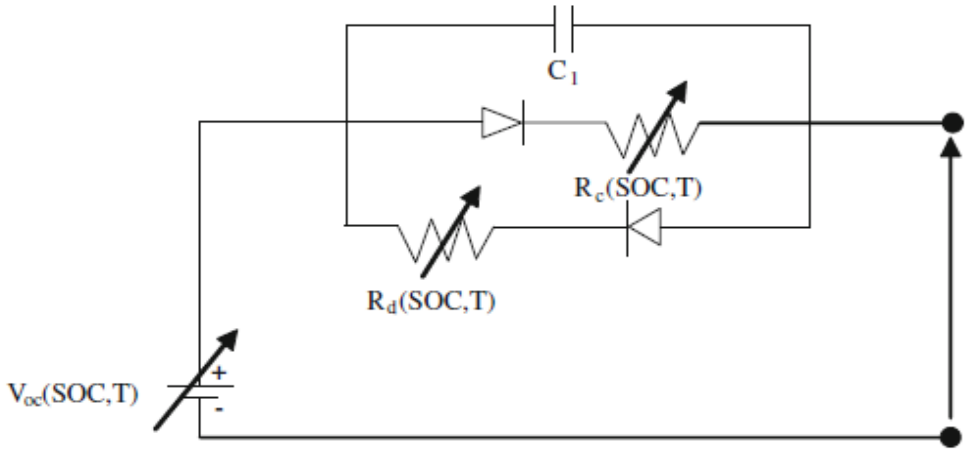

Figure 2.19: Battery nonlinear model [81].

2.5.1.3. Power converters

Power converters are a very important component in PV Hybrid Systems, especially in view of evolution not just only in their quality and performance in recent years but rather for having arisen new challenges along with new opportunities. So, in

those types of systems the following power converters often are used as: battery charging systems and PV inverters.

2.5.1.3.1. Battery charging systems

They are based on the charge controller. Battery charge controllers regulate the flow of electricity from the photovoltaic generator to the battery. Its function is to regulate the voltage and current from the photovoltaic arrays to the battery in order to prevent overcharging and over discharging.

There are four general types of charge controllers, categorized by the method used to regulate the charge from the solar modules to the batteries [85, 86]: shunt type charge controllers, series type charge controllers, PWM (pulse width modulation) charge controllers and MPPT charge controllers.

2.5.1.3.1.1. The shunt charge controller

The shunt charge controller is the first type of chargers developed and are the simplest ones still on the market today. They short-circuit the energy from the solar panel when the battery reaches the full charge. In general, shunt type charge controllers are low cost and reliable, with simple design and suitable for small off grid photovoltaic systems [87].

2.5.1.3.1.2. Series type charge controllers

This type is very similar to shunt type charge controller, instead of short-circuiting the solar panel output they open the circuit, interrupting the path to the batteries. For disconnecting the circuit, this type of controllers uses a relay or a solid-state switch. After the batteries reach a set voltage value, the solar module is disconnected from the batteries. When the battery state of charge goes down, the switch is reset and the panel is once again connected to the batteries [87].

2.5.1.3.1.3. Pulse width modulation charge controllers

It simulates a variable charging current, given by variable power output of the solar panel or by the battery state of charge, switching a series element at a high frequency for variable periods [87].

2.5.1.3.1.4. The MPPT controllers

They are DC–DC converters, as a matching interface between the PV generator and the battery. The main function of a MPPT controller is to adjust the PV generator output in order to transfer maximum energy to the batteries [88, 89]. This offers a high efficiency over a wide range of operating points. About their electrical specifications four important parameters must be taking into consideration: the nominal battery voltage, the MPPT inputs, the input voltage and the shade-tolerant Maximum Power Point Tracking. Regarding to the nominal battery voltage, two ranges are found: the first one with 12, 24 o 48 VDC (low voltage) and another one with 120, 240 and 480 VDC (high voltage). And the input voltage is related to maximum open circuit voltage of the PV array admissible to be connected to the equipment. The benefit of using a high voltage charge controller is the ability to have one long series string of solar panels wired together, or fewer strings in a system. This reduces the number of cables, reduces wire size and voltage drop issues, and reduces the number of breakers in the system for easier wiring and faster installation.

And, another important parameter is the ability or not for obtaining the MPPT under solutions shaded of the PV arrays. However, this topic is focused practically to domestic applications [90, 91].

Nowadays, charge controllers provide several communication options. They can use a proprietary protocol and/or non-proprietary open standard such as MOD-BUS™ and MODBUS TCP/IP™ protocols for RS-232, EIA-485, and Ethernet networks [87].

2.5.1.3.2. PV inverters implemented in PV Hybrid systems

They can be divided into two categories: stand-alone and grid-connected inverters. Stand-alone inverters are further subdivided into stand-alone inverter, grid-Interactive inverter, bidirectional inverter and multiport inverter (called hybrid inverter too). We are interested only in stand-alone inverters.

2.5.1.3.2.1. Stand-alone inverter

This converter is designed for remote stand-alone application, or off-grid power system, with battery backup where the inverter draws its DC power from batteries charged by PV array and converts to AC power. On the market today there are three

different types of power inverters: square wave, modified sine wave and pure sine wave inverter. Table 2.1 Summarized the characteristics of the different types of off-grid inverters.

Table 2.1: Characteristics of the different types of off-grid inverters.

Square wave inverters	**Modified sine wave inverter**	**Sine wave inverter**
Simple technology	Better efficiency	Technique similar to inverters used for connecting to grid but with simpler circuits and no protection from or synchronization with grid
Risk of generating odd harmonics	Fewer harmonics than square wave inverters. Precise regulation of voltage	Elevated efficiency
No regulation of outgoing voltage (varies with charge and incoming voltage)	Appropriate for powering many devices (televisions, engines, table saws)	Suitable for practically every type of user

2.5.1.3.2.2. Grid-interactive inverter

This inverter can operate on both grid-tied and stand-alone off-grid operations, according to figure. 2.20. When the utility power is available, the inverter can operate as grid-tie inverter that converts DC power generated by PV generator into AC power to supply the load and feed the excess energy back to utility grid line. When utility power is not available, the inverter can operate as backup power source to supply power from PV panels and battery, see figure 2.21.

In a grid-interactive system, the inverter is a much smarter, more agile device and capable of doing three things as opposed to the one-trick grid-tied inverter [92]: like a grid-tied inverter, a grid-interactive type can convert solar-generated DC power to AC power; it can also function as a battery charger and store energy in a battery system designed for residential and commercial applications and it can convert battery-produced DC during an outage into useable AC power and charge those batteries during the day from the PV generator or a genset. It can even turn a generator on as

needed. Having battery-back up taking care of power needs in the evening means the generator's run time and fuel consumption can be greatly reduced during an outage.

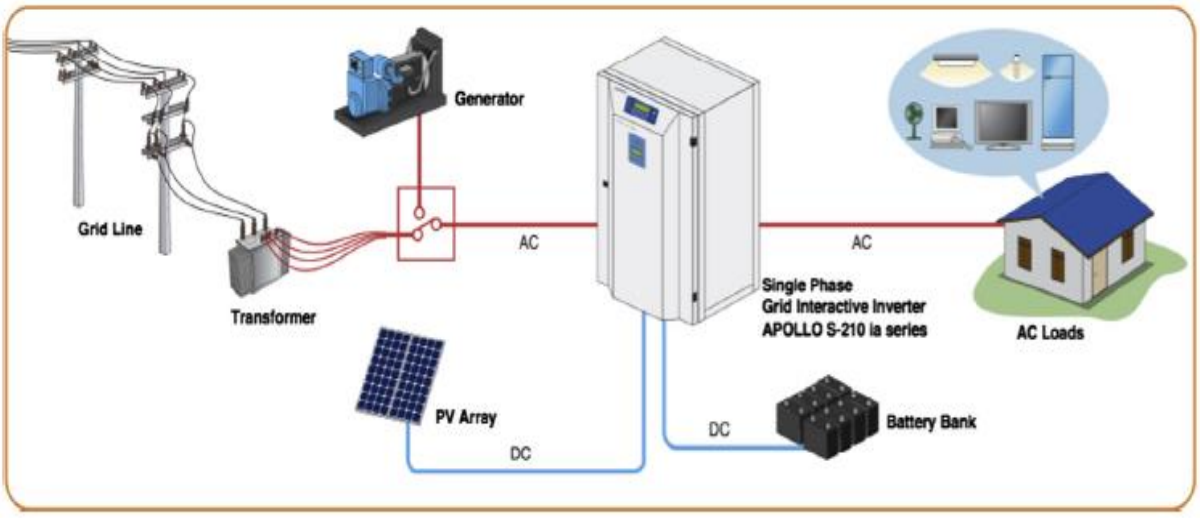

Figure 2.20: PV grid-interactive inverter. Source: Leonics.

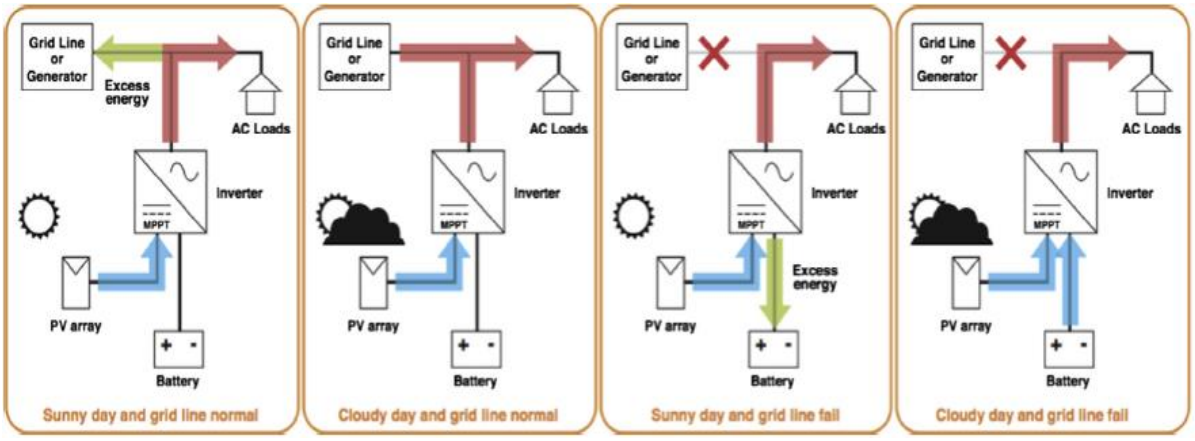

Figure 2.21: Operation of a PV grid-interactive inverter. Source: Leonics.

2.5.1.3.2.3. Bidirectional inverter (BDI)

This inverter has two ports: AC and DC ports. In the DC port is connected a battery bank, so, this type of inverter is called as battery inverter too. In some models have some extra input where can be connected coming from the output of the charge controller. And in the AC side is connected the AC line, where the utility grid or a genset(s) (AC configuration) can be coupled and the AC loads too. Sometimes some equipment can have two independent AC outputs, one of these as an auxiliary output (non-critical load). They have a dual control, therefore the bidirectional inverter operates in two modes: VCVSI (Voltage Control Voltage Source Inverter) mode, as

rectifier, and like CCVSI (Current Control Voltage Source Inverter) mode, operating as off-grid inverter [93]. In addition, it has Intelligent Battery Management for charging and discharging the batteries. The BDI (Bidirectional Inverter) can be integrated in the AC coupled topology [94, 95]. Currently, the BDI (Bidirectional Inverter) is marketed as a single compact enclosure for ranges between 0.8 kW up to 1800 kW. According to table 2.2, it can be seen with the battery voltage, there are two types of BDI: with low voltage (12V, 24V and 48V) and with high voltage (330V, 820V). In addition, it can be distinguished between single-phase (up to 20 kW) or three-phase (up to 1800 kW). Although there are much more models for single-phase (with brands as Leonics, Outback, SMA, Studer, Schneider, Victron and Zigor) than for three-phase (with only three brands: Ingeteam, Leonics and Zigor). The BID permits a modular design of any PV off-grid plant. So, it is possible to design any three-phase system with single-phase units, tabl e 2.3. For example, SMA uses the SMA multicluster technology where the off-grid systems can be extended at any time as the energy demand increases, from 3 to 300 kilowatts (see figure 2.22). Bidirectional inverters can operate as simple converter and also as controller of grid-connected inverters in an AC coupled configuration [96].

The active power of the grid-connected inverter can be controlled without any communication. In addition, a function for voltage dependent power reduction can be implemented to prevent from over voltage caused tripping. There is also a possibility to implement communication between the bidirectional and the grid-connected inverter or to implement load measurement to limit the maximum power that is to be consumed by the BDI. This can be done by using an external controller. Finally, it is also possible to control BDI with a proprietary protocol and/or non-proprietary open standard such as MOD-BUS™ and MODBUS TCP/IP™ protocols for RS-232, EIA-485, and Ethernet networks. Additionally, HTTP, SMTP, and SNMP are often supported for web page, email, and network message support [87].

Table 2.2: Off-grid BDI for different brands. Single-phase and three-phase [87].

Manufacturer	**Model**	**Phase**	**Range of power (kW)**	**Battery voltage (V)**
Ingeteam	Ingecon Hybrid AC Link	3	60–250	330–820
Leonics	Apolo S	1	3–30	48
	Apolo STP	3	15–100	48
	Apolo M	1	5–20	120–240
	Apolo MTP	3	15–2400	120–480
Outback	FX and VFX	1	2–3	12–48
SMA	Sunny Island	1	5–8	48
Studer	Compact and Xtender	1	0.5–7	12–48
Schneider	Conext XW	3	7	48
Victron	Multiplus	1	0.8–5	12–48
Zigor	HIS1	1	1.2–8	24–48
	HTDI	3	150–1800	672

Table 2.3: Three-phase off-grid PV Hybrid system options for a AC coupled configuration [87].

Three-phase system	**String inverter**	**Central inverter**	**Bidirectional single-phase**	**Bidirectional three-phase**
Option 1	X		X	
Option 2	X			X
Option 3		X	X	
Option 4		X		X

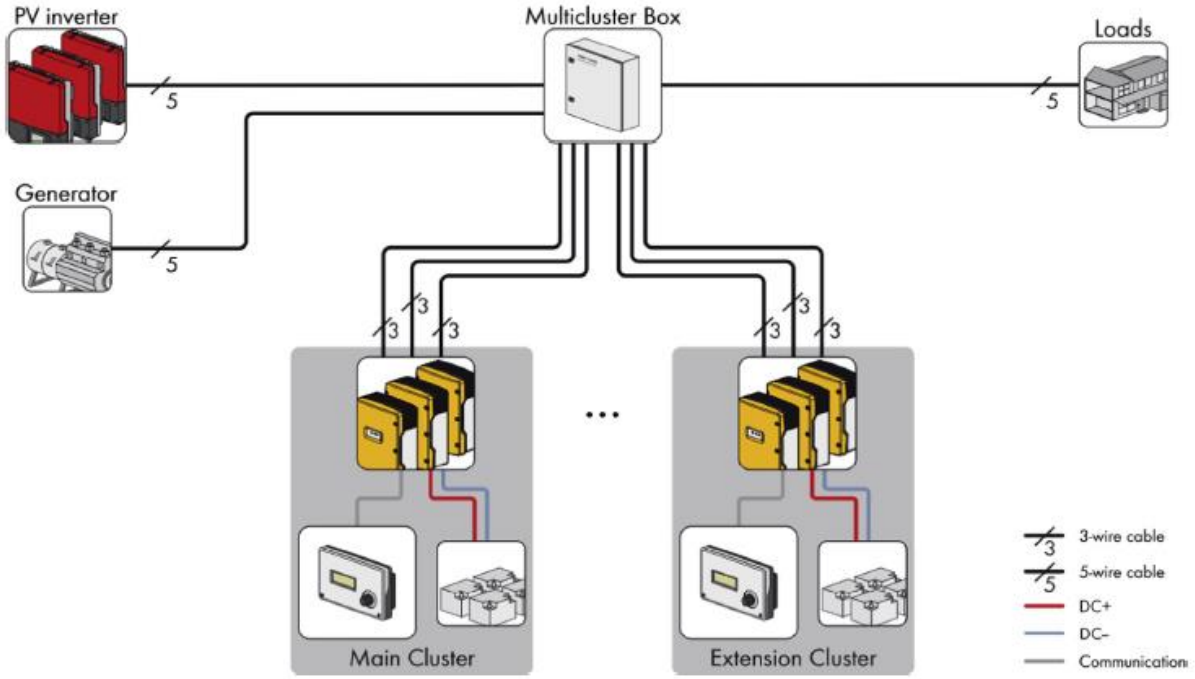

Figure 2.22: Block circuit diagram for a three-phase multi-cluster Off-grid system. Source: SMA.

2.5.1.3.2.4. Multiport input/multi output inverter

In a photovoltaic hybrid system with batteries, the PV and the batteries need a power electronic interface to be connected to the load. One solution is to use a system formed by a hybrid inverter that consist of two inverters, operating in parallel whose outputs are tied to the AC output through a multi-winding step-up transformer [87]. Another possible configuration can be a multi input DC/DC converter with an additional AC/DC inverter stage for feeding the AC loads, or with the power stage according to [97]. However, in both cases, they consist of multiple power processing stages that contribute to lowering the efficiency of the overall system. An alternative to the previous topologies, a single-stage multi-input high frequency topology [98] that simplifies and reduces the cost of those inverters while increasing their reliability and it is able of both stepping up or down the voltage. It is based on the single input/single-output partial resonant AC Link converter [99]. In all topologies shown before, in fact, the final inverter implemented is a multiport inverter with three ports: two for input and one for output, implemented in a single compact enclosure (see figure 2.23). Then, those inverters incorporate a PV input where the PV field can be connected directly to the inverter without using another extra output inverter. The PV input has MPPT

management too. Also, as in the bidirectional inverters, the multiport inverter has implemented a battery management technology that ensures the maximum life of the storage system, by controlling constantly the battery temperature (often using a three-wire PT100 sensor). From the energy point of view, the inverter implemented will have four possible power flow scenarios, depending on the power generated by PV modules, the battery state of charge, and the load requirements: (1) from the PV modules to the load; (2) from the battery to the load; (3) from the PV modules to the load and the battery; (4) from the PV modules and the battery to the load [87].

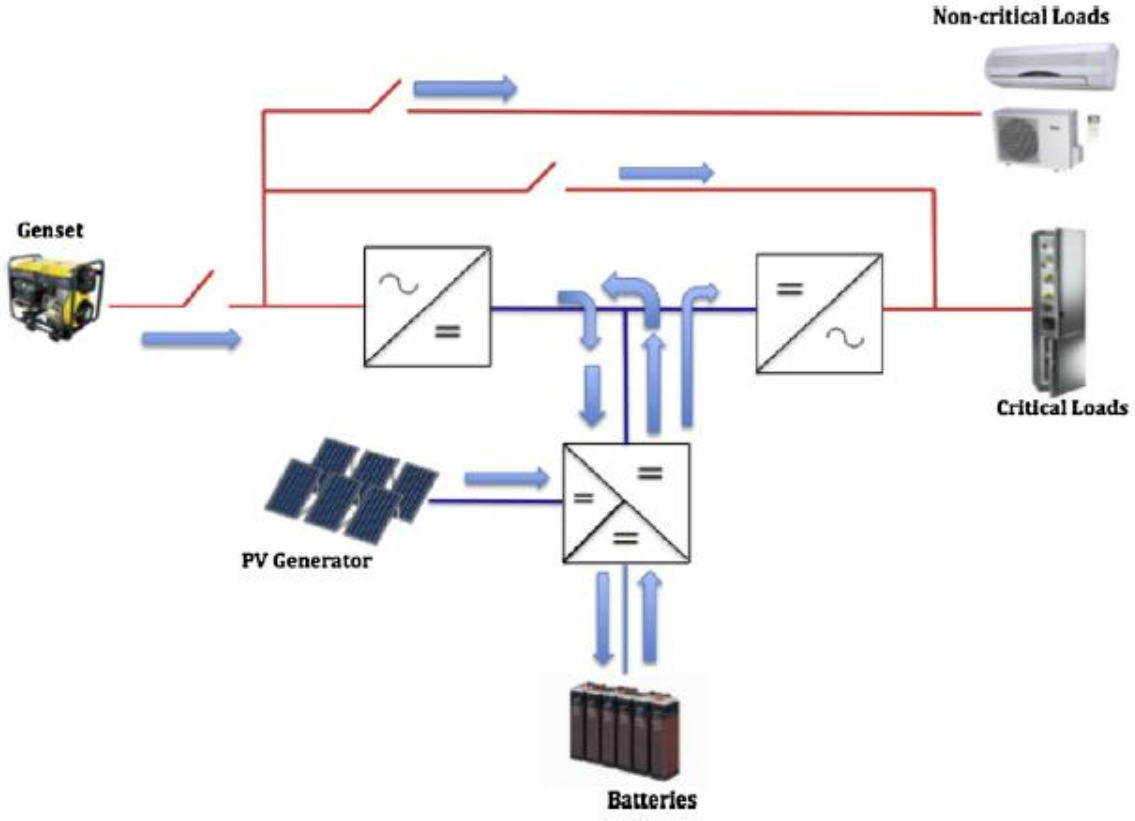

Figure 2.23: The schematic block diagram of the multiport input/multi output inverter.

2.5.1.3.2.5. Inverter Parameters

According to the PV penetration (the fraction of PV power installed with respect to the load profile), the integration of the PV into pre-existing or new diesel systems can be divided into: Low penetration systems (PV penetration < 20%); Medium penetration systems (where the control is needed), the PV penetration is 20 to 65% and High penetration systems with PV penetration between 65% and 100% and where energy storage systems must be installed [100]. The implementation of those configurations according with the penetration chosen can be done: decentralized (by

using string inverters and small bidirectional inverters) or centralized (by using central inverters and large bidirectional inverters) [87].

The parameters that characterize an inverter, usually specified by manufacturers in the data sheet, are summarized below [40].
At input:

- Maximum DC power, which represents the absolute allowable maximum power under any operating conditions.
- Maximum DC voltage, which represents the absolute allowable maximum voltage under any operating conditions. When sizing a PV array, it should be compared to highest voltage that occur at high irradiance (typical G = 1000 W/m^2) and low temperature (e.g. -15 ºC for Eastern Europe).
- Maximum DC current, which represents the absolute maximal current admissible at the input of the inverter. When sizing a PV array, it is assumed to be equal to the short-circuit current at STC.
- Power threshold, i.e., the minimum input power needed to operate. It is admitted to be the internal inverter operating consumption.

In addition to these parameters, another important parameter to be considered is the distortion factor (or total harmonic distortion—THD), describing the quality of the alternative voltage produced. The distortion factor is defined by the ratio of the sum of the actual AC voltage V_i harmonics and the same sum of harmonics plus the actual value V_1 of the fundamental oscillation:

$$DF = \frac{\sqrt{\sum_{i=2}^{\infty} V_i^2}}{V_{tot}} \tag{2.24}$$

Another quality parameter of an inverter is the output power factor Q, which is defined as the ratio of active power and apparent power:

$$Q = \frac{P_{active}}{P_{apparent}} \tag{2.25}$$

For proper operation this ratio should be close to 1.

The most important characteristic of an inverter is the efficiency η. It is defined as the ratio of AC power P_{AC} output to DC power P_{DC} input:

$$\eta = \frac{P_{AC}}{P_{DC}} = 1 - \frac{P_L}{P_{DC}} \tag{2.26}$$

In the above equation, AC output power is substituted with the difference between the DC power input P_{DC} and the power loss P_L. The efficiency is affected at low input power by internal consumption of the inverter and at high power mainly due to resistive losses, P_L includes three independent power losses in the conversion process: (1) Inverter power electronic circuits supply, p_i, (2) The losses of the power semiconductor switching devices, which are linearly dependent on the inverter output power, vp_{ac}, (3) Ohmic losses, increasing with the square of the AC power, rp_{ac}^2. Thus, with good approximation p_l can be represented by a second-order polynomial:

$$p_l = \frac{P_L}{P_N} = p_i + vp_{ac} + rp_{ac}^2 \tag{2.27}$$

In order to obtain dimensionless expressions of the coefficients, all measured powers are divided by the nominal power P_N of the inverter. From Equations 2.27 and 2.28:

$$\eta = \frac{p_{dc} - \left(p_i + vp_{ac} + rp_{ac}^2\right)}{p_{dc}} \tag{2.28}$$

The three loss coefficients p_i, v, and r can be calculated from three values of efficiency η_1, η_2 and η_3 provided by most manufacturers in the data sheet (commonly at p_1 =0,1, p_2 =0,5 and p_3 = 1. The efficiency of inverters can reach very high values, beyond 98 % [101].

2.5.1.3.2.6. Inverter Model

As for the inverter, there are two main functions of the inverter in PV systems. First, in stand-alone PV system the inverter is responsible of converting the DC signal to an AC signal. Thus, the required model here should be in terms of conversion efficiency. However, in grid connected PV systems, inverters are responsible of synchronizing the output signal with the grid in terms of frequency and phase shift [102].

Figure 2.24 shows an efficiency curve for a commercial inverter obtained from the datasheet. The curve describes the inverter's efficiency in terms of input power and inverter rated power. The efficiency curve can be described by a power function as follows [102]:

$$\begin{cases} \eta = c_1\left(\frac{P_{PV}}{P_{INV_R}}\right)^{c_2} + c_3 \quad \text{with } \frac{P_{PV}}{P_{INV_R}} > 0 \\ \eta = 0 \qquad \text{with } \frac{P_{PV}}{P_{INV_R}} = 0 \end{cases} \tag{2.29}$$

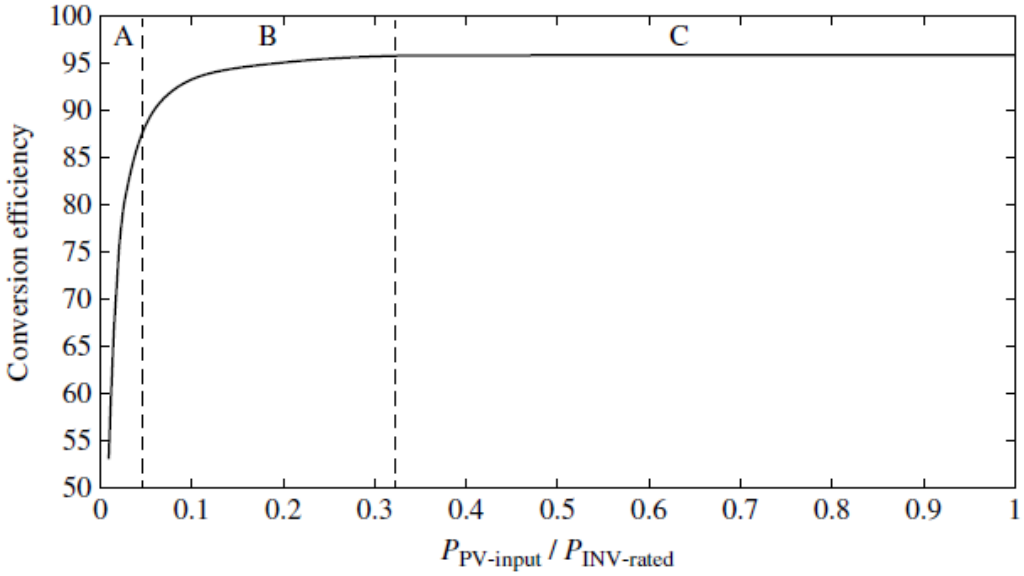

Figure 2.24: Typical efficiency curve for an inverter [102].

Where P_{PV} and P_{INVR} are PV module output power and inverter's rated power, respectively, while c_1, c_2 and c_3 are the model coefficients.

The grid connected inverters models are quite different as they need also to consider signal specifications.

2.5.1.4. Diesel generator

Diesel generators are used as a backup energy source in hybrid power systems. When there is no output power from the PV panel and the battery bank has discharged all the stored energy within its allowable depth, the diesel generator will start working and its power rating should be at least equal to the maximum peak load in the daily

load curve. The fuel consumption of the diesel generator can be calculated by using the following equation [102]:

$$F = F_0 \cdot Y_{gen} + F_1 \cdot P_{gen} \tag{2.30}$$

Where F_0 is the fuel curve intercept coefficient, F_1 is the fuel curve slope, Y_{gen} the rated capacity of the generator (kW), and P_{gen} is the electrical output of the generator (kW). The units of F depend on the measurement units of the fuel. If the fuel is denominated in liters, the unit of F is L/h. If the fuel is denominated in m^3 or kg, the units of F are m^3/h or kg/h, respectively.

2.5.2. Energy flow modeling

The size and performance of PV systems strongly depend on meteorological variables such as solar energy, and ambient temperature, and therefore, to optimize and control PV systems, accurate models must be developed in order to simulate system's performance. PV system models can be divided into two types: energy flow models and current-based models. Energy flow models are used for system sizing, while current-based models are mainly use to demonstrate system control strategies [102].

The hybrid PV/diesel power system is supposed to have the PV array as a main source with a backup battery, while the diesel generator (DG) is operated in deficit time. Here the deficit time is defined as the time in which the instantaneously produced energy form the PV array and battery is not enough to cover the load demand. The implementation of an energy flow model for hybrid PV-diesel system is different from the hybrid PV-wind and stand-alone PV systems. Figure 2.25 shows the flowchart of simulating the PV-diesel system.

The system first supplies the load as there is no diesel generator in the system. Meanwhile the diesel generator will be operated in the time that the energy produced by the PV array and the battery is not enough to cover the load demand. The energy at the front end of the system or at the load side is given by:

$$E_D(t) = \sum_{i=1}^{365} \left(E_{PV}(t) + E_{DG}(t)\right) - E_L(t) \tag{2.31}$$

The following part represents the case that the energy generated by the PV array is more than the load demand and consequently there is no generated energy neither by the diesel generator nor the battery. In addition, there is no energy deficit in this case, while the energy to be damped equals to the difference between the energy generated by PV and the load demand.
The second case is when the energy generated by the PV array and the battery is less than the energy demand. In this case, the diesel generator must cover the load demand that is not covered by the PV array and the battery. In addition to that, the diesel generator is used to charge the battery. At this point, there are four scenarios:

1. The first is that the diesel generator produced the maximum possible energy to supply the load and to charge the battery, while the battery state of charge (SOC) is less than or equal maximum SOC.
2. The second is that the battery SOC reaches the maximum value and the diesel generator at this point must stop charging the battery.
3. In the third, the diesel generator could not cover all the demanded energy by the load, and it is consequently not able to charge the battery.
4. Finally, the case that the battery is able to cover the load demand alone. Here the diesel generator is used to charge the battery as well.

The diesel generator is supposed to keep the battery fully charged to be ready for deficit times. This is because the fact that the use of the energy stored in a battery is easier than operating a diesel generator since the diesel generator needs a start-up time. Moreover, the frequent on/off states of a diesel generator affects its lifetime negatively. However, in this part also the SOC of the battery must be controlled in order not to exceed the allowable SOC.

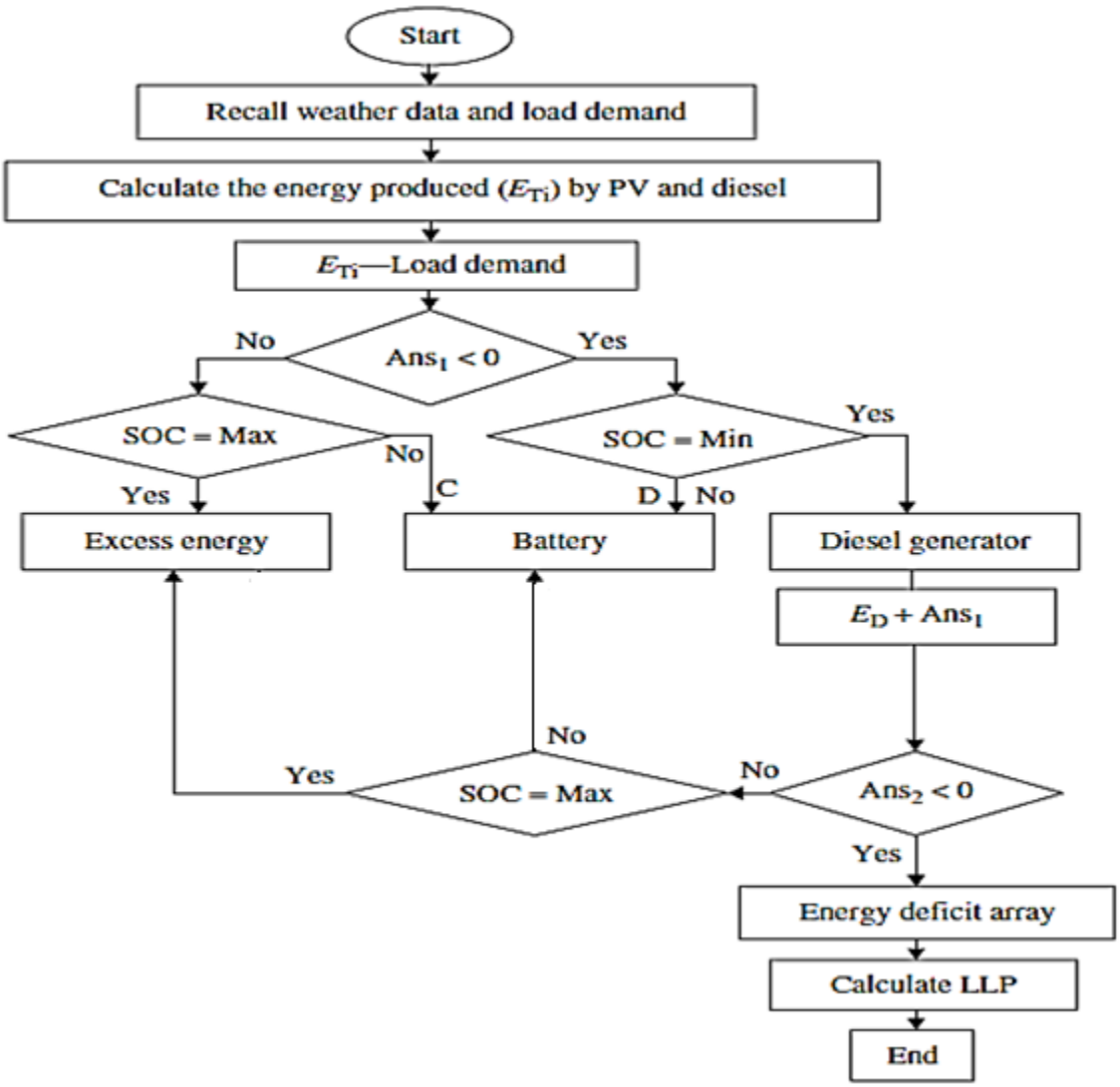

Figure 2.25: Flowchart of simulating the PV-diesel-battery system.

2.5.3. Dispatch strategies and system controls

In general, there are two main control strategies of hybrid PV-diesel-battery system. These strategies are load following strategy and cycle-charging strategy.

2.5.3.1. Load Following Dispatch Strategy

In the load following strategy, when the generator operates, it produces only enough power to meet the primary load. Charging the battery bank or serving the deferrable load are left to the renewable power sources.

There is a “Frugal” option that can be applied in all the strategies. The Critical Discharge Load (L_d) is the net load above which the marginal cost of generating energy with the diesel generator is less than the cost of drawing energy out of the batteries. If the Frugal option is applied, then the Diesel generator meets the net load whenever the net load is above the critical discharge load, regardless of whether or not the battery bank is capable of meeting the net load. The cost of generating energy with the diesel generator and the cost of drawing energy out of the batteries are equal when the net load is [103]:

$$B.P_{Ngen} \cdot \Pr_{fuel} + C_{O\&Mgen} + C_{rep\_gen\_h} + A \cdot \Pr_{fuel} \cdot L_d = \frac{C_{cycling\_bat} \cdot L_d}{\eta_{inv}} \tag{2.32}$$

Than L_d can be calculated as follows:

$$L_d = \frac{\eta_{inv}\left(B \cdot P_{Ngen} \cdot \Pr_{fuel} + C_{O\&Mgen} + C_{rep\_gen\_h}\right)}{C_{cycling\_bat} - \eta_{inv} \cdot A \cdot \Pr_{fuel}} \tag{2.33}$$

Where:

$C_{O\&Mgen}$ is the diesel generator’s hourly operation and maintenance cost ($/h), Pr_{fuel} is the fuel price ($/l), A = 0,246 l/kWh and B = 0,08415 l/kWh are the fuel curve coefficients [104]. The fuel cost of 1h DG running, C_{fuel} is:

$$C_{fuel} = \Pr_{fuel} \cdot \left(B \cdot P_{Ngen} + A \cdot P_{gen}\right) \tag{2.34}$$

P_{gen} is the diesel generator output power in this hour (kW). $C_{rep\_gen\_h}$ ($/h) is the DG hourly replacement cost:

$$C_{rep\_gen\_h} = \frac{C_{gen}}{life_{gen}} \tag{2.35}$$

C_{gen} is the diesel generator acquisition cost plus O&M cost throughout diesel generator lifetime (€) and $Life_{gen}$ is the diesel generator lifetime (h), $C_{cycling\_bat}$ ($/kWh) is the cost of cycling energy through the batteries [103]:

$$C_{cycling\_bat} = \frac{C_{bat}}{C_N \cdot N_{bat\_P} \cdot U_{DC} \cdot N_{cycles\_eq} / 1000} \tag{2.36}$$

C_{bat} is the batteries bank acquisition cost plus O&M cost throughout batteries lifetime (€), C_N is the nominal capacity of one battery (Ah), N_{bat_p} is the number of batteries in parallel, U_{DC} is the batteries bank voltage and N_{cycles_eq} is the number of full cycles of battery life. We have assumed that the batteries can cycle a certain amount of energy, which divided by its nominal capacity, gives the equivalent cycles (full cycles). It is true that the energy that a battery can cycle depends on the depth of discharge, but is almost constant if the discharge is never allowed to fall below SOC_{min}, this being greater than 20% [103]. The figure 2.26 illustrates the performance of the hybrid PV-diesel-battery system under cloudy day using load-following dispatch strategy.

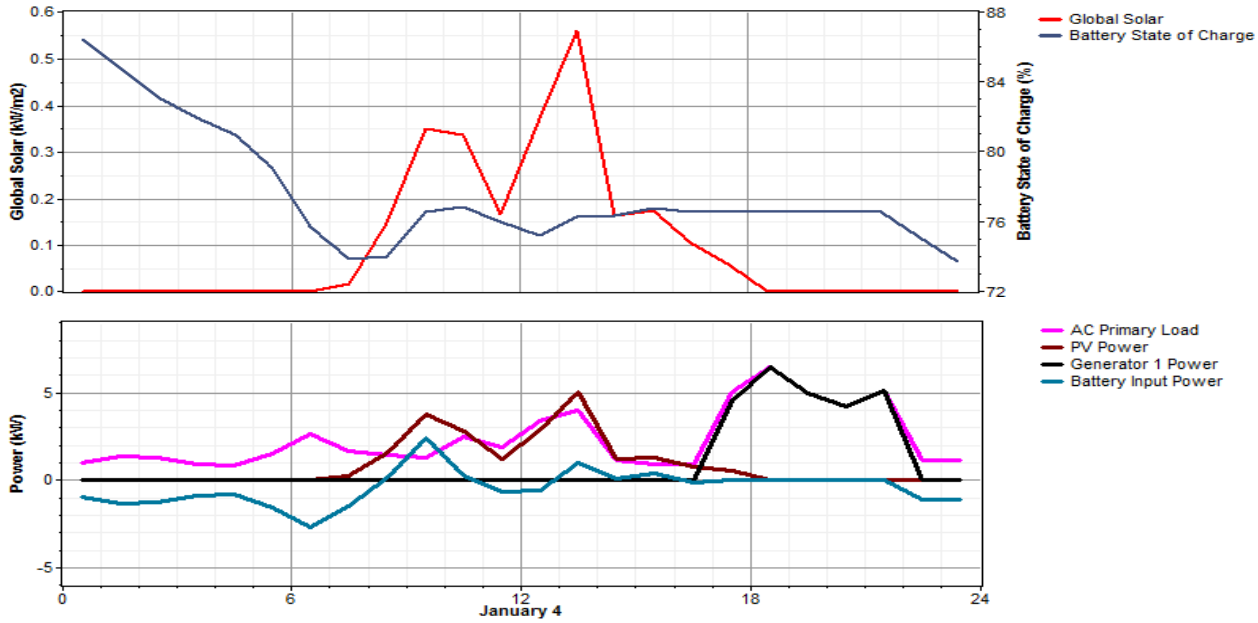

Figure 2.26: Performance of the hybrid PV-diesel-battery system under cloudy day using load-following dispatch strategy.

2.5.3.2. Cycle Charging Dispatch Strategy

In cycle charging strategy, whenever the generators operate, they produce more power than required (or at a rate not exceeding the maximum energy that batteries are capable of absorbing) to serve the load with surplus electricity going to charge the battery bank [105]. If a *SOC* set point is applied, the diesel generator will continue running until the batteries reach this *SOC* set point. The Frugal option also can be applied in this strategy [103]. The figure 2.27 illustrates the performance of the hybrid PV-diesel-battery system under cloudy day using cycle charging dispatch strategy.

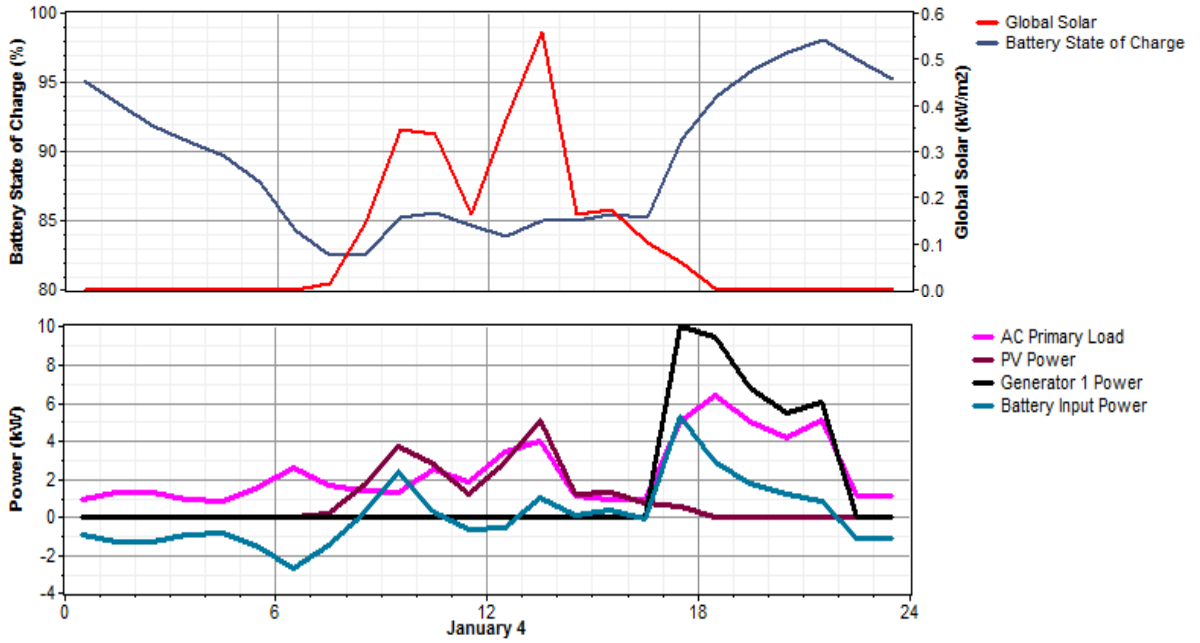

Figure 2.27: The performance of the hybrid PV-diesel-battery system under cloudy day using cycle charging dispatch strategy.

2.6. Conclusion

The design of a hybrid PV system is complex process due to the number of components to be dimensioned and optimized, the technical constraints of each component, and the challenge in the selection of the best control strategy for the system. In this chapter, we have presented first the PV technology with the different types of solar PV systems. Then, we focused on the hybrid PV-diesel-battery system, the characteristics and the modelling of its components, in addition to the energy flow and the control strategies of the hybrid PV-diesel-battery system. The complexity of some presented models allowed us to choose the appropriate models for our study which give good results without excessive computation time.

CHAPTER 3

OPTIMAL SIZING METHODS OF THE HYBRID ENERGY SYSTEM

3.1. Introduction

The major components of the hybrid PV-diesel-battery system with their technical details, models and relevant control strategies have been discussed earlier in chapter 2. The optimal design of hybrid energy system such as PV-diesel-battery system is a complicated task since the optimal configuration depends on the knowledge of energy sources, technical, economic and environmental specifications, with the load profiles characteristics. There are different optimization techniques that are applied in many researches for hybrid renewable energy system sizing like:

- Graphic construction methods.
- Probabilistic methods.
- Analytical methods.
- Iterative methods.
- Linear programing
- Artificial intelligence methods.

In this chapter, we will summarize these techniques. Also we will present the methods and material used in the two approaches of our study, the PSO (particle swarm optimization) based approach and the techno-economic analysis approach.

3.2. Sizing methods

3.2.1. Graphic construction methods

The technique is based on the condition that the average value of the demand must be satisfied by the average values of solar radiations for a definite size of PV generator. “the sizing curve”. The solution can be displayed in a convenient graphical form using the sizes of the components as coordinates in a Cartesian plane [106]. This is a basic and easily understandable method with no complexity, but this technique is not used currently as it is not flexible and based on various approximations [107].

3.2.2. Probabilistic methods

The probabilistic method like Monte Carlo method is one of the simplest sizing methodologies but the results thus obtained may not be suitable for finding out the best possible solution. Generally, a very few performance parameters are considered to be optimized in order to size the system. Solar radiation, ambient temperature, etc. Data, most of the time are unavailable for a remote rural area. They must be statistically generated by insufficient data available for proper designing of HES for the locality. Disadvantage of this probabilistic approach is that it cannot represent the dynamic changing performance of the hybrid system [106].

3.2.3. Analytical methods

In these methods, hybrid energy systems are represented by means of computational models which describe the hybrid system size as a function of its feasibility. Analytical methods require less time than Monte Carlo simulation in obtaining the required size for a definite demand [108]. The major advantage of this technique is that the design and the system size calculation are very straightforward, while the disadvantage of this technique is that these equations are location-dependent factors as well as the difficulty of finding the coefficients of these equations is another point [39].

3.2.4. Iterative methods

In iterative method is a mathematical procedure that generates approximate solutions for problems. This is a recursive process which stops when the best configuration is reached as per specifications. In hybrid renewable energy research, iterative approach is used from beginning to design and optimize. Iterative optimization method requires more computational efforts [107].

3.2.5. Linear programming techniques

The linear programming method was first developed by Leonid Kantorovich in 1939 and is a widely used technique for sizing and optimization of renewable systems. Among all the techniques discussed above, linear programming technique is found to be best than other approaches as it improves the quality of decision. Also linear

programming technique is more flexible than other methods and a wide range of problems can be solved easily [107].

3.2.6. Optimization computer software tools

Many software tools have been used in optimization of renewable energy systems. Recently, HOMER, RETScreen and iHOGA, have been mostly used for sizing a standalone hybrid energy system (HES).

HOMER can optimize and simulate energy systems including renewable and conventional sources, as well as an energy storage system in standalone and grid-connected modes. Optimization can be conducted using previous meteorological data according to monthly averaged or hourly data based on the site location. Many researches have been conducted using this optimization tool in Algeria [109-112].
The improved version of the software has some added features such as optimizer, multi-year module, advanced battery, load profile options, monthly demand limits, and ability to link with the Matlab software [113, 114]. The software is widely used for sizing a standalone hybrid PV and WT energy system and other energy sources and storage systems integrated with it [112, 115-117]. The software is limited as it performs only a single-objective optimization by minimizing NPC and the input variables should be inserted by the user [118].

RETScreen is feasibility study tool and is freely downloadable software developed by Ministry of Natural Resources, Canada [119] for evaluating both financial and environmental costs and benefits of different renewable energy technologies for any location in the world. RETScreen was released in 1998 for on-grid applications. RETScreen PV model also covers off-grid PV applications and include stand-alone, hybrid and water pumping systems also. It has a global climate database of more than 6000 ground stations (month wise solar irradiation and temperature data for the year), energy resource maps (i.e. wind maps), hydrology data, product data like solar photovoltaic panel details and wind turbine power curves. It also provides link to NASA climate database [120]. Retscreen software is also largely used in the optimization of renewable energy systems [121-123].

iHOGA is a hybrid energy system optimization software developed by the electric engineering department of the University of Zaragoza [124]. The optimization can be conducted by using input data of component, economic, and constraints resources. The simulation is carried out for one-hour interval in which all system variables remain unchanged throughout the simulation. This software utilizes GA to perform the size optimization of single or multi-objective optimization and optimal control strategies with less computational time compared to the use of GA alone. In addition, it utilizes Monte Carlo Simulation to perform probabilistic analysis [125] . It also can perform analysis for buy and sell for electric energy when the hybrid system is connected to the utility grid with different cases of net metering [106] and allows for selling the surplus hydrogen produced by the electrolyzer [124]. It allows to include the MPPT function in the PV charge regulator and estimate the lifetime of the lead-acid batteries [126] based on model predication of lead-acid batteries [127]. In addition, it considers the efficiency of the inverter as a function of the power output. Moreover, it considers the height of the wind turbine, and atmospheric pressure and air density in the optimization problem [124].

These software tools are used to find the optimal design of HES for different locations worldwide by considering the main objective function of minimizing NPC and subjecting it to numerous environmental, reliability, and social constraints.

3.2.7. Artificial Intelligence Methods

Artificial intelligence is a term that in its broadest sense would mean the ability of a machine or artefact to perform similar kinds of functions that characterize human thought. In recent research works for optimization of a Renewable Energy unit, there is an increase in usage of evolutionary computations, due to their suitability for multi-objective issues by implementing a heuristic algorithm. Researchers applied multi-objective evolutionary algorithms (MOEA) to solve one of those problems. O. Erdinc & Uzunoglu [128] reviewed the state-of-art of hybrid system sizing approaches. Also, M. Fadaee et Radzi [129] presented a review of multi-objective optimization methods applied to different Hybrid Renewable Energy Systems (HRES) like genetic algorithm (GA), particle swarm optimization (PSO) from the point of view of placement, sizing, operation, design, planning and control. Chicco & Mancarella [130] presented a

comprehensive review of many different approaches for the characterization, planning, evaluation and optimization of such systems. Aim of the optimization is often the overall cost minimization or that of environmental impact: the better optimal hourly, daily or annual operation strategy is evaluated able to satisfy users' requirement. Many research papers have been carried out to find the optimization method for distributed generation installation using analytical, numerical and heuristic methods [124, 131, 132]. we will discuss some of these methods such as: Artificial Neural Network (ANN), Genetic Algorithms (GA), Fuzzy Logic (FL),

3.2.7.1. Artificial Neural Network (ANN)

Artificial Neural Networks are relatively crude electronic models based on the neural structure of the brain. This brain modeling promises a less technical way to develop machine solutions. ANN does not utilize traditional programming but involves the creation of massively parallel networks and the training of those networks to solve specific problems. This field also utilizes words very different from traditional computing, words like behave, react, self-organize, learn, generalize, and forget [67]. The structure or topology of artificial neural networks is shown in figure 3.1. In this structure some of the neurons interfaces to the real world to receive its inputs. Other neurons provide the real world with the network’s outputs. This output might be the particular character that the network thinks that it has scanned or the particular image it thinks is being viewed. All the rest of the neurons are hidden from view.

Neuron connection weights are not just modified in one pass. The process by which neuron weights are modified occurs over iterations. The neural network is presented with training data, and the results are then observed. These results must in some way change the connection weights in order for the neural network to be learn. The exact process by which this happens is determined by the learning algorithm [67].

ANN have been used in many researches in the field of HES. In [133], an artificial neural network based controller is proposed to control a diesel generator on/off status in PV-diesel system. The proposed ANN aims to maintain a minimum loading level on the generator under light load and high solar radiation levels. In addition to that the proposed model aims to save the diesel generator energy by switching it off when it is not required and it based on predicted information. Different

point of view of controlling hybrid PV systems has been also reported in [134-136]. These researchers focused on control of system's power electronic features in order to achieve maximum system overall efficiency [137].

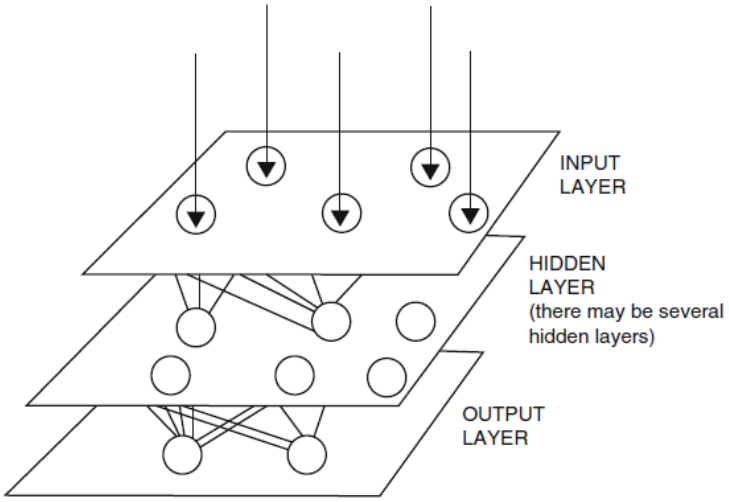

Figure 3.1: A simple neural network diagram [67].

3.2.7.2. Genetic Algorithms (GA)

One of the optimization methods operates in terms of the genetic process for biological mechanisms and is called GAs, which have the ability to present a problem solving method for difficult real-world problems [138, 139]. Holland was the first to represent the concept of GAs [140], and afterward, it was widely utilized in many applications, case studies, and information mining. The Genetic Algorithm (GA) model is done by the creation within a machine of a population of individuals represented by chromosomes, in essence a set of character strings that are analogous to the base-4 chromosomes. The individuals in the population then go through a process of simulated "evolution". Genetic algorithms are used for a number of different application areas. An example of this would be multidimensional optimization problems in which the character string of the chromosome can be used to encode the values for the different parameters being optimized [67]. There many published articles that regard GA usage in hybrid systems like in [103, 141], Lopez et al. [103] programmed hybrid optimization based on Genetic Algorithms (HOGA), as a simulation application to plan compounds of stand-alone hybrid energy systems with content from renewable sources and typical diesel generators.

3.2.7.3. Fuzzy logic (FL)

Fuzzy Logic was initiated in 1965 by Lotfi A. Zadeh, professor for computer science at the University of California in Berkeley. Basically, Fuzzy Logic (FL) is a multivalued logic that allows intermediate values to be defined between conventional evaluations like true/false, yes/no, high/low, etc. These intermediate values can be formulated mathematically and processed by computers, in order to apply a more human way of thinking. Fuzzy logic can be blended with conventional control techniques [67]. Fuzzy systems don't necessarily replace conventional control methods. In many cases fuzzy systems augment them and simplify their implementation. Figure 3.2 shows a fuzzy expert system consists of four components namely, the fuzzifier, the inference engine, and the defuzzifier, and a fuzzy rule base. Fuzzy logic is applied in photovoltaic solar energy systems, solar tracking system, to predict solar radiation and in solar powered energy. Fuzzy logic controllers are applied to control solar air-conditioning system, for maximum power point tracking, and in charge controllers. Combination of neural networks and fuzzy logic are applied as ANFIS systems to predict solar radiation and temperature. The ANFIS systems are also applied to model the power supply of PV systems [67].

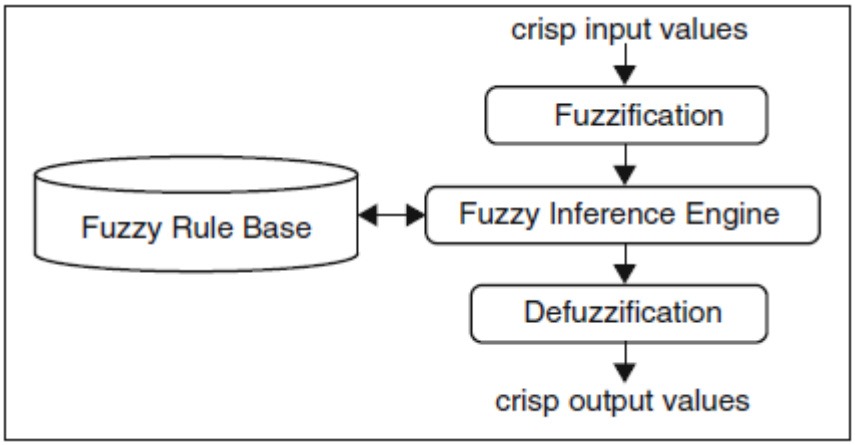

Figure 3.2: Fuzzy expert system model.

3.3. Methods and Materials of our study

The objective of this research is to study the feasibility of the hybrid PV-diesel-battery system as an electrification solution for rural, Saharan and remote villages,

then to translate the results of the study into recommendations that can be used by decision makers. To reach this objective, it is essential to design an optimal and efficient energy system, hence, two approaches have been used: the first is based on the Particle Swarm optimization method and the second is based on techno-economic analysis. The following sections are dedicated to present these methods.

3.3.1. Methodology

This work is a feasibility study of the hybrid PV-diesel-battery system, hence the key technique used by the research was the optimization of hybrid energy system by computer modelling.

To answer our research question, we followed five stages. With the help of the Electricity Distribution Company (societé de distribution d'éléctricité du centre, SDC) in the gathering of data, stage one involves the selection of a group of un-electrified villages, located far from the grid along with the collection of the local meteorological data. Afterward, a selection of one village to be consider as case study or model for the first approach which was the village of Tiberkatine located in the district of Tazrouk. Moreover, the rural Saharan village of Terhananet has been selected for the techno-economic analysis approach. Next, the electricity demand of the sites has been achieved based on hourly winter and summer patterns.

In third stage: After the mathematical modeling of the hybrid PV-diesel-battery system components, the optimization of the hybrid system using PSO based approach and ε- constraint method were achieved in the first approach. Next, an energy balance of the system has been derived from the simulation of the system, following by a sensitivity analysis of three parameters (the load consumption, ε_{CO2} and ε_{LLP} constraints) on the behavior of the optimal hybrid system.

In the second approach, three electrification scenarios are considered and compared: the standalone PV system, the diesel based system and hybrid PV-diesel-battery system. The three systems have been simulated and analyzed their performance. In fourth stage, a sensitivity analysis has been performed to evaluate the system's behavior based on the variation of the load consumption and diesel price. The last part has been dedicated to discuss the potential and the contribution of the

hybrid PV-diesel-battery system in the electrification of six other rural villages in the province of Tamanrasset.

3.3.2. PSO based method approach

3.3.2.1. Particle Swarm Optimization (PSO)

The concept of PSO is characterized as a simple heuristic of well-balanced mechanism with flexibility to enhance and adapt both global and local exploration abilities. It uses a stochastic search technique with reducing memory requirement, computationally effective and easier to be implemented compared to other metaheuristics of evolutionary computation and swarm intelligence fields [142]. PSO is a population based stochastic optimization technique developed by Dr. Eberhart and Dr. Kennedy in 1995 [143] which is inspired by social behavior of bird flocking or fish schooling [144]. PSO to some extents, has similarities with evolutionary computation techniques such as GA. However, unlike GA, PSO never utilizes evolution operators such as crossover and mutation [145]. Moreover, PSO has several advantages compared to other optimization methods as follows [146]:

- It is a derivative-free algorithm unlike many conventional techniques.
- It has the flexibility to be integrated with other optimization techniques to form a hybrid tool.
- It is less sensitive to the nature of the objective function, i.e., convexity or continuity.

The particle moves towards an optimum solution through its present velocity and its individual best solution obtained by itself in each iteration and global best solution is obtained by all particles. In a physical dimensional search space, updated position and velocity of the 'ith' particle are represented as:

$$v_i^{k+1} = K\left[v_i^k * \omega + C_1 * R_1 * \left\{p_{best}(i) - x_i^k\right\} + C_2 * R_2 * \left\{g_{best} - x_i^k\right\}\right] \quad (3.1)$$

$$x_i^{k+1} = x_i^k + v_i^{k+1} \quad (3.2)$$

Where:

$x_i = [x_{i1}, x_{i2,} \dots \dots \dots \dots \dots \ x_{id}]$
$v_i = [v_{i1}, v_{i2,} \dots \dots \dots \dots \dots \ v_{id}]$
} 1,2, …. , d shows possible dimensions for i = 1,2, …. , n particles with position x and velocity v

$\mathrm{p_{best}(i)} = [\mathrm{X_{i1P_{best}}}, \mathrm{X_{i2P_{best}}}, \dots \dots \mathrm{X_{idP_{best}}}]$ is the individual best positions of particle i.

$g_{best} = [X_{1G_{best}}, X_{2G_{best}}, \ldots\ldots\ldots X_{nG_{best}}]$ is the global best positions

k represents the iteration number for total n iterations. K is constriction factor, C_1 and C_2 are non-negative coefficients called acceleration factors, R_1 and R_2 are two random numbers different from each other and generally distributed in the range [0,1]. ω is inertia weight, suitable selection of ω provides a balance between global exploration and local exploitation and reduces the total number of iterations [143].

The best interval for PSO parameters ω, C_1, C_2, R_1 and R_2 are suggested according to literature: acceleration coefficients C_1 and C_2 are set within the range of [0-4], R_1 and R_2 are random numbers set within range of [0-1]. In this study, we use the formula suggested to calculate the inertia weight (ω) [142]:

$$\omega(i) = \omega_0 \cdot \exp\left(\frac{i}{\max\ i}\right)^n \tag{3.3}$$

PSO is considered as one of the most used algorithm in HES size optimization due to its good performance, flexibility, and simplicity [147].

3.3.2.2. The ε-constraint method

The ε-constraint method is a simple MOP (Multi-Objective optimization) technique that can be used where one objective is chosen to be optimized. The remaining objectives are considered as constraints bound by given target levels (ε_i) [148]. By varying these levels, the non-inferior solutions of introduced problem can be obtained. Consider the following MOP:

$$Min\{f_1(x), f_2(x), \ldots\ldots\ldots, f_k(x)\} \tag{3.4}$$

Where x is the decision vector, $f_i\ (i = 1,2, \ldots, k)$ are objective functions.

A solution x* is said to be non-inferior if there exists no other feasible solution x such that:

$f_i\ (x) \leq f_i\ (x^*)$ for all i = 1, 2, ..., k, and at least, one inequality is strict.

In the ε-constraint method, if $f_j\ (x)$, j ϵ {1, .., k} is the objective function chosen to be optimized, and $f_i\ (x)$ is objective considered as the constraint, we have the following problem [148, 149].

$$Min\ f_j(x)\ j \in \{1, \ldots\ldots, k\}\ \ subject\ to\ f_i(x)\ \leq \varepsilon_i\ \forall\ i \in \{1, \ldots\ldots, k\}, i \neq j, x \in S \quad (3.5)$$

Where S is the feasible solution space, k is the number of objective functions, and ε_i is assumed values of the objective function that must not be exceeded.

3.3.2.3. Objective Function and Constraints

Performance parameters are used for the determination of reliability & feasibility and also help the system designer to design hybrid energy system (HES) for a required locality. These parameters can be technological, economic or environmental. In our study we consider three parameters: LLP (Loss of load probability), Annualized cost of system (ACS), and CO_2 emissions.

3.3.2.3.1. Loss of load probability (LLP)

As the solar is a random and intermittent source of energy, the determination of the reliability of the system becomes an important consideration. One of the parameters that helps us to access the system's reliability is loss of load probability (LLP). It is defined as the ratio of the total energy deficit to the total demand during the considered period [150, 151]:

$$LLP = \frac{\sum_{t=1}^{8760} shortage(t)}{\sum_{t=1}^{8760} D(t)} \quad (3.6)$$

Where, $\mathrm{LLP} \leq \varepsilon_{\mathrm{LLP}}$ and D(t) is electricity demand, and shortage (t) is unmet load during time period t [150].

3.3.2.3.2. Annualized cost of system (ACS)

The system costs consist of the annual capital cost (ACC), annual operation and maintenance cost (AOM), annual fuel cost (AFC), and annual replacement cost (ARC), ACS is calculated using the following equation:

$$ACS = ACC + AOM + ARC + AFC \quad (3.7)$$

Annual capital cost of each unit that does not need replacement during project lifetime such as DG, PV, and inverter is calculated as follows:

$$ACC = C_{cap} \cdot CRF(i, y) \tag{3.8}$$

Where C_{cap} is the capital cost of each component in US$, y is the project lifetime in a year. CRF is capital recovery factor, a ratio to calculate the present value of a series of equal annual cash flows. This factor is calculated as follows:

$$CRF = \frac{i(1+i)^y}{(1+i)^y - 1} \tag{3.9}$$

Where i is the annual real interest rate. Annual real interest rate consists of nominal interest i' and annual inflation rates f. This rate is calculated as follows:

$$i = \frac{(i' - f)}{(1+f)} \tag{3.10}$$

Annual operation and maintenance cost of system (AOM) as a function of capital cost, reliability of components (λ) and their lifetime can be determined using the following equation [152, 153]:

$$AOM = C_{cap}(1-\lambda)/y \tag{3.11}$$

ARC is annual cost value for replacing battery banks during the project lifetime. Economically, annual replacement cost is calculated using the following equation [153]:

$$ARC = C_{rep} \cdot SFF(i, y_{rep}) \tag{3.12}$$

Where C_{rep} is the replacement cost of battery banks in US$, y_{rep} is the lifetime of battery banks in a year. SFF is the sinking fund factor, a ratio to calculate the future value of a series of equal annual cash flows. This factor is calculated as follows [154]:

$$SFF = \frac{i}{(1+i)^y - 1} \tag{3.13}$$

3.3.2.3.3. CO_2 emissions

The annual CO_2 quantity produced (in kg) by diesel generator is considered to represent the pollutant emission and it is calculated using the following equation [150, 151]

$$CO_{2_{emission}} = \sum_{t=1}^{8760} fuel(t) \cdot EF \tag{3.14}$$

EF is the emission factor for a diesel generator. It depends on the type of fuel and diesel engine characteristics. it is considered between 2.4 kg/L and 2.8 kg/L [150].

3.3.2.3.4. Constraints of the system

The annual cost of the system (ACS) is considered as objective function. The CO_2 emission and LLP during one year are considered as the constraint bounds.

Where, $LLP \leq \varepsilon_{LLP}$ and Where $CO_{2_{emission}} \leq \varepsilon_{CO_2}$

Some other feasible operation constraints should be considered:

- The constraints of the number of PV modules and batteries and capacity of DG:

$$N_{PV}, N_{bat}, P_{n-DG} \geq 0 \quad (3.15)$$

- The constraints of the capacity of batteries:

$$C_{B\min} \leq C_B(t) \leq C_{B\max} \quad (3.16)$$

- The energy flow (energy produced by or entered to each component) in every time ($E_j(t)$) should be less than the capacity of the component. Where Δt is the time interval (Δt =1h).

$$E_j(t) = P_j \cdot \Delta t \quad (3.17)$$

3.3.3. Techno-economic approach

Whichever sizing and optimization technique are used, they must ultimately search for an optimum combination of the system reliability and the system cost [155]. To search for the optimum solutions that guarantee the lowest investment and the best technical performance, the techno-economic analysis of stand-alone hybrid PV diesel system approach is based on the minimum total net present cost (NPC) and the minimum cost of energy (COE) methods. The simulation of long-term performance of the hybrid system is performed. a range of equipment options are evaluated over varying constraints and sensitivities to optimize small power systems. The flexibility of the software makes it useful in the evaluation of design issues in the planning and early decision-making phase of rural electrification projects [156]. energy balance

calculations is calulated for each system configuration. When sensitivity variables are defined as inputs, the optimization process for each sensitivity variable is repeated [157]. The cost-minimizing combination of power generating technologies that would suit the load profiles is identified [158]. To calculate the total net present cost (NPC) and the levelized cost of energy (COE), the capital, replacement, maintenance, and fuel costs, along with the salvage value and any other costs or revenues for each component are combined to find the component's annualized cost. The annualized costs of each component were summed along with any miscellaneous costs, such as penalties for pollutant emissions, to find the total annualized cost of the system, the NPC and COE of the system [157]. The total net present cost is calculated using the following equation [105]:

$$C_{NPC} = \frac{C_{ann,tot}}{CRF\left(i, R_{proj}\right)} \tag{3.18}$$

Where, $C_{ann,tot}$ is the total annualized cost, i is the annual real interest rate (the discount rate), R_{proj} the project lifetime, and CRF is the capital recovery factor, was given by equation (3.9).

The levelized cost of energy is calculated using the following equation:

$$COE = \frac{C_{ann,tot}}{E_{prim} + E_{def} + E_{grid,sales}} \tag{3.19}$$

Where, $C_{ann,tot}$ is the total annualized cost, E_{prim} and E_{def} are the total amounts of primary and deferrable load, respectively that the system serves per year, and E_{grid}, sales is the amount of energy sold to the grid per year.

3.4. Conclusion

This chapter started by summarizing the different techniques in literature used to find the optimal sizing of renewable energy systems. Furthermore, the adopted methodology and the range of methods used in this study are presented such as the particle swarm optimization, ε-constraint method, objectives functions and constraints. Given the need to increase hours of electricity services and to design a sustainable electrification system for rural Saharan community, hence, these methods mentioned previously have been employed in the optimization process

to evaluate the feasibility and the potential of hybrid PV-diesel-battery energy system in different case studies. The results of our study are presented and discussed in the next chapter.

CHAPTER 4

FEASIBILITY STUDY OF HYBRID PV-DIESEL-BATTERY SYSTEM

4.1. Introduction

This chapter studies the feasibility and potential of a hybrid PV-diesel-battery energy system as an electrification solution for rural, scattered, and non-electrified villages in the province of Tamanrasset, the Sahara region, in the southern part of Algeria. Two approaches are considered. First, a particle swarm optimization (PSO) and the ε-constraint method are used to minimize simultaneously the total cost of the system, unmet load and the greenhouse gases emission of the system. A sensitivity analysis is performed on the optimal hybrid system to study the impact of three parameters (the load consumption, ε_{CO2} and ε_{LLP} constraints) on the behavior of the system. Second, a feasibility study of hybrid PV-diesel-battery system is performed, the study contains a technical, economic, and environmental analyses between the hybrid PV-diesel-battery system, the standalone PV system, and the diesel-based system. A sensitivity analysis is subsequently used to evaluate the variation of the load consumption and diesel price on the hybrid system's behavior.

4.2. Proposed approaches

Two approaches are used in our work:

- Particle swarm optimization approach.
- Techno-economic analysis.

4.2.1. First approach (PSO based approach)

The aim of this approach is the optimal sizing of hybrid PV-diesel-battery system by using PSO and ε-constraint method in order to electrify a rural Saharan village called Tiberkatine located in the province of Tamanrasset. Three objectives functions are considered (the total cost of the system, the total CO_2 emissions produced by diesel generator, and the loss of load probability LLP). Design variables included in the optimization process are: the size of the PV panels N_{pv}, the size of the battery bank

N_{bat}, and the rated capacity of the diesel generator (DG) unit $P_{n\text{-}DG}$. These variables are defined in a vector named particle $x_i=[N_{PVi},N_{bati},P_{n\text{-}DGi}]$. Each particle represents a different configuration of the system. Total cost, which is a function of design variables is considered as the fitness of particles for particles evaluation while CO_2 emission and unmet load are considered as constraints bounds. The optimization and simulation flowchart of the approach is shown in figure 4.1. After entering the initial parameters and different constraints of the system such as the hourly load demand, hourly meteorological data, lifetime of the project, cost of the components etc. The next step is the initializing of the first population of particles, particles are generated randomly then in each iteration and for each particle, the energy flow between components is evaluated, the LLP and CO_2 emission are calculated. The results of the simulation procedure are sent back to the optimization model to calculate the fitness value for each particle and check its feasibility (if it meets the constraints of the model).

The simulation model is run for one year to evaluate the performance of each particle. And it is carried out based on weather data (insolation, temperature, etc.). The simulation model calculates the annual fuel consumption of diesel generator unit, the CO_2 emission and the yearly-unmet load for each particle. These values are sent to the optimization algorithm to check if the particle meets the constraints (the desirable level of unmet load and CO_2 emission). If the particle did not meet the constraints, it is modified and sent back to simulation. Each iteration feasible particles are evaluated in the PSO algorithm based on their fitness until termination criterion is checked. After terminating the cycle, the optimal solution will be returned.

The optimization of hybrid PV-diesel-battery energy system using PSO based approach and ε- constraint method to electrify a remote Saharan village of Tiberkatine, Tazrouk district in the province of Tamanrasset, the south of Algeria (latitude 23°25’ N and longitude 6°15’E). The village has 20 un-electrified households. The electrical load is considered based on the local needs. The daily load is 47 kWh/day and the peak demand is 4.5 kW. PSO and ε-constraint method have been used to minimize simultaneously the total cost of the system, unmet load, and fuel emission. The hybrid system included PV generator, Diesel generator and battery bank. In addition to that, a sensitivity analysis was accomplished to study the impact of three parameters on the hybrid system (the load consumption, ε_{CO2} and ε_{LLP} constraints).

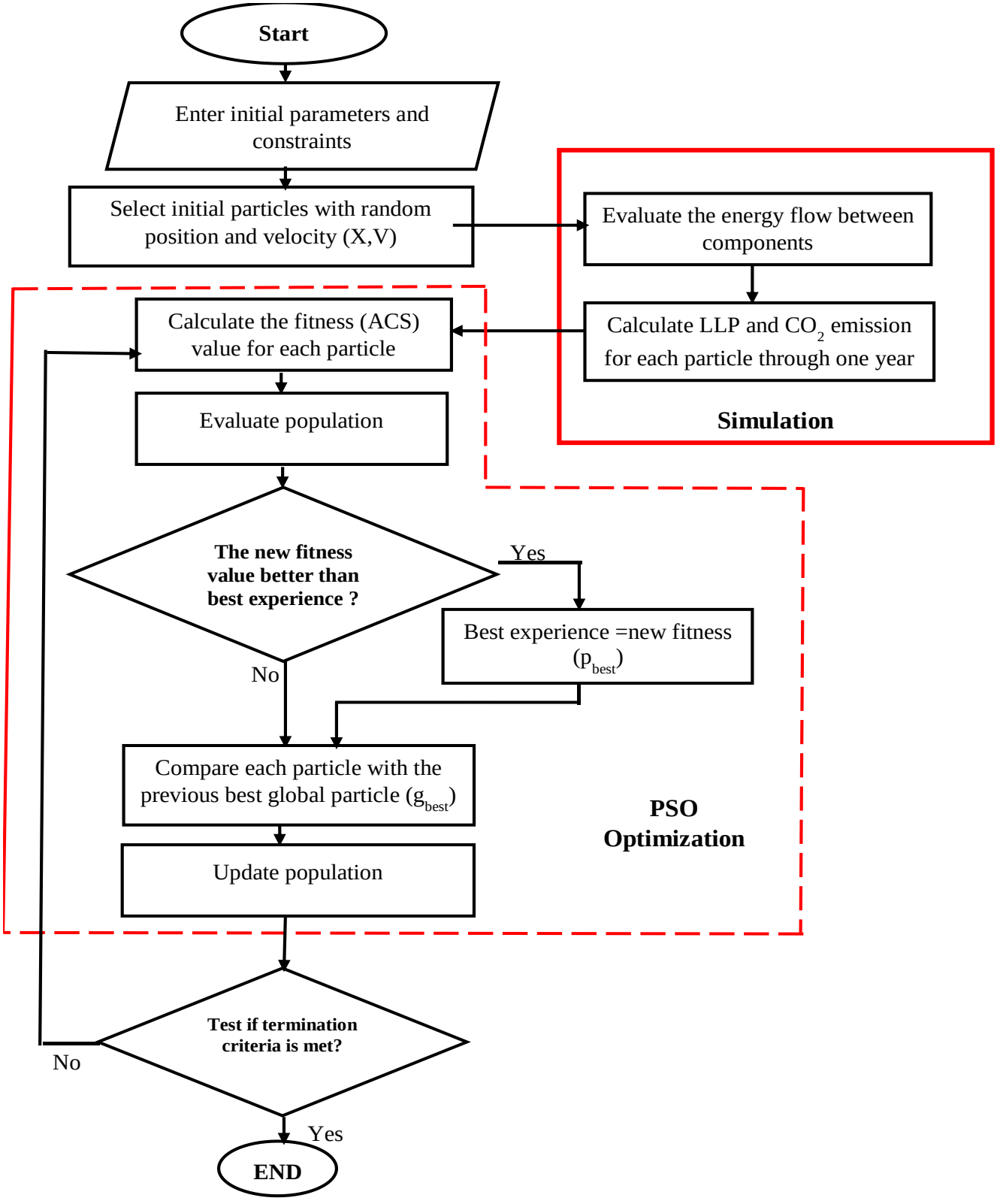

Figure 4.1: Simulation and optimization flowchart of the hybrid PV-diesel-battery system.

4.2.2. Second approach (Techno-economic Analysis)

The second approach used a techno-economic analysis of stand-alone hybrid PV diesel battery system to search for the optimum solutions that guarantee the lowest investment and the best technical performance, the optimization approach is based on the minimum total net present cost (NPC) and the minimum cost of energy (COE) methods.

4.3. Case study

The study was focused on the un-electrified rural Saharan villages located in the province of Tamanrasset. Two cases studies were selected:

- The village of Tiberkatine was chosen for the PSO based approach.
- Seven (07) rural un-electrified villages located in Tamanrasset were selected for the second approach.

The villages with number of un-electrified households are listed in table 4.1 and the locations of these villages on map are shown in figure 4.2.

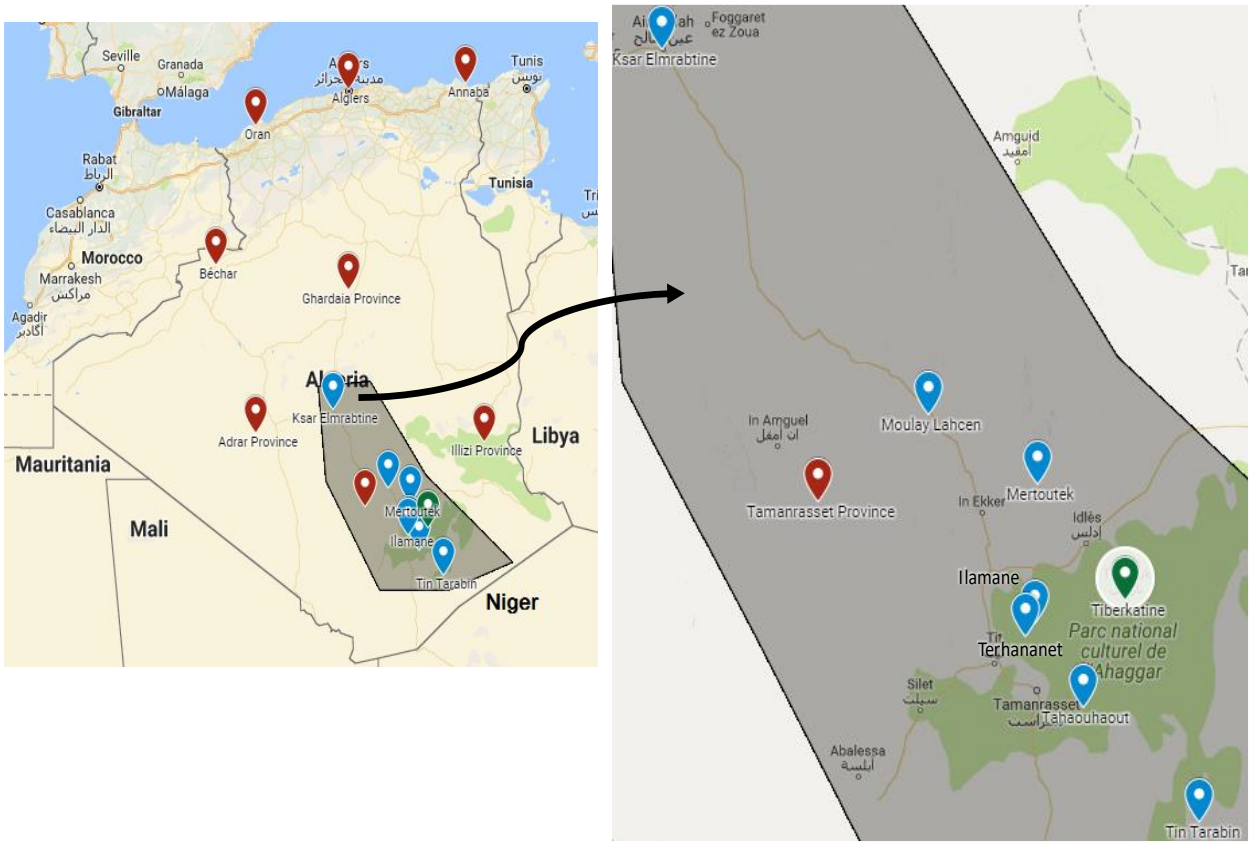

Figure 4.2: The location of the rural villages.

Table 4.1: The selected villages for the study.

Village	**Number of households**
Terhananet	100
Moulay lahcen	40
Mertoutek	190
Tahaouhaout	180
Ilamane	60
Ksar elmrabtine	100
Tin Tarabine	100
Tiberkatine	20

4.3.1. Meteorological Data

To analyze and evaluate the performance of an existing system, or to predict energy consumption or energy generated from a system in the design stage, an appropriate meteorological data is required [159]. The solar radiation and clearness index of each location were sourced from the NASA Surface Meteorological dataset, the other set of data containing the air temperature is obtained from measured data of the year 1992 and implemented in the software database. Figure 4.3 shows the meteorological characteristics (ambient temperature, clearness index and daily radiation) of the selected sites. The province of Tamanrasset has a desert climate, thus the ambient temperatures are very high. The solar potential in all villages is significant, it is observed that the village of Tiberkatine has the highest solar radiation with an annual average 6.36 kWh/m^2/d and an annual clearness index of 0.69.

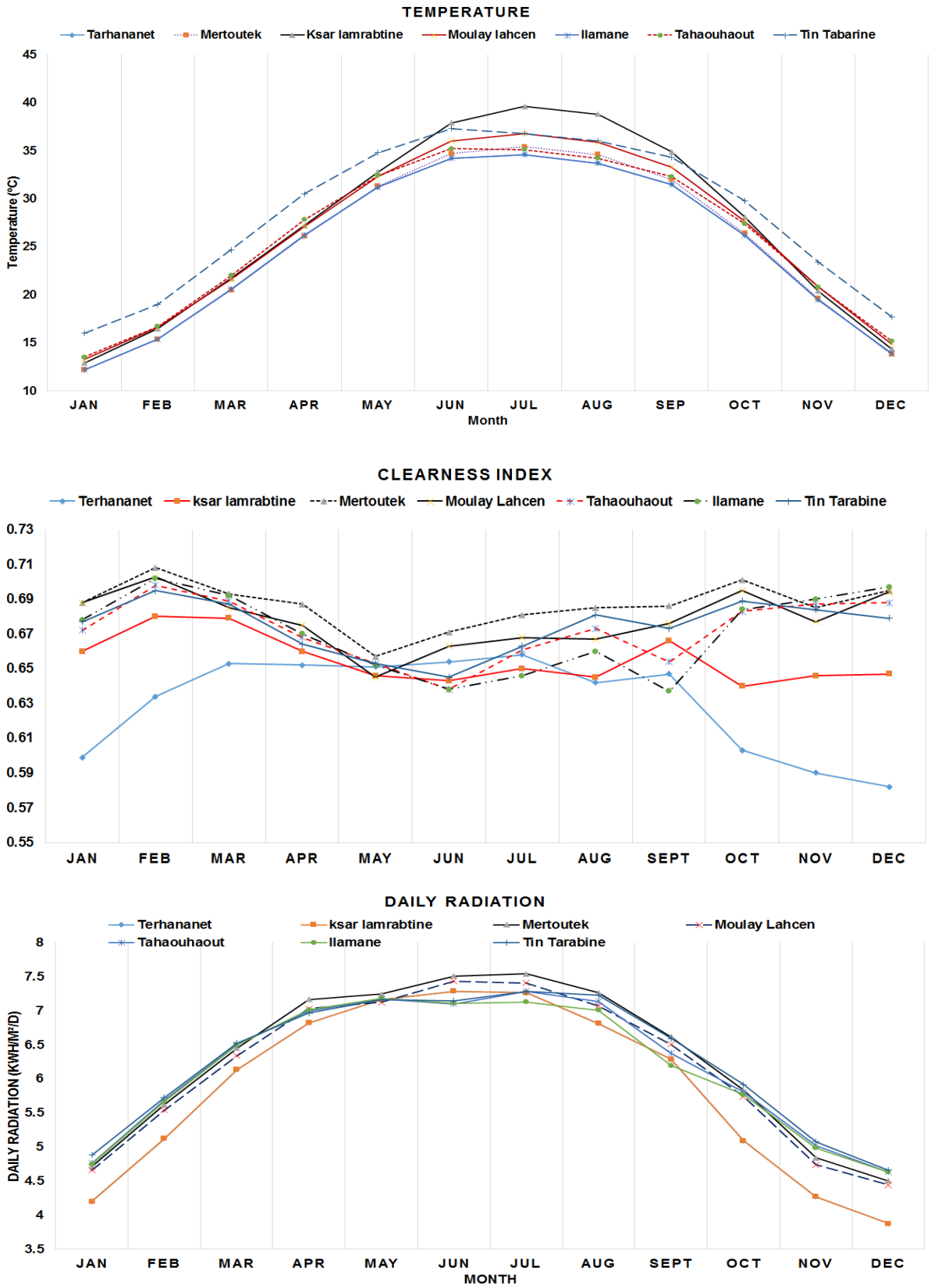

Figure 4.3: Meteorological data (ambient temperature, clearness index and daily radiation) of the villages.

4.3.2. Load Profile

The proposed load profile [160] for our study based on an investigation nearby the inhabitants of the rural villages in the southern of Algeria. The load profile considered standard of living, traditions, behavior and habits.

The load profile was formulated by using assumptions on electric appliances functioning periods. The load profile of household covers the basic power needs (lighting, refrigeration, TV, radio, ventilation). We considered the following hypotheses:

- The dwelling is occupied continuously throughout the year.
- Utilization of low energy electrical appliances.
- Two patterns are considered for winter and summer.

Figure 4.4 illustrates daily load profile. The two seasonal patterns show a prominent peak in the evening corresponding to lighting use, a midday peak and base peak in the morning, and during the night the load is very low.

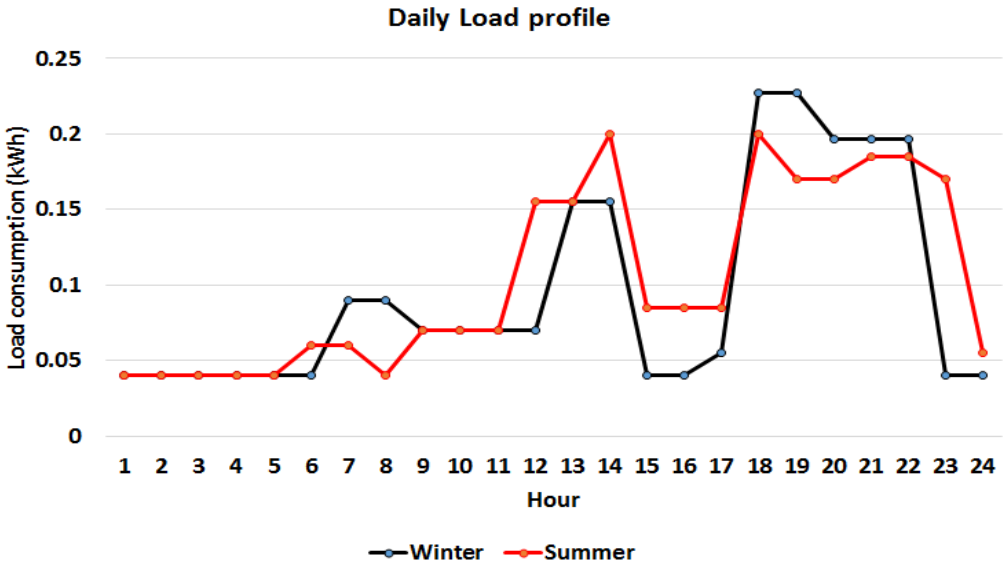

Figure 4.4: Daily load profile for a household.

4.4. PSO results

The swarm size of PSO algorithm consist of 30 particles, the particle is a vector of three elements [the size of PV panels, the number of batteries, and the capacity of diesel generator]. Each vector represents a certain configuration of the system. The

considerable size for a PV, battery bank and diesel generator respectively are: Npv ϵ [10-95], Nbat ϵ [2-48] and Pn-DG ϵ [5-10] (kW).

The best interval for PSO parameters ω, C_1, C_2, R_1 and R_2 are suggested according to literature: Acceleration coefficients C_1 and C_2 are set within the range of [0-4], R_1 and R_2 are random numbers set within range of [0-1].

. The goal of the PSO and ε-constraint approach is to minimize one objective function at a time which is the ACS of the system, and considering the other objectives as constraints bound (LLP and CO_2 emissions) by some allowable levels (ε_{CO2}, ε_{LLP}). By varying these levels, the non-inferior solutions of the problem can be obtained. Preliminary analysis is required to identify proper starting values for ε_{CO2}, ε_{LLP}. To design a sustainable electrification solution for a rural Saharan community, one optimal solution was chosen after the optimization phase. The selection criteria are based on the high load growth potential in rural areas after the installation of the hybrid system and the environmental sustainability of the energy system, therefore, to handle the growth of the load demand and to avoid the maximum GHG emissions, in our case, the optimal solution with $\varepsilon_{CO2} \leq 2000$ kg/year, $\varepsilon_{LLP} \leq 0.5$ % is picked. The optimal size of the components is 11.4 kWp of PV generator, 42 kWh of battery bank and 6 kW of diesel generator.

ACS of the optimal system is 8585.14 $, COE is 0.38 $/kWh, the cost of the battery bank is the dominant cost of the system with 51.4 % of the ACS. The economical results of the system are reported in table 4.2.

Table 4.2: The economic results of the optimal size.

Component	**ACC (US$)**	**AOM (US$)**	**ARC (US$)**	**AFC(US$)**	**ACS (US$)**
PV subsystem	2704.7	126.19	0	0	2830.89
Diesel generator	231.96	108.22	0	133	473.18
battery bank	1731.9	808.07	1873.4	0	4413.37
converter	439.89	205.19	222.63	0	867.71
Total	5108.45	1247.67	2096.07	133	8585.14

The optimal size of the components is 11.4 kWp of PV generator, 42 kWh of battery bank and 6 kW of diesel generator. An example of simulating intra-hourly

energy fluctuations of the hybrid system in winter day (the 3rd of January) and summer day (23rd of July) is represented in figure 4.5: when the energy produced by the PV modules is more than the load requirement, the load is satisfied by the PV subsystem. When the energy produced by PV modules cannot meet the load, the battery bank assists the PV subsystem to cover the load based on the state of charge of batteries. Otherwise, the diesel generator is used as a backup unit to satisfy the load demand. The local weather variation (mainly the solar radiation) has direct influence on the operation and the energy contribution of the diesel generator, and it was clearly shown in winter day.

The size of the components is enough to satisfy the load demand without any unmet load. The monthly variation of the energy production from PV, diesel generator and the storage capacity of the battery bank are presented in figure 4.6. The PV production has a significant impact on the storage capacity and the diesel production, the PV production and the storage capacity of the battery bank are linearly related, when the PV production is favorable (months of October and March), the storage capacity is maximal and when the PV production decreased the storage capacity also decreased. Unlike the storage capacity, the PV production and the DG production are inversely related because the DG was used as back up unit when the PV subsystem cannot meet the load requirements.

4.4.1. Sensitivity Analysis

Sensitivity analysis is performed to investigate the impact of the variation of the input parameters on the behavior of the system and to identify the most sensitive parameters. In this chapter, the parameters are: the load consumption, ε_{CO2} constraint and ε_{LLP} constraint.

4.4.1.1. Load consumption

The load consumption is varied from 49.4 kWh/d to 89.4 kWh/d, the sizes of PV, battery bank, and diesel generator are remained the same. To cover the capacity shortage due to the growth of the load, the system relies mainly on the diesel generator. As shown in figure 4.7 and Table 4.3, the dependence on the diesel subsystem increases the ACS from 8585 $ to 9347 $ (an increase of 8.8 %) due to the increasing costs of the fuel consumption. It is also observed that the COE

decreases from 0.38 $/kWh to 0.26 $/kWh due to the decreasing of the PV penetration from 93 % to 59 % (see Figure 4.8), which means that the fuel cost influences the COE more than the cost of the PV (the cost of the conventional energy is less than the cost of the PV energy). Subsequently, the CO_2 emissions increases from 2429.8 kg/yr to 13428 kg/yr as shown in figure 4.8. and the LLP increases from 0 % to 7.46 %.

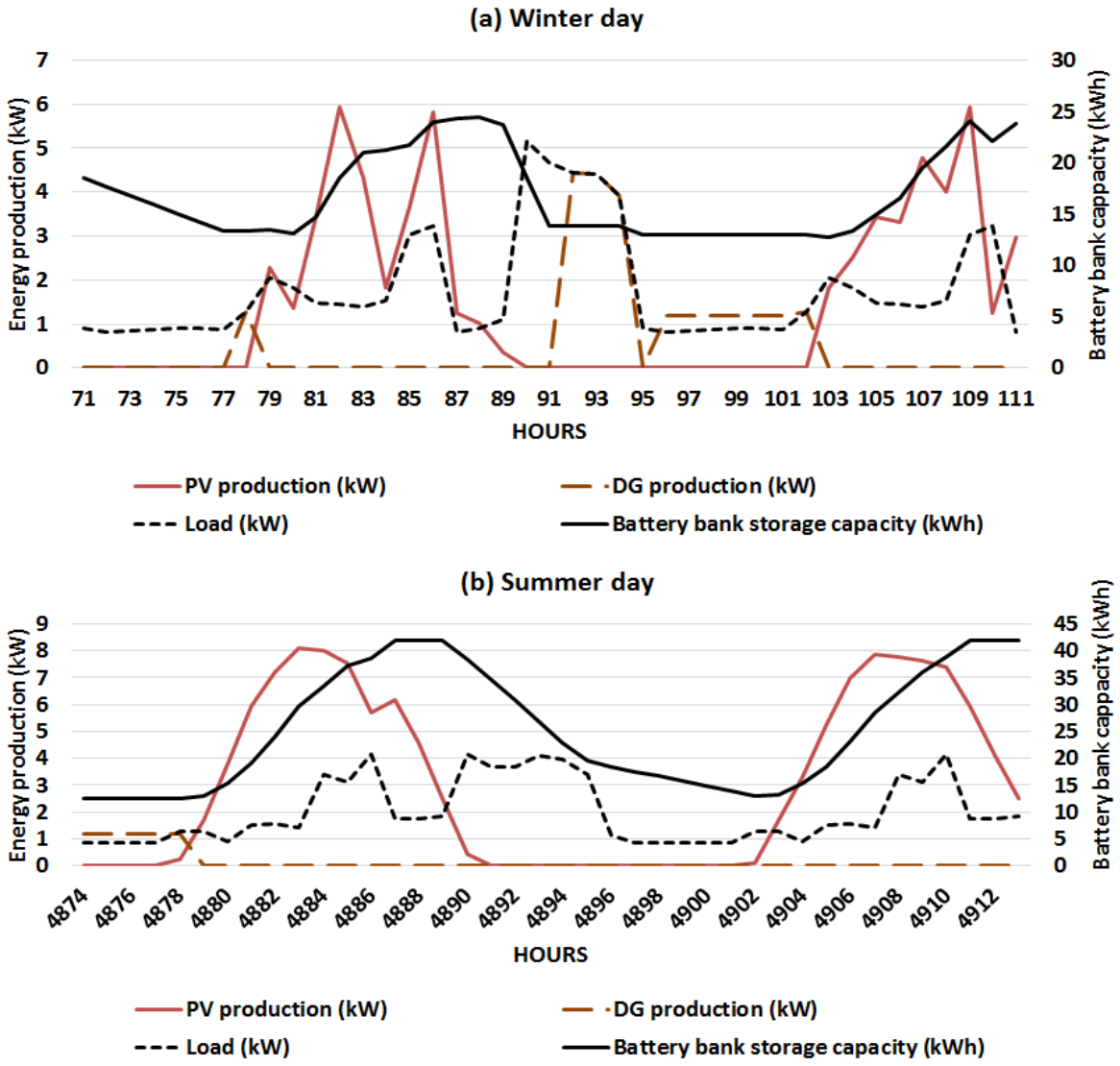

Figure 4.5: Simulating intra-hourly energy fluctuations of the hybrid system.

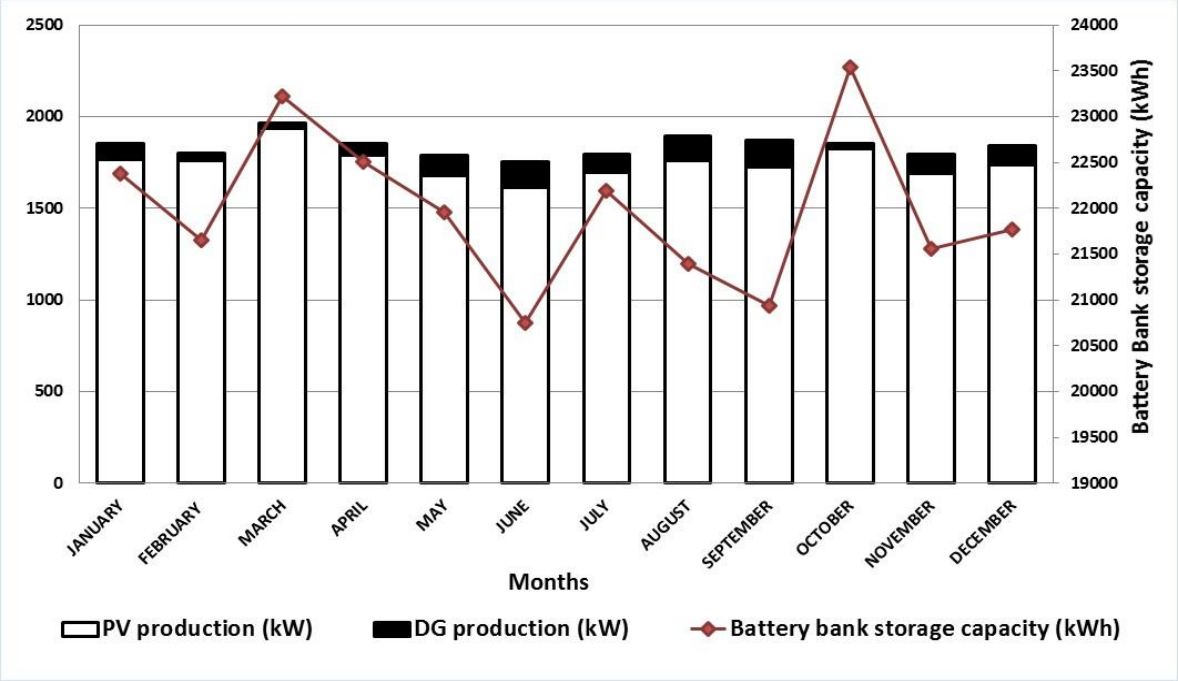

Figure 4.6: The monthly variation of the energy production from PV, diesel generator and battery bank storage.

4.4.1.2. ε_{CO2} and ε_{LLP} constraints

Figure 4.9 depicts the effect of ε_{CO2} on the size of the PV, battery and diesel generator. ε_{CO2} has a significant impact on the size of the system basically the size of the battery bank, this latter increases from 26 kWh to 46 kWh when ε_{CO2} ranges from 7000 kg/yr to 50 kg/yr. Whereas for the effect of ε_{LLP} on the size of the system, the size of the battery bank is also the most influenced, it decreases from 22 kWh to 18 kWh when ε_{LLP} ranges from 0 % to 2 % as shown in Figure 4.10.

Figure 4.11 shows the effect of the variation of ε_{CO2} on the PV penetration, the PV penetration is inversely related to ε_{CO2}, it increases from 74.5 % to 99.9 % when ε_{CO2} is varied. As for the effect of the variation of ε_{LLP}, the PV penetration decreases slightly from 72 % to 67 % as depicted in Figure 4.12.

Figure 4.13 shows the effect of the variation of ε_{LLP} on different costs. ACS is inversely related to ε_{LLP} of the system, ACS decreases by 717.4 $. Furthermore, COE ranges between 0.24 $/kWh and 0.27 $/kWh when ε_{LLP} is varied.

Whereas for the effect of the variation of ε_{CO2} on different costs, ACS is also inversely related to ε_{CO2} of the system as seen in Figure 4.14, ACS increases from

6662.8 $ to 11231.3 $ (an increase of 4568.4 $). As for the impact of ε_{CO2} on COE, it can be observed that COE ranges between 0.29 $/kWh and 0.38 $/kWh.

Table 4.3: Effect of varying the load consumption on PV penetration, LLP, CO_2 emission, ACS and COE.

The added load (kW/day)	**PV penetration (%)**	**LLP (%)**	**CO_2 (kg/year)**	**ACS (US$)**	**COE ($/kWh)**
1	92.15	0	2429.8	8614.1	0.38
2	90.97	0	2818.9	8640.1	0.37
3	89.58	0	3326.9	8673.9	0.37
4	88.43	0	3717.6	8700	0.36
5	87.21	0	4156.9	8729.3	0.36
6	86.13	0	4530.2	8754.1	0.36
7	85.09	0	4895.7	8778.5	0.35
12	80.24	0	6427.9	8880.7	0.34
15	77.62	0	7070	8923.5	0.33
20	73.30	0.37	8225	9000.5	0.31
25	69.19	1.67	9645.6	9095.2	0.30
30	65.41	3.71	10788	9171.3	0.28
35	61.95	5.62	12078	9257.3	0.27
40	58.80	7.46	13428	9347.3	0.26

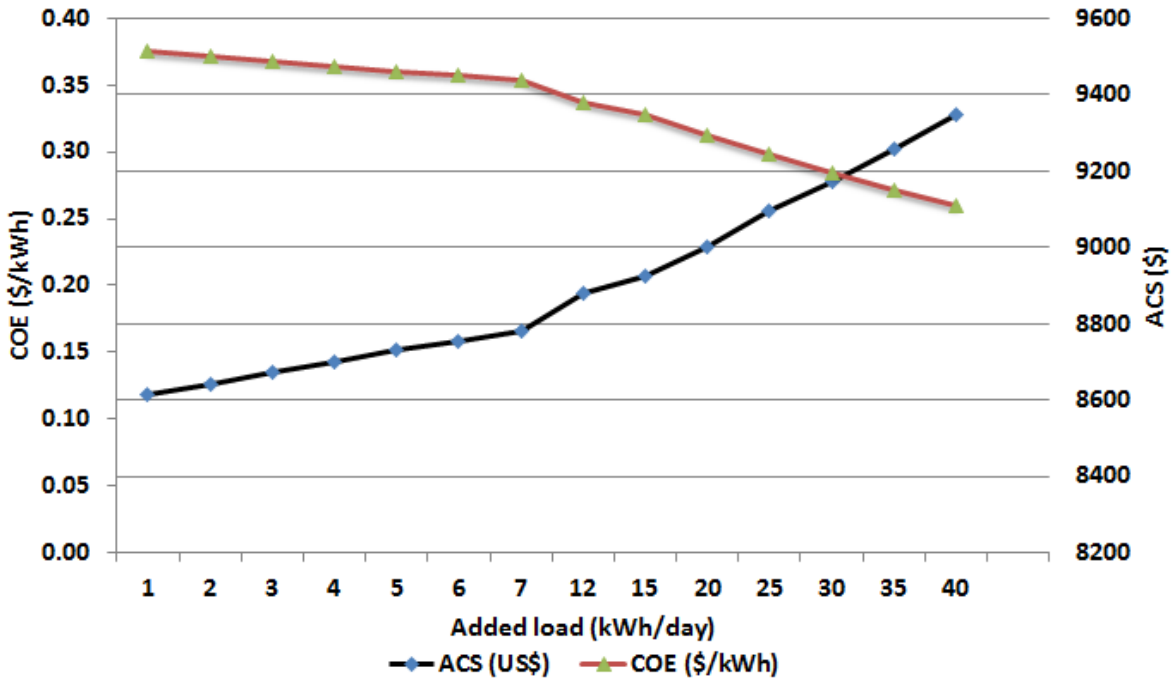

Figure 4.7: Impact of load variation on the NPC and COE of the system.

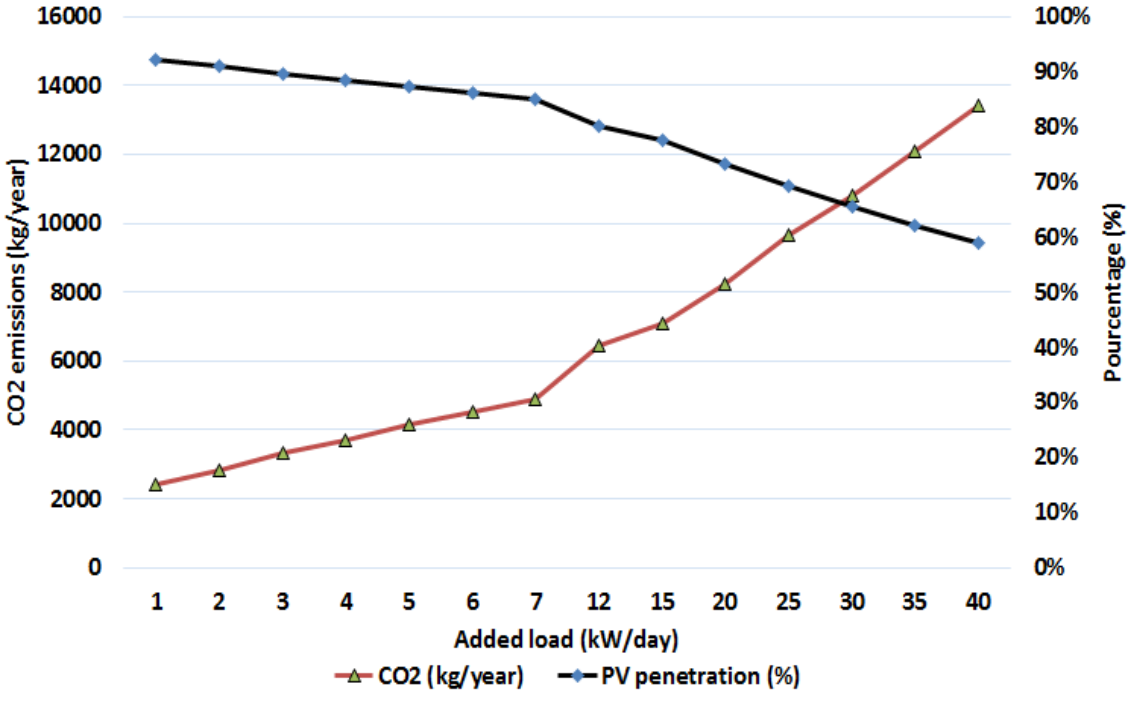

Figure 4.8: Effect of load variation on the PV penetration and CO_2 emission.

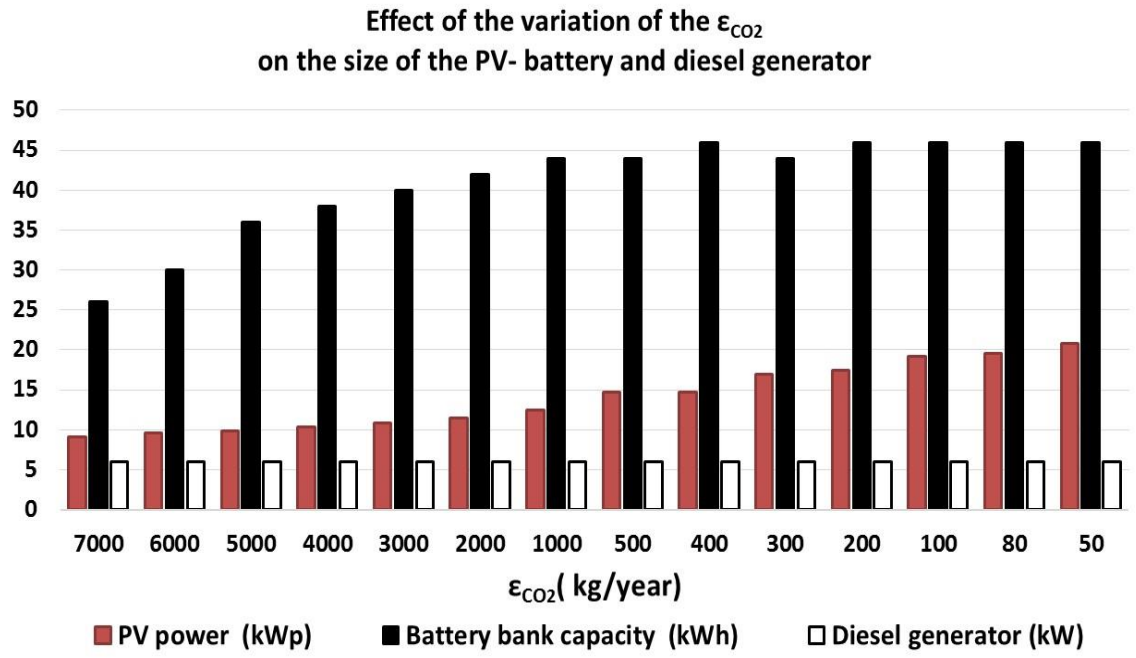

Figure 4.9: Effect of the ε_{CO2} on the size of the PV-battery and diesel generator.

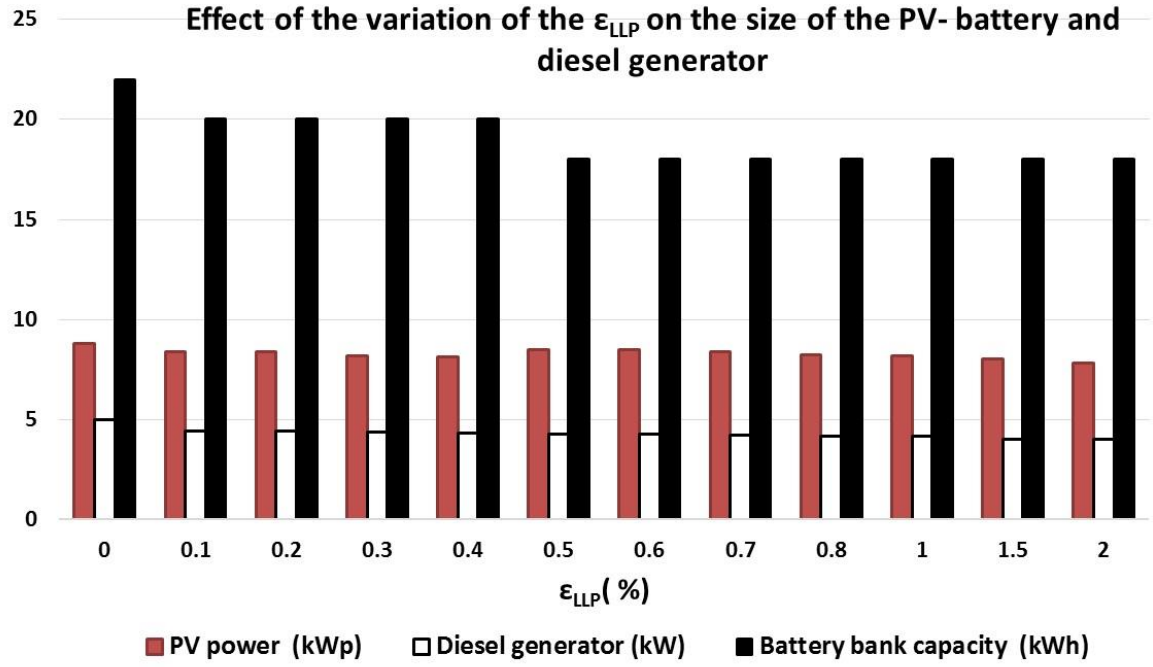

Figure 4.10: Effect of the ε_{LLP} on the size of the PV-battery and diesel generator.

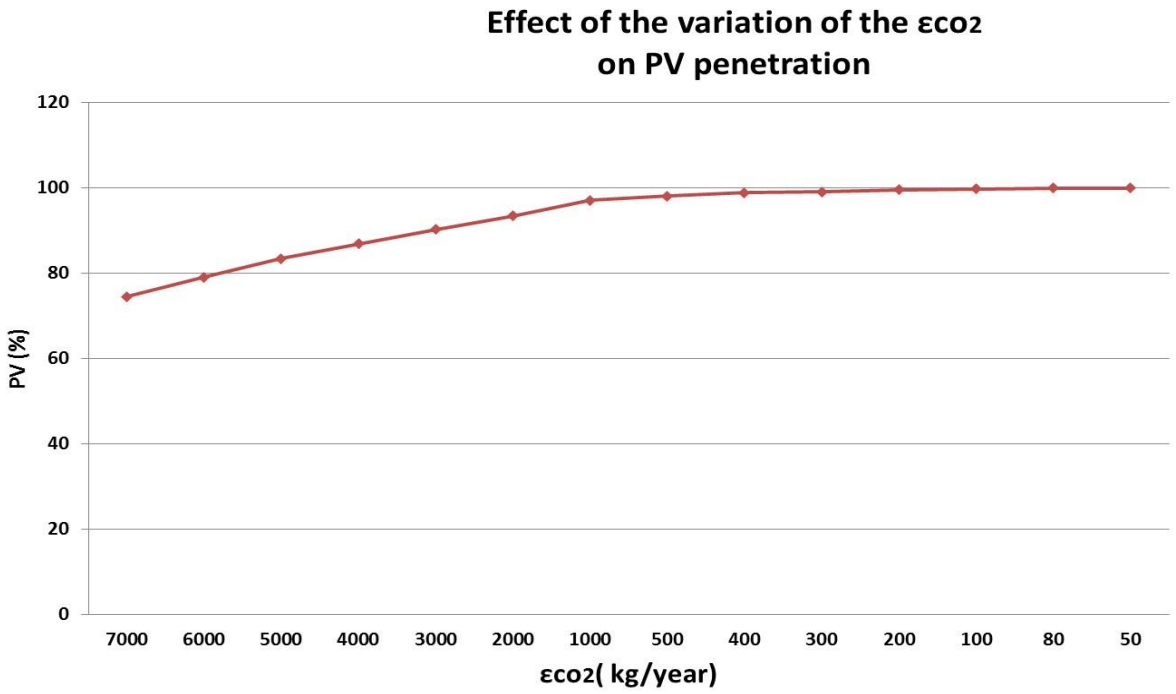

Figure 4.11: Effect of the variation of the ε_{CO2} on the PV penetration.

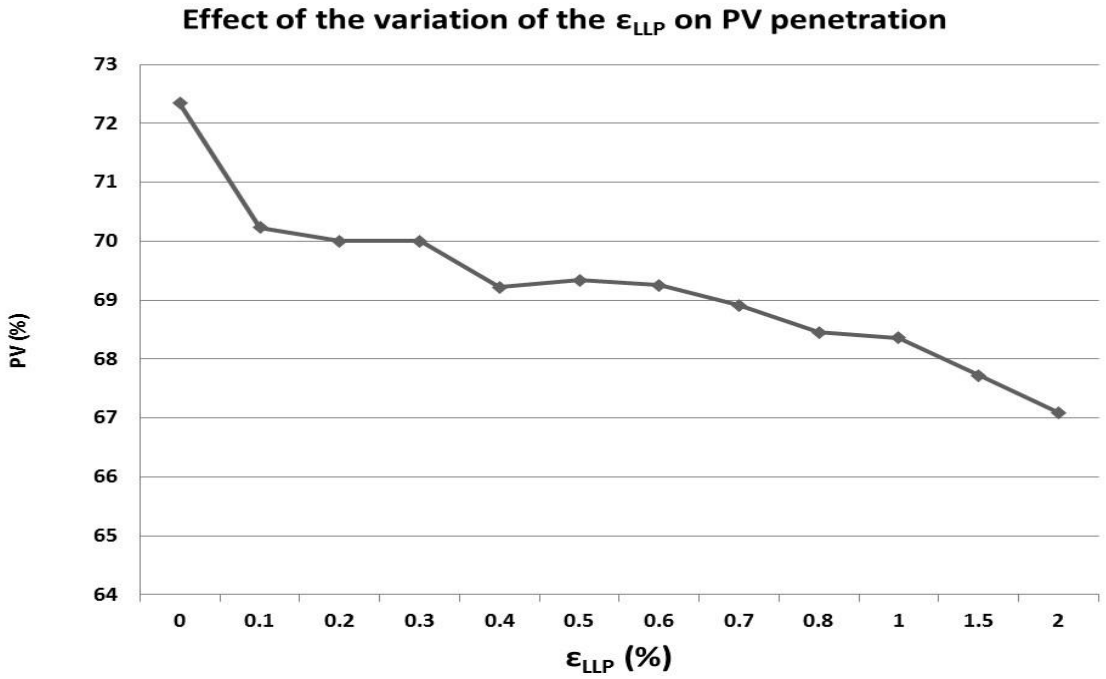

Figure 4.12: Effect of the variation of the ε_{LLP} on the PV penetration.

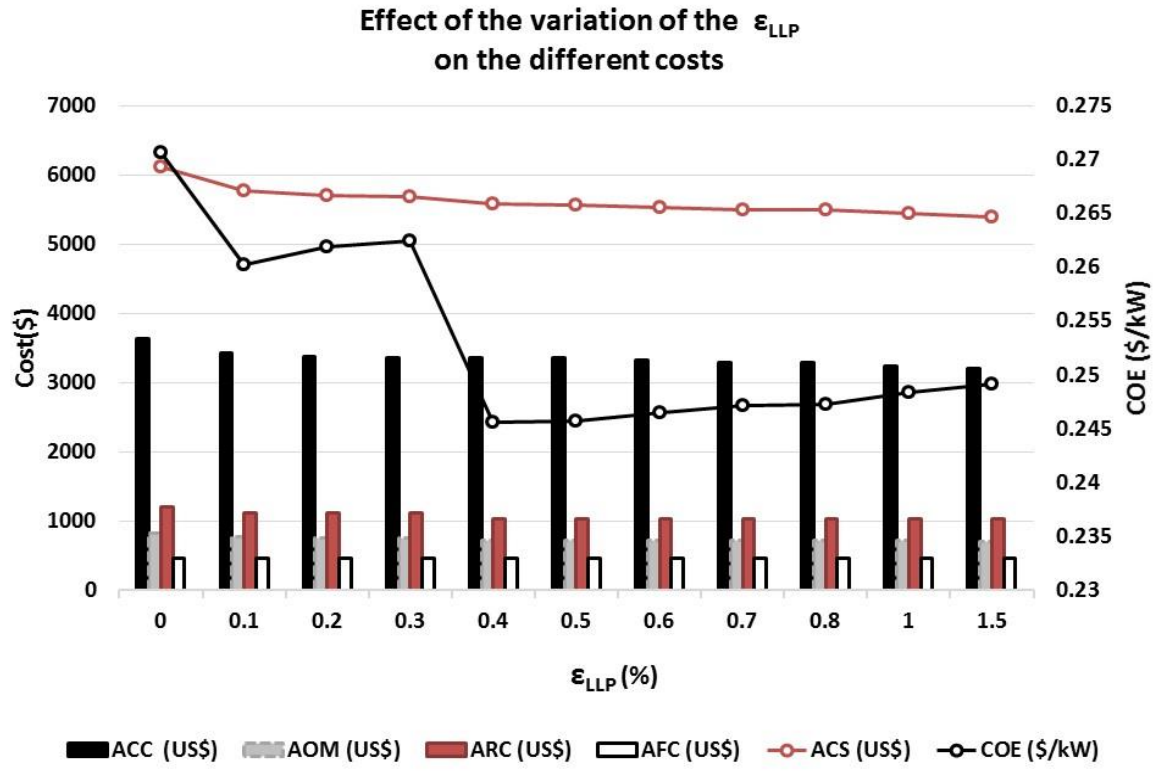

Figure 4.13: Effect of the variation of the ε_{LLP} on the different costs.

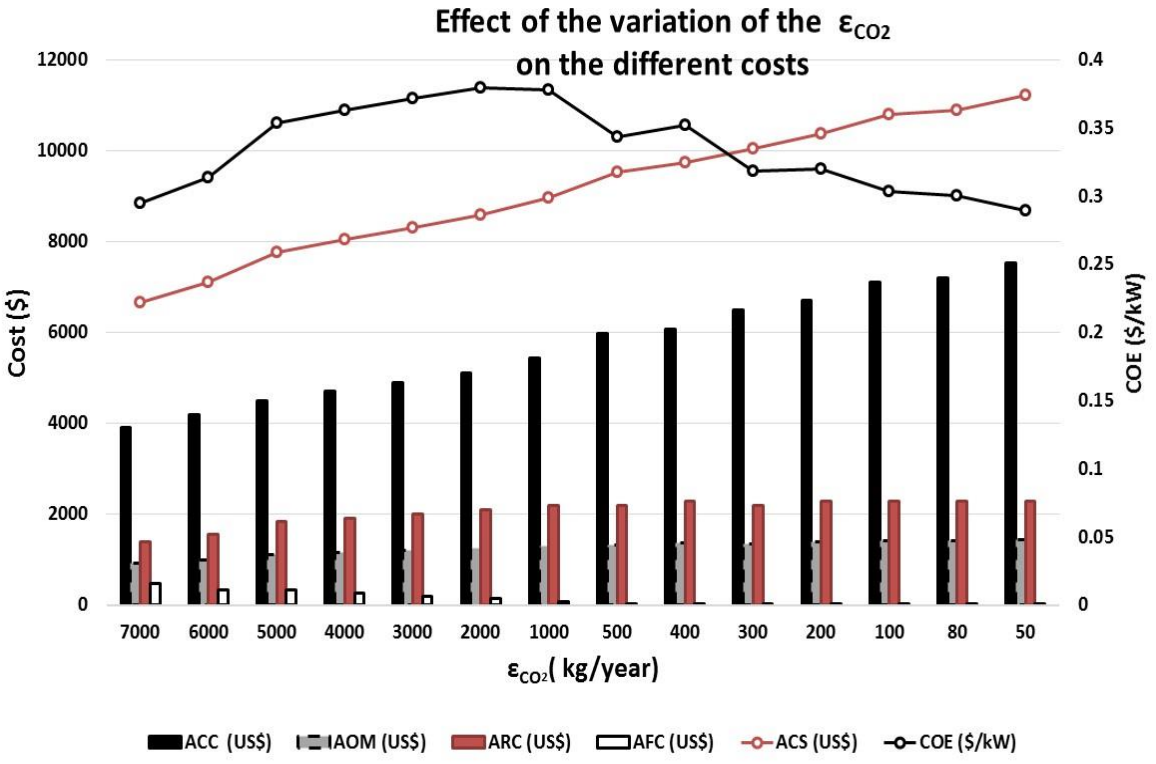

Figure 4.14: Effect of the variation of the ε_{CO2} on the different costs.

4.4.2. Analysis of the PSO based approach results

An optimization model based on PSO and ε-constraint method is effectively established to search for the optimal design of an off-grid hybrid PV-diesel-battery system as rural reliable electrification solution. Three objectives functions are considered (annualized cost of the system ACS, loss of load probability LLP, and CO_2 emissions). Hybridizing PSO with other algorithms can complicate the system, but in our case, the ε-constraint method is used to handle constraints and multiple objectives of the system with simplicity and computational efficiency. The results indicate that the optimal system satisfies 100 % of the load demand, the COE of the optimal system is 0.38 $/kWh, the PV penetration is 93 %, the CO2 emission is 1994 kg/year and the dominant cost of the system is the cost of the Battery bank (51%) plus the PV subsystem (33%). A sensitivity analysis is performed on three parameters shows that the load consumption growth has direct impact on reducing the PV penetration and increasing the COE of the system, whereas, the diesel generator satisfies the supplementary load. The fuel consumption, the CO_2 emission and the O&M cost also increase, which leads to increase the ACS. Moreover, The CO_2 emissions constraint ε_{CO2} strongly affects the cost of the system, the size of the battery bank and the size of the PV panels. Decreasing the ε_{CO2} has increased the ACS, PV penetration and the size of the PV panels, and the capacity storage of the battery bank. It is also found that decreasing the ε_{LLP} has increased the ACS and the size of the PV subsystem and the battery bank.

4.5. Techno-economic approach results

An annual growth of the load will be expected during project lifetime and it will affect the share of each energy source in the hybrid system [70]. Also providing fuel and maintenance to isolated and rural villages is very difficult, so we are chosen a PV penetration in the range of 80% to maintain the supply of the load demand.
Sites with the same number of households have the same technical and economic inputs.

4.5.1. Input data

Simulation and analysis of the systems were performed by inserting resources data, economic constraints, control methods, and inputs on component types, their

numbers, costs, efficiency, longevity, etc. Description of these components is given in the following section:

- Dispatch strategy:

  The cycle charging strategy is used as a dispatch strategy, so when the diesel generator is operating, it uses as much power as possible to charge the batteries in addition to meet the load consumption.
- PV array:

  A PV module (CEM200M-72) made in Algeria by Condor company is used in this study. The cost of PV module is (111150 DA/kW) [161]. Taking on consideration the installation and transportation costs, in this study the capital cost of the PV module is 2300 $/kW. The operating and maintenance cost is 23 $ (1% of the capital cost [162]), the replacement cost is specified as zero, lifetime is 20 years, no tracking system, and the effect of temperature is considered. Table 4.4 shows the technical characteristics of the PV module [163].
- Battery bank:

  The Lead Acid Battery Hoppecke 24 OPzS 3000 is used in this study. The capital cost of the battery is 0.4 $/ Wh [164] , the replacement cost is 0.4 $/Wh, the operating and maintenance cost is 10 $/year, the bus voltage is 48 V, minimum battery life is considered 6 years.
- Bidirectional converter:

  The capital cost of the converter is 0.711 $/W, the replacement cost is 0.711 $/W, the operating and maintenance cost is 7 $/year, lifetime is 15 years, and the efficiency is 95 % as a rectifier and 98% as an inverter
- Diesel generator:

  The CUMMINS diesel generator with rated power of 40 kW is chosen. The table 4.5 outlines the diesel generator fuel consumption per hour in liter. The capital cost of the diesel generator is considered 300 $/kW, the replacement cost is 300$/kW, the operating and maintenance cost is 0.05 $/hr, lifetime (operating hours) is 15000 hours. Taking into account the transportation costs, the fuel price is specified as 0.2 $/L.

- A random variability is used (day to day variability = 15 % and time step to time step variability = 20 %) in the load profile. The project lifetime is 20 years and the annual real interest is 6%.

Table 4.4: CEM200M-72 module characteristics.

Technical characteristics	
Dimensions	1580 mm x 808 mm x 45 mm
PV module rated power	200 Wp
Maximum Voltage	36.9 V
Maximum current	5.42 A
Open circuit voltage	45.6 V
Short Circuit Voltage	5.80 A
NOCT	45 $\pm$ 2° C
Efficiency	13 %

Table 4.5: the diesel generator fuel consumption per hour in liter.

Output Power (kW)	**Fuel Consumption (L/hr)**
½ load	7.27
¾ load	9.54
Full load	12.72

4.5.2. Results and discussion

Three electrification scenarios have been considered to electrify the village of Terhananet: standalone PV system, a diesel generator based power system and hybrid PV-diesel-battery system. A comparison between these systems has been analyzed. Afterwards, a sensitivity analysis has been performed to evaluate the system's behavior under different operating inputs. The parameters are: the price of the fuel and the load consumption. Furthermore, the others un-electrified villages have been sized and simulated to evaluate the techno-economical and environmental performance of the hybrid PV-diesel-battery system in different locations of the province and discuss the contribution of the hybrid system in the enhancement of the electrification situation in the province of Tamanrasset.

All system configurations have been simulated in search of feasible systems that satisfy the technical constraints at the lowest life-cycle cost [105]. The optimal solutions or the optimization results are feasible systems with the minimum total net present cost (NPC) and the minimum cost of energy (COE).

4.5.2.1 Simulation and comparison

The hybrid PV-diesel-battery system with 82% of PV penetration consists of a PV generator of 50 kWp, DG of 40 kW, battery bank of 288 kWh and converter of 40 kW. The system produce enough energy to cover the load consumption without any unmet load (84951 kWh/yr from PV and 18944 kWh/ yr from the DG), the excess of energy is about 7.32 % of the energy production and the autonomy of the battery is 20.5 hours with an expected lifetime of 9.32 years. The fuel consumption of the hybrid system is 38122 l/yr. The NPC of the hybrid system is 471093 $ and COE of the system is 0.477 $/kWh.

The DG based system consists of diesel generator with 40 kW rated power. The system satisfies the load consumption without any unmet load, the excess of energy reaches 30.5 % and the annual fuel consumption is 618210 L. The NPC of the system is 1706093 $ and the COE is 1.72 $/kWh.

The standalone PV system consists of a PV generator of 76 kWp, battery bank of 576 kWh and converter of 40 kW. The energy produced is 129126 kWh/ yr, which it is enough to cover the load demand, the excess is 26 %, the autonomy of the battery is 18.2 years, the NPC of the system is 489479 $ and the COE is 0.496 $/kWh.
Table 4.6 summarized the techno-economic and environmental results between the three systems. It has been found that:

- The initial capital cost of the diesel generator based system is the smallest compared to the initial capital cost of the hybrid system and the standalone PV system, but the fuel cost and O&M cost of a diesel generator is very high (represent respectively 83 % and 11 %) resulting to the highest COE and NPC. Likewise, the DG based system has the high electricity excess (30.5%) and the highest quantity of released dioxide carbon (1.62 tons of carbon dioxide) with other pollutants.
- The standalone PV system is the most environmental effective with zero emissions. The capital cost is the dominant cost of the system with 92 %, the cost of the battery

bank and the PV generator represent respectively 45 % and 34 % of the total cost of the system.

- The hybrid PV-diesel-battery system with 82% of PV penetration is the most cost effective compared to the other two systems with lowest COE (0.477 $/kWh). Furthermore, the hybrid system has the lowest electricity excess (7.32%), also it has the shortest breaking grid extension distance (12.6 km) which is the Economical Distance Limit (EDL) from the grid at which the net present cost of grid extension equals the net present cost of the hybrid system, figure 4.15 shows the electrification cost between the grid extension and the hybrid PV-diesel-battery system. The results show that the hybrid system will be more cost effective for a community situated at a distance greater than 12.6 km from the national grid, otherwise it will be better to use the extension of national grid. This hybrid PV-diesel-battery system is better option than the grid extension for the selected community, because our village is at 30 km from the transmission line of the national grid.

Figure 4.15: Comparison of the electrification cost between the grid extension and the hybrid PV-diesel- battery system.

Based on the results obtained from the comparison of the three systems, the hybrid system can be considered the best scenario for the electrification of the rural village economically and technically. Also, the hybrid system can reduce the GHG emission of DG based system about 93%. So, the hybridization of the DG system can

combine the benefits and reduce the disadvantages of both systems (DG based system and PV standalone system).

4.5.2.2. Sensitivity analysis

Sensitivity analysis is performed to evaluate the system's behavior under different operating inputs. The parameters are: the price of the fuel and the load consumption. The figure 4.16 is a surface plot that shows the effect of the variation of the fuel price and load consumption on COE of the system, the range of the fuel price is 0.2 $/L - 1.4 $/L and the range of load consumption is 236 kWh/d - 280 kWh/d. The load consumption is represented on the x-axis, and diesel price variation on the y-axis. As the load consumption increases, the NPC and the COE of the system increase as well due to the increase in the fuel cost. The same thing happened to the diesel price, the NPC increases as well as the diesel price increases.

Table 4.6: Comparison between DG system, Standalone PV system and hybrid PV-diesel-battery system.

Parameters	**DG based system**	**hybrid PV-diesel- battery system**	**Standalone PV system**
Fuel consumption (L/yr)	618210	38122	0
Excess of electricity (%)	30.5	7.32	10.6
NPC ($)	1706093	471093	561243
COE ($/kWh)	1.72	0.477	0.568
Capital ($)	12000	270640	518940
Replacement ($)	76201	117653	1867
O&M ($)	200930	33240	36348
Fuel ($)	1418164	87451	0
Salvage ($)	-1202	-37891	-5912
Carbon dioxide (kg/yr) (CO2)	1627950	100387	0
Carbon monoxide (kg/yr) (CO)	4018	248	0
Unburned hydrocarbons (kg/yr) (UHC)	445	27.4	0
Particulate matter (kg/yr) (PM)	303	18.7	0
Sulfur dioxide (kg/yr) (SO2)	3269	202	0
Nitrogen oxides (kg/yr) (NOX)	35856	2211	0
Breaking grid extension distance (km)	54.5	12.6	13.2

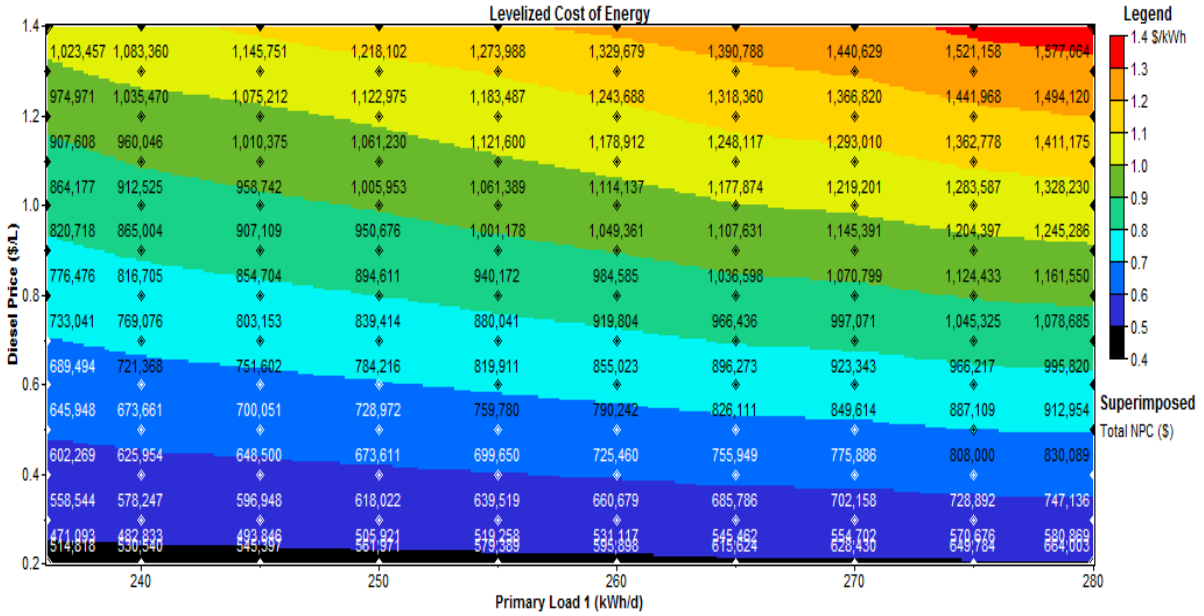

Figure 4.16: Effect of the variation of the fuel price and load consumption on COE of the system.

4.5.2.2.1. Variation in fuel price

The fuel price can vary significantly based on market price, region, and transportation costs. The rise in the fuel price increase steadily the NPC and COE of the system, the NPC increased from 471092 $ to 1023456 $ (an increase of 552364 $), and the COE increased from 0.476 $/kWh to 1.03 $/kWh (see figure 4.17).

As shown in figure 4.18, the increase in the diesel price reduces the battery life from 9.32 years to 9.25 years, as for the excess of electricity fraction, the excess decreases from 7.32 % to 7.12 % when the diesel price increase from 0.2 $/l to 1.2 $/l, then the excess increases it can be explain by the variation in marginal cost of the dispatchable power source (generators, battery bank), which is negligible in both cases, the same for the renewable fraction, it increases in little way as well as the diesel price increases (see figure 4.19), as for the breakeven distance for grid extension, the distance varies from 12.5 km to 31.5 km, as mentioned before, the village is at 30 km from the grid, meaning that the hybrid system becomes no longer the best option for the village electrification at diesel price above 1.3 $/L , this is due to the increase in the NPC of the system.

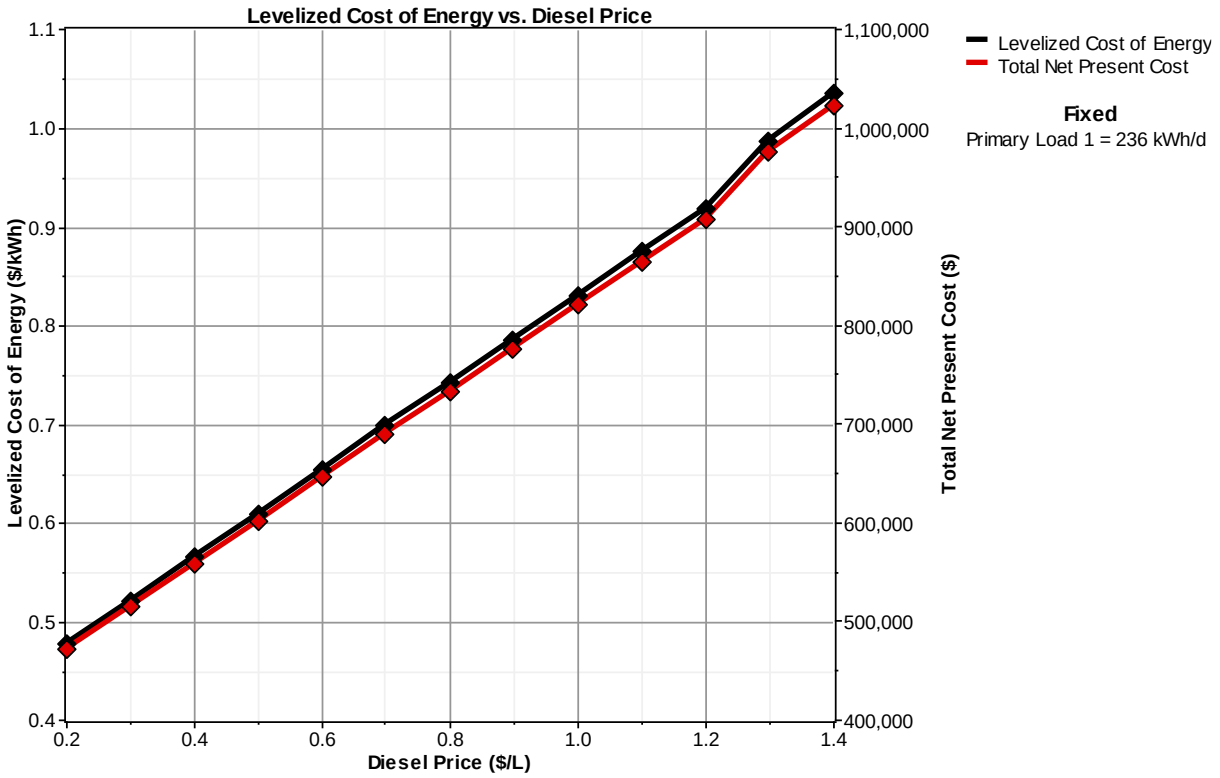

Figure 4.17: Effect of the variation of the fuel price on NPC and COE of the system.

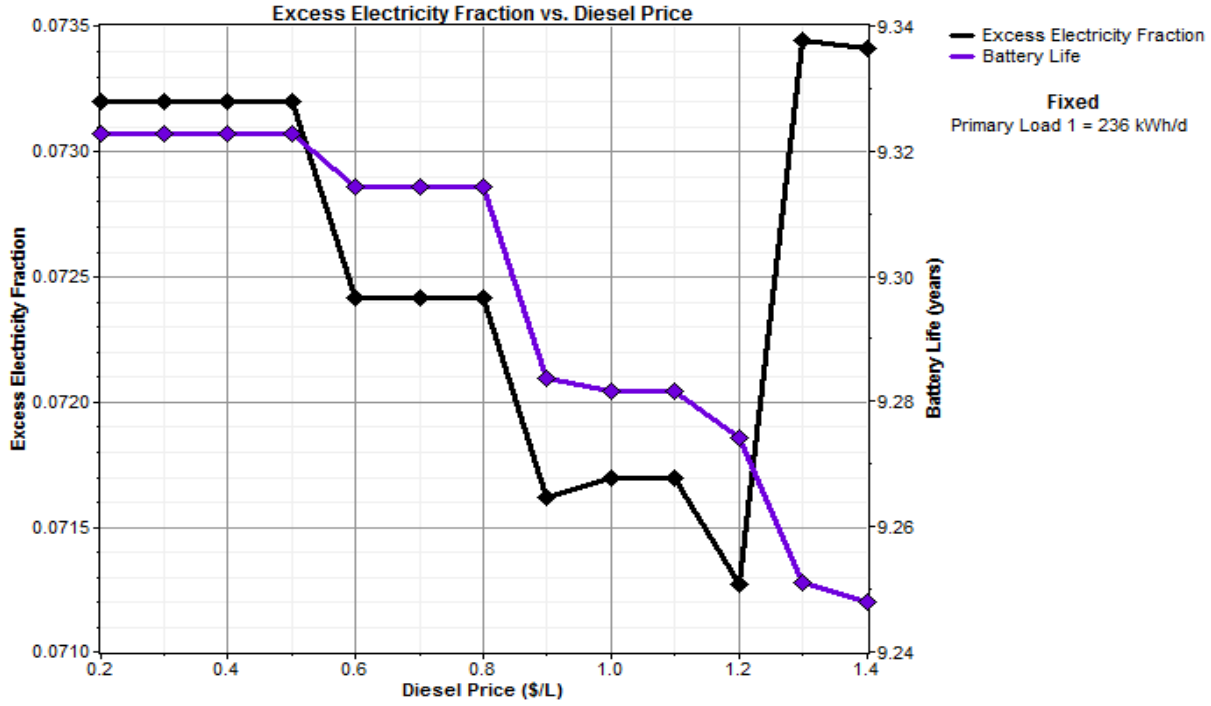

Figure 4.18: Effect of the variation of the fuel price on battery life and excess electricity fraction of the system.

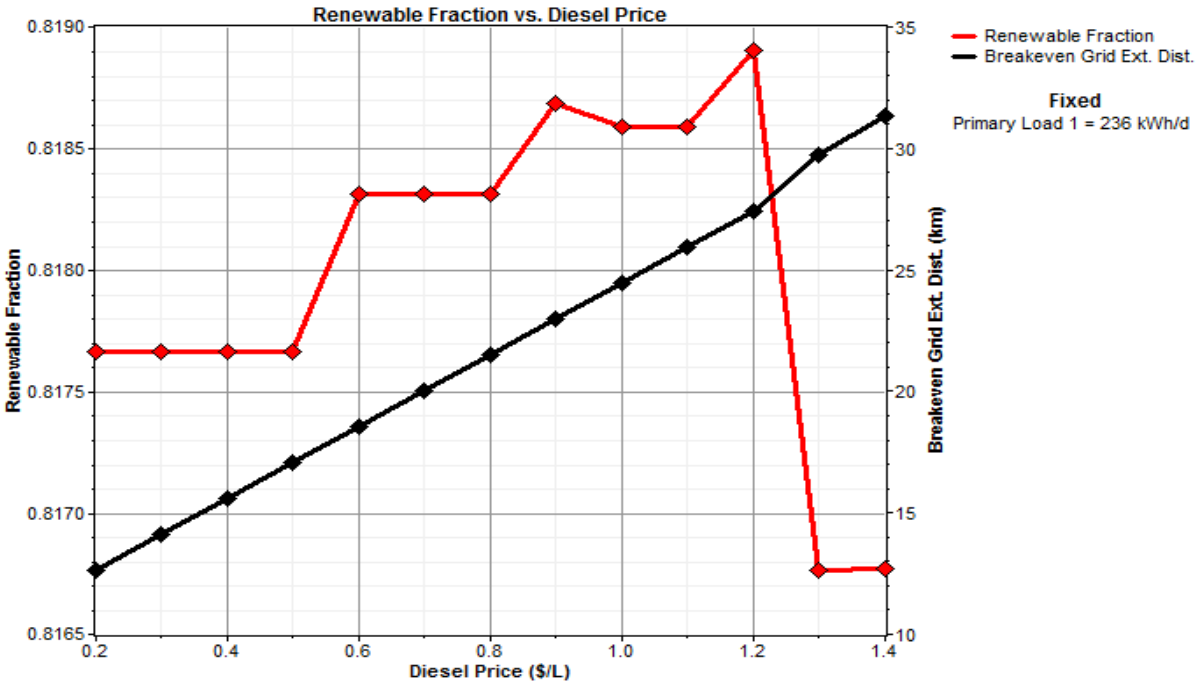

Figure 4.19: Effect of the variation of the fuel price on PV fraction and breakeven grid extension distance of the system.

4.5.2.2.2. Variation of the load demand

The electricity consumption of a rural village expects to increase after the installation of the hybrid system, this growth is caused mainly by adding new electrical appliances to the load consumption, also the emerging of new needs as result of the annual growth of the community. In our case we increase the load consumption from 236 KWh/d to 280 kWh/d, the sizes of PV, battery bank, and diesel generator are remained the same. As shown in figure 4.20, the NPC of the system increased from 471092 $ to 580869 $ (an increase of 18.8 %). COE also increase from 0.476 $/kWh to 0.496 $/kWh due to the increasing of O&M costs and the increasing of fuel cost, the system relies mainly on diesel generator to cover the capacity shortage. As result, the PV penetration decreases from 81% to 70%. The breakeven distance for grid extension varies from 12.5 km to 15.9 km, meaning that the hybrid system remains better than the extension of the grid to electrify the village (see figure 4.21). The increasing of the fuel consumption from 38122 l/yr to 72246 l/yr increases the CO_2 emissions from 100387 kg/yr to 190863 kg/yr as shown in figure 4.22. The battery lifetime and the electricity excess fraction decrease from 9.32 yr to 8.34 yr and from 7.32 % to 47.4 % respectively as shown in figure 4.23.

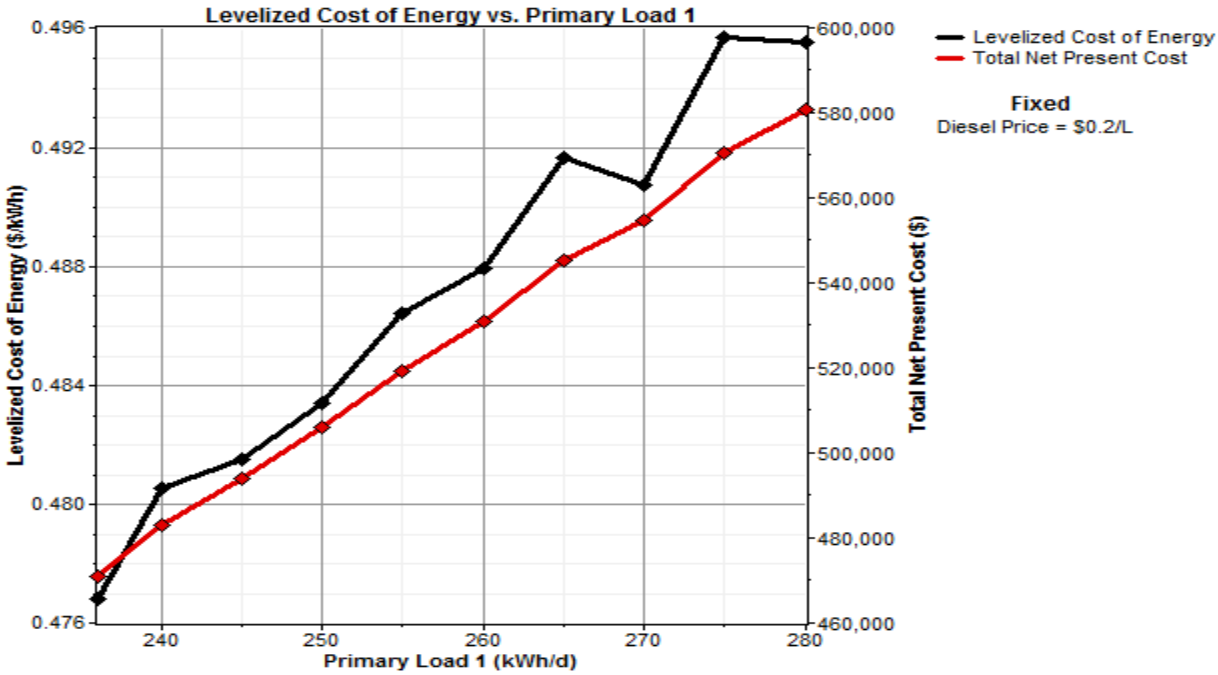

Figure 4.20: Effect of the variation of the load demand on NPC and COE of the system.

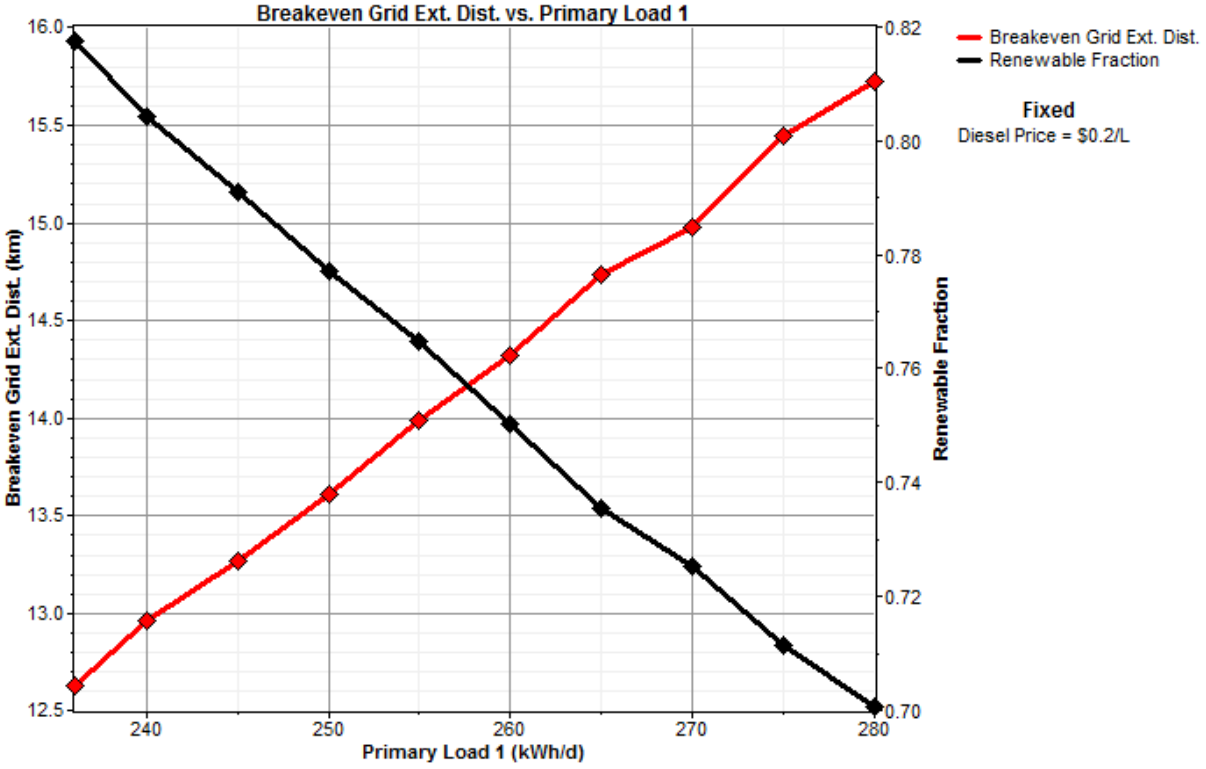

Figure 4.21: Effect of the variation of the load demand on PV fraction and breakeven grid extension distance of the system.

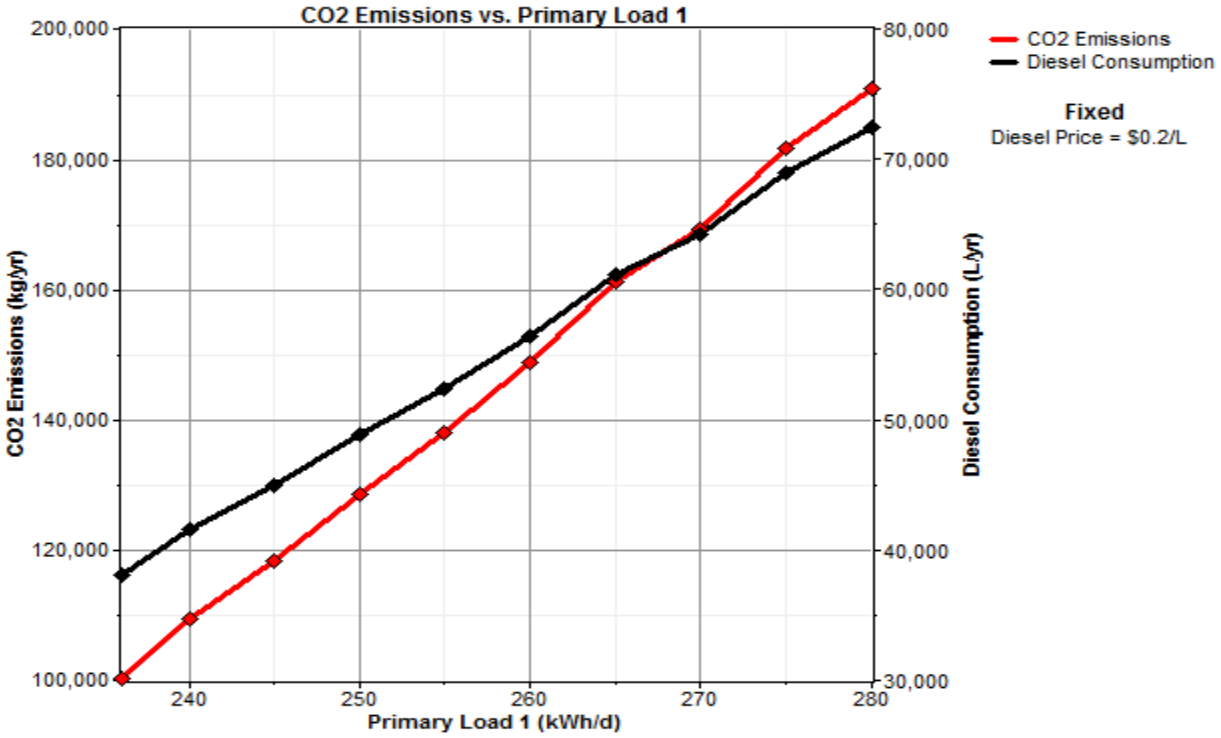

Figure 4.22: Effect of the variation of the load demand on diesel consumption and CO_2 emissions of the system.

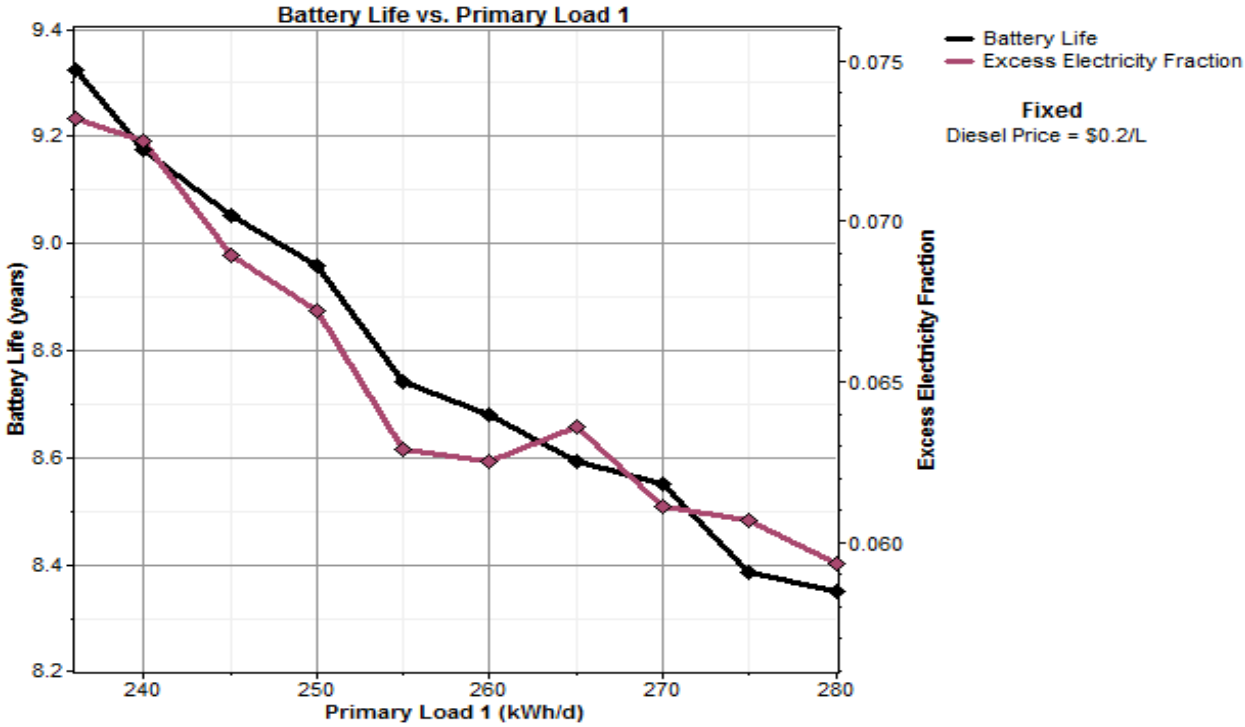

Figure 4.23: Effect of the variation of the load demand on battery life and excess electricity fraction of the system.

4.6. Feasibility of the hybrid PV-diesel-battery system

To study the feasibility and suitability of utilizing hybrid PV-diesel-battery energy system as electrification solution, the proposed hybrid system is used to meet the energy requirement of six other villages with different meteorological data and load consumption in the province of Tamanrasset, the locations of these villages are shown in figure 4.2. The energetic, economic and environmental results are summarized in tables 4.7, 4.8 and 4.9 respectively.

4.6.1. Energetic impact of the hybrid PV-diesel-battery system

The hybrid system supplies the load consumption in all villages without an unmet load, the PV penetration ranges between 84 % and 87 %, the excess of energy is between 4.16 % and 8.38 %. The villages of Ksar lamrabtine and Tin Tabarine have the same load consumption as Terhananet and the same optimal solution (PV generator of 50 kWp, diesel generator of 40 kW, 288 kWh battery bank and converter of 40 kW rated power) with slight difference in the performance of the hybrid system. The village of Tin Tabarine has the highest PV penetration (87 %) which means less diesel consumption. this can be explained by the fact that the village of Tin Tabarine has a bit more favorable meteorological conditions (solar potential and ambient temperature) compared to ksar Lamrabtine and Terhananet.

The load demand in the villages of Mertoutek and Taghaouhaout is the same (471 kWh/day). The optimal solution is (PV generator of 95 kWp, diesel generator of 80 kW, 576 kWh battery bank and converter of 80 kW rated power), the PV penetration in Mertoutek (85 %) is a bit more than Taghaouhaout (84 %), resulting in 6.22 % more diesel consumption, 7.74 % decrease in the electricity excess and 1.85 % augmentation in the NPC of the hybrid system in Taghaouhaout. The lowest electricity excess is obtained in the village of Moulay lahcen (4.16 %). With capacity of 338 kW of PV, 280 kW of diesel generators and 2064.6 kWh of batteries, the total electrical production of the systems is 722915 kWh/year including 617331 kWh/year from PV (85.39 %) and 105584 kWh/year (14.6 %) from diesel generators. From the energetic results, it is clear that the hybrid PV-diesel-battery system is a suitable and a reliable electrification solution to all the investigated villages due to the favorable meteorological conditions such as the high solar radiation.

The hybrid PV-diesel-battery system can enhance the electrification situation of the province by providing access to electricity to households located in remotes and rural un-electrified villages.

4.6.2. Economic viability of the hybrid PV-diesel-battery system

The economic viability of the hybrid PV-diesel-battery system is influenced by the optimal system size. The capital cost the system is very decisive in the decision-making process. The capital cost represents a significant share in the NPC of the system, it ranges between 50.7 % (Taghaouhaout) and 69.2 % (Moulay Lahcen). The battery bank is the dominant cost in all villages and it varies between 50.05 % (Moulay Lahcen) and 37.9 % (Taghaouhaout). The COE of the hybrid system ranges between 0.44 $/kWh (Ilamane) and 0.529 $/kWh (Taghaouhaout).

The village of Taghaouhaout has the highest COE (0.529 $/kWh). The village of Ilamane has the lowest COE (0.44 $/kWh) followed by the village of Moulay Lahcen (0.446 $/kWh). The Hybrid PV-diesel-battery system can be considered as the optimal economic solution compared to the diesel only system, PV standalone system and grid extension.

If the grid is extended to the rural villages during the lifetime of the hybrid system the hybrid system can be interconnected to the national grid, the diesel generator and the battery bank will not be required any more. Then the hybrid system will consist only by the PV subsystem and the inverter, thus the energy generated by the hybrid system can be sold to the national grid.

4.6.3. Environmental impact of the hybrid PV-diesel-battery system

According to the IPCC, the anthropogenic greenhouse gas (GHG) emissions contributing most evidently to Global Warming in terms of relative radiative forcing are CO_2, CH_4, halocarbons and N_2O, CO_2 dominates GHG emissions. About 77% of annual CO_2 emissions world-wide originate from fossil-fuel combustion [165]. The influence of the GHG emissions on the environment as well as on human health must be considered in the reliability and long term performance of the systems. In addition to the electrification role, the hybrid PV-diesel-battery system will also have a significant environmental impact, mainly due to the reduction of GHG emissions on long-term basis. In our case CO_2 emissions of the hybrid PV-diesel-battery system

(which are 848.15 tonnes/year) are compared to the emissions of diesel generator system emissions. The total PV penetration of the systems is around 85 %, this means that by using the hybrid PV-diesel system, CO_2 emissions can be reduced by 4806.2 tonnes/year compared with diesel generator based system.

Table 4.7: Energetic results of the villages.

Sites	PV (kW)	DG (kW)	Battery (kWh)	Converter (kW)	Electrical production		Fuel consumption (L/yr)	Excess of electricity (%)	Daily Load (KWh/d)
					PV (%)	DG (%)			
Ksar lamrabtine	50	40	288	40	84	16	32763	7.58	236
Moulay Lahcen	19	16	144	17	87	13	5366	4.16	94
Ilamane	29	24	192	24	86	14	12346	6.1	141
Taghaouhaout	95	80	576	80	84	16	125982	6.43	471
Tin Tabarine	50	40	288	40	87	13	27490	8.38	236
Mertoutek	95	80	576	80	85	15	118139	6.97	471

Table 4.8: Economic results of the villages.

Sites	NPC ($)	COE ($/kWh)	PV cost (%)	Battery cost (%)	DG Cost (%)	Capital ($)	Replacement ($)	O&M ($)	Fuel ($)	Salvage ($)
Ksar lamrabtine	457256	0.463	28,03	42.9	20.83	270640	117847	31657	75157	-38044
Moulay Lahcen	176193	0.446	29.8	50.05	11.06	121987	34633	15076	12310	-7813
Ilamane	259675	0.44	28.63	47.5	15.16	167764	49373	20107	28321	-5890
Taghaouhaout	1043269	0.529	23.34	37.91	31.52	529780	237314	61720	289000	-74545
Tin Tabarine	445177	0.451	28.79	44.49	18.26	270640	118809	30097	63061	-37430
Mertoutek	1023911	0.519	23.78	38.73	30.94	529069	237531	60447	271009	-74145

Table 4.9: GHG emissions of the villages.

Sites	Carbon dioxide (kg/yr) (CO_2)	Carbon onoxide (kg/yr) (CO)	Unburned hydrocarbons (kg/yr) (UHC)	Particulate matter (kg/yr) (PM)	Sulfur dioxide (kg/yr) (SO2)	Nitrogen oxides (kg/yr) (NOX)
ksar lamrabtine	86275	213	23.6	16.1	173	1900
Moulay Lahcen	14131	34.9	3.86	2.63	28.4	311
Ilamane	32510	80.2	8.89	6.05	65.3	716
Taghaouhaout	331751	819	90.7	61.7	666	7307
Tin Tabarine	72389	179	19.8	13.5	145	1594
Mertoutek	311099	768	85.1	57.9	625	6852

4.7. Conclusion

This Chapter analyzed the potential and the feasibility of the hybrid PV-diesel-battery system as a solution to supply electricity to rural and un-electrified communities in the province of Tamanrasset. Two approaches have been considered to find the optimal system: the PSO based approach and techno-economic analysis approach.

The optimization results and sensitivity analysis of the hybrid PV-diesel-battery system in both approaches confirmed the sustainability and the techno-economical feasibility of the hybrid PV-diesel-battery system for isolated and scattered Saharan communities. Considering the meteorological data, the load demand and other characteristics of the site, we concluded that the hybrid PV-diesel-battery system is sustainable and suitable solution technically, economically and environmentally for the electrification of remote, rural communities in the south of Algeria, but the main issue of the implementation of hybrid PV-diesel-battery system was the high initial cost compared to conventional energy, however, the decreasing cost of the components of this technology and the importance given by Algeria to renewable energy specially solar energy will promote and subsidize rural electrification by integration and exploitation of this technology through the country basically in rural Saharan regions. So, the integration of the hybrid PV-diesel-battery energy system in the national and regional rural electrification programs will be a sustainable contribution to the rural development.

GENERAL CONCLUSION AND RECOMMENDATIONS

The main goal of this thesis is to design and optimize a hybrid PV-diesel-battery system and take the competitive advantages of each technology to reach a reliable and sustainable electrification solution for rural scattered communities particularly in Sahara region.

The first step of our study was the selection of a group of un-electrified villages, located far from the grid, along with detailed study on data input collection such as the local meteorological data and renewable energies resources. Next, a load profile for a rural Saharan settlement has been proposed based on an investigation nearby the inhabitants of the rural villages in the southern of Algeria. The load profile considered standard of living, traditions, behavior and habits, and it considered two hourly patterns, winter and summer patterns. Before starting the optimization phase, modelling of the hybrid PV-diesel- battery system was elaborated using mathematical models for different components of the system. Afterwards, two approaches were considered in the optimization phase, the PSO based approach and the techno-economic approach.

PSO and ε-constraint method have been used to find the optimal system in order to electrify the rural Saharan village of Tiberkatine located in the province of Tamanrasset. Three objectives functions are considered: the total cost of the system, the total CO_2 emissions produced by diesel generator, and the loss of load probability LLP. The optimization results show that the optimal size of the components (11.4 kWp of photovoltaic generator, 42 kWh of battery bank and 6 kW of diesel generator power) is enough to satisfy the load consumption without any unmet load. The cost of energy generation is estimated at 0.38 $/kWh. Considering the meteorological data, the load demand and other characteristics of the site, this methodology can be applied to optimize and size other composition of the hybrid system.

In the second approach, three electrification scenarios are considered and compared: the standalone PV system, the diesel based system and hybrid PV-diesel-battery system, the three systems have been simulated and analyzed their performance. Based on the results obtained from the comparison of the three systems, the hybrid system was the best scenario for the electrification of the rural village

economically and technically. Also, the hybrid system can reduce the GHG emissions of DG based system significantly. The hybridization of the DG system combines the benefits and reduces the disadvantages of both systems, the DG based system and PV standalone system. However, the economic viability of the hybrid system depends also on the breakeven grid extension distance from the national grid. It has been found that the long distances to the grid make the hybrid PV-diesel-battery a more acceptable electrification option for remote rural communities.

A sensitivity analysis has been performed to evaluate the system's behavior based on the variation of the load consumption and diesel price in both approaches, the results predict that the variation of load demand for the same size of the system has a strong influence on the PV penetration, the fuel consumption, and the GHG emissions, the system will rely more on diesel generator which leads to increasing the NPC and the COE of the hybrid system. As for the impact of the fuel price, the results showed that increasing the fuel price will increase directly the NPC and COE of the system as well.

To study the feasibility and suitability of utilizing hybrid PV-diesel-battery energy system as electrification solution, the proposed hybrid system is used to meet the energy requirement of six other villages with different meteorological data and load consumption in the province of Tamanrasset. Meteorological characteristics especially the global solar radiation of the site has an impact on the efficiency of the hybrid system, it appears in the performance of the hybrid system in villages with the same inputs and different geographical locations, also if the site has more favorable meteorological conditions the GHG emissions will be reduced.

The analysis of the energetic, economic and environmental potentials of the hybrid PV-diesel-battery system as an alternative to diesel generators shows that it is more capable of meeting the energy needs of the rural Saharan communities than the diesel generators. This is due to the ability of the hybrid system analyzed in this study to extend electricity availability and meet the required energy needs to 24 hours and achieve a higher level of electricity production. The hybrid PV-diesel-battery system may cost more to implement than diesel generator, but the advantage of higher electricity production could justify the higher cost. Also, in Algeria, the electricity is subsidized (end users do not pay the real cost of electricity), this implies that shifting

from a diesel based power plant to PV-diesel-battery hybrid system requires the change of the subsidy from the operating costs to the initial investment, which is a substantial challenge for the utility in charge of subsidizing rural electrification. Furthermore, the decreasing cost of the components of this system will promote and help shifting from diesel only systems to hybrid PV- diesel-battery systems. Finally, we can conclude that the hybrid PV-Diesel-Battery system is sustainable and suitable solution for the electrification of remote, rural communities in the south of Algeria exactly the rural villages of the province of Tamanrasset.

To ensure a successful implementation of the hybrid PV-diesel-battery system as an electrification solution for a rural Saharan community, it is essential to provide periodic maintenance for the system, but keeping skilled personnel in rural areas is difficult, so the possibility of training local users and increasing the community awareness can overcome this constraint.

The following further studies can be conducted from this work:

- System performance monitoring for empirical validation and post-evaluation of the different impacts on the hybrid PV-diesel-battery system after the physical implementation of the system such as the variation of the load consumption on the outcomes of the hybrid system.
- Exploitation of another local renewable source such as wind energy to ensure a large share of renewable energy in the hybrid system.
- Amelioration of the storage system through the use of higher efficiency storage techniques with the modelling of operation and optimization of the energy systems.
- Study the impact of different control strategies on the behavior of the hybrid system.

APPENDIX

LIST OF SYMBOLS AND ABBREVIATIONS

A.1. LIST OF SYMBOLS

ACC	: annual capital cost	$
ACS	: Annualized cost of system	$
AFC	: annual fuel cost	$
AM	: Air Mass	
AOM	: annual operation and maintenance cost	$
A_{pv}	: total area of the photovoltaic generator	m^2
ARC	: annual replacement cost	$
$C_{ann,tot}$	: total annualized cost	
C_{Bmax}	: maximum capacity of battery	Ah
C_{Bmin}	: minimum capacity of battery	Ah
C_{cap}	: capital cost of each component	$
$C_{cycling\_bat}$	: cost of cycling energy through the batteries	$/kWh
C_{fuel}	: fuel cost of 1h DG running	$/h
C_{gen}	: DG acquisition cost plus O&M cost	$
C_N	: nominal capacity of one battery	Ah
$C_{O\&Mgen}$	: DG's hourly operation and maintenance cost	$/h
COE	: cost of energy	$/kWh
$C_{rep\_gen\_h}$	: DG hourly replacement cost	$/h
CRF	: capital recovery factor	
D(t)	: electricity demand	kWh
DF	: distortion factor	
e	: elementary charge	ev
E_{def}	: total amount of deferrable load	kWh
$E_{Diffuse}$	: Global radiation	W/m^2

E_{Direct}	: Direct radiation	W/m^2
EF	: Emissions factor for a diesel generator	kg/L
E_G	: Global radiation	W/m^2
E_{grid}	: Amount of energy sold to the grid per year	kWh
E_{prim}	: Total amount of primary load	kWh
E_S	: Solar constant	W/m^2
ET	: Equation of time	
F	: Fuel consumption of the diesel generator	l/h
f	: Annual inflation rates	
F_0	: Fuel curve intercept coefficient	l/kWh
F_1	: Fuel curve slope	l/kWh
FF	: Fill factor	
f_i	: Objective function	
g_{best}	: Global best positions	
h_S	: elevation of the Sun	o
I_{MPP}	: Maximum courant	A
I_{Ph}	: Photocurrent	A
I_S	: Saturation current	A
k	: Boltzmann's constant	J/ºK
L_d	: The critical discharge load	kWh
$Life_{gen}$	: DG lifetime	h
LT	: Legal time	
MST	: Mean solar time	
Nbat	: Number of batteries	
N_{cycles_eq}	: Number of full cycles of battery life	
NPC	:Net present cost	$
NPV	: number of PV modules	
p_{best}	: Individual best positions of particle	
P_{gen}	: Diesel generator output power in this hour	kW
P_{MPP}	: Maximum power	W
$P_{n\text{-}DG}$	: nominal power of DG	kW
Pr_{fuel}	: Fuel price	$/l
P_{Sun}	: amount of radiation from the Sun	W

Q	: Output power factor	
R_0	: Initial resistance of the fully charged battery	Ω
R_{batt}	: Resistance of the battery	Ω
R_P	: Parallel resistance	Ω
Rproj	: Project lifetime	years
R_S	: Series resistance	Ω
SFF	: The sinking fund factor	
shortage (t)	: Unmet load during time period t	kWh
T	: Temperature	^oK
T_{jref}	: reference temperature of the PV cell	^oK
TST	: True solar time	
UT	: Universal time	
V_D	: A diffusion voltage	V
v_i	: Velocity of particle	
V_{MPP}	: Maximum voltage	V
V_{OC}	: Open circuit voltage	V
V_T	: Thermal voltage	V
x_i	: Particle of swarm	
Y_{gen}	: Rated capacity of the generator	kW
y_{rep}	: Lifetime of battery banks	years
α_{sc}	: Relative temperature coefficient of short-circuit current	$/^oK$
Γ	: Day angle	rad
γ_{MPP}	: Relative maximum power temperature coefficient	$/^oK$
δ	: Solar declination	o
ε_{CO2}	: CO_2 emissions constraint	Kg/year
ε_{LLP}	: LLP constraint	%
η_{pv}	: Efficiency of the photovoltaic generator	
θ_z	: Azimuth	rad
σ	: Standard deviation	
φ	: Longitude	o
ϕ	: Latitude	o

A.2. LIST OF ABBREVIATIONS

ANN : Artificial Neural Network
BDI : Bidirectional Inverter
BSRN : Baseline Surface Radiation Network
CAISO : California Independent System Operator
EMR : Electromagnetic Radiation
FERC : US Federal Energy Regulatory Commission
FL : Fuzzy Logic
GA : Genetic Algorithms
GHG : Greenhouse gases
HES : Hybrid Energy System
ISO : International Organization for Standardization
LLP : Loss of load probability
MAE : Mean Absolute Error
MBE : Mean Bias Error Or Bias
MOEA : Multi-Objective Evolutionary Algorithms
MOP : Multi-Objective optimization
MPP : Maximum Power Point
MPPT : Maximum Power Point Tracker
MSE : Mean Square Error
NWP : Numerical Weather Prediction Models
O&M : Operation and Maintenance
PSO : Particle Swarm Optimization
PV : Photovoltaic
PVGIS : Photovoltaic Geographical Information System
RMSE : Root Mean Square Error
Satel-Light : European Database of Daylight and Solar Radiation
SDC : Societé de Distribution d'éléctricité du Centre
SDE : standard deviation or σ
SOC : State Of Charge
SoDa : The project Solar Data

STC : Standard Test Conditions

THD : Total Harmonic Distortion

VCVSI : Voltage Control Voltage Source Inverter

WMO : World Meteorological Organization

WRDC : World Radiation Data Center

WT : Wind Turbines

REFERENCES

[1] BP, “Electricity generation, BP Statistical Review of World Energy”, https://www.bp.com/content/dam/bp/business-sites/en/global/corporate/pdfs/energy-economics/statistical-review/bp-stats-review-2019-full-report.pdf

[2] IEA_indicators, “Algeria Indicators , International Energy Agency IEA”, http://www.iea.org/statistics/statisticssearch/report/?year=2014&country=ALGERIA&product=Indicators.

[3] Bank, W., “Rural population (% of total population), World Bank”, July 2016, http://data.worldbank.org/indicator/SP.RUR.TOTL?locations=DZ&view=chart.

[4] Stambouli, A.B., “Algerian renewable energy assessment: The challenge of sustainability”, Energy Policy, V. 39, n° 8, (2011), 4507-4519.

[5] Bélaïd, F., and Abderrahmani, F., “Electricity consumption and economic growth in Algeria: A multivariate causality analysis in the presence of structural change”, Energy Policy, V. 55, (2013), 286-295.

[6] Fodhil, F., Hamidat, A., and Nadjemi, O., “Performances d’une électrification rurale à l’aide d’un système hybride photovoltaïque-diesel : Cas d’un village à Tamanrasset”, in 2ème Conférence Internationale sur les Energies Renouvelables ICRE’2012, Université de Béjaia, Algérie, (15-16 Avril 2012).

[7] Häberlin, H., “Photovoltaics System Design and Practice”, Wiley, (2012).

[8] Mertens, K., “Photovoltaics: Fundamentals, Technology and Practice”, Wiley, (2014).

[9] Sen, Z., “Solar Energy Fundamentals and Modeling Techniques: Atmosphere, Environment, Climate Change and Renewable Energy”, Springer London, (2008).

[10] Stacey, F.D., “Physics of the earth”, 3rd ed, Brookfield Press, Brisbane, (1992).

[11] Iqbal, M., “An introduction to solar radiation”, Academic Press, (1983).

[12] Duffie, J.A., and Beckman, W.A., “Solar Engineering of Thermal Processes”, Wiley, (2006).

[13] Spencer, J.W., “Fourier Series Representation of the Position of the Sun,” Search, V. 2, n° 5, (1971).

[14] Quaschning, V., “Understanding Renewable Energy Systems”, Earthscan, (2005).

[15] SOLARGIS, “Global horizontal irradiation map for Algeria”, July 2017, http://solargis.com/products/maps-and-gis-data/free/download/algeria.

[16] Sonnenenergie, D.G.f., “Planning and Installing Photovoltaic Systems”.

[17] Meteonorm, “Meteonorm database”, (2017), http://www.meteonorm.com/.

[18] Benmouiza, M.K., “Quantification of solar radiation in Algeria, application to the sizing of photovoltaic systems”, Phd, Abou Bekr Belkaid, Tlemcen, (May 2015).

[19] Lacis, A.A., and Hansen, J., “A parameterization for the absorption of solar radiation in the earth's atmosphere”, Journal of the atmospheric sciences, V. 31, n°1, (1974),118-133.

[20] Bird, R.E., and Hulstrom, R.L., “Simplified clear sky model for direct and diffuse insolation on horizontal surfaces”, Solar Energy Research Inst., Golden, CO USA, (1981).

[21] Hay, J.E., and Davies, J.A., “Calculations of the solar radiation incident on an inclined surface”, In: Hay, J.E., Won, T.K. (Eds.), Proc. of First Canadian Solar Radiation Data Workshop, 59. Ministry of Supplyand Services, Canada.

[22] Liu, B.Y., and Jordan, R.C., “The interrelationship and characteristic distribution of direct, diffuse and total solar radiation”, Solar energy, V. 4, n° 3, (1960),1-19.

[23] Temps, R.C., and Coulson, K., “Solar radiation incident upon slopes of different orientations”, Solar energy, V. 19, n° 2, (1977), 179-184.

[24] Angstrom, A., “Solar and terrestrial radiation, Report to the international commission for solar research on actinometric investigations of solar and atmospheric radiation”, Quarterly Journal of the Royal Meteorological Society, V. 50, n° 210, (1924), 121–126.

[25] Garg, H., and Garg, S., “Prediction of global solar radiation from bright sunshine hours and other meteorological data”, Energy Conversion and Management, V. 23, n° 2, (1983),113-118.

[26] Hussain, M., “Estimation of global and diffuse irradiation from sunshine duration and atmospheric water vapour content”, Solar Energy, V. 33, n° 2, (1984), 217-220.

[27] Frutos, F., Ruiz, V., and Gutirrez, J., “Correlation between the solar diffuse and global radiation for Madrid”, Revue Internationale d’Heliotechnique, V. 1, (1985), 7.

[28] Page, J., “The estimation of monthly mean values of daily total short wave radiation on vertical and inclined surfaces from sunshine records 40S-40N”, in Proceedings of the United Nations Conference on New Sources of Energy: Solar Energy, Wind Power and Geothermal Energy, Rome, Italy, (1967), 378-390.

[29] Delorme, C., Gallo, A., and Olivieri, J., “Quick use of Wefax images from Meteosat to determine daily solar radiation in France”, Solar Energy, V. 49, n° 3, (1992), 191-197.

[30] Yang, K., Huang, G., and Tamai, N., “A hybrid model for estimating global solar radiation”, Solar energy, V. 70, n° 1,(2001), 13-22.

[31] Pelland, S., Remund, J., Kleissl, J., Oozeki, T., and De Brabandere, K., “Photovoltaic and solar forecasting: state of the art”, IEA PVPS, Task, V. 14, (2013),1-36.

[32] Jones, L., “Strategies and Decision Support Systems for Integrating Variable Energy Resources in Control Centers for Reliable Grid Operations - Global Best Practices, Examples of Excellence and Lessons Learned”, Alstom Grid Inc., Washington, DC, United States, (2011).

[33] Kleissl, J., “Solar Energy Forecasting and Resource Assessment”, Academic Press, (2013).

[34] Chow, C.W., Urquhart, B., Lave, M., Dominguez, A., Kleissl, J., Shields, J., and Washom, B., “Intra-hour forecasting with a total sky imager at the UC San Diego solar energy testbed”, Solar Energy, V. 85, n° 11, (2011), 2881-2893.

[35] Perez, R., Kivalov, S., Zelenka, A., Schlemmer, J., and Hemker Jr, K., “Improving the performance of satellite-to-irradiance models using the satellite’s infrared sensors”, in Proceedings of ASES Annual Conference, Phoenix, Arizona, USA, (2010).

[36] Traunmüller , W., and Steinmaurer, G., “Solar irradiance forecasting, benchmarking of different techniques and applications of energy meteorology”, In Proceedings of the EuroSun conference, (September 28 – October 1, 2010).

[37] Beyer, H.G., Polo Martinez, J., Suri, M., Torres, J.L., Lorenz, E., Müller, S.C., Hoyer-Klick, C., and Ineichen, P., “D 1.1. 3, Report on Benchmarking of Radiation Products”, Report under contract, n° 038665, (2009).

[38] Madsen, H., Pinson, P., Kariniotakis, G., Nielsen, H.A., and Nielsen, T.S., “Standardizing the performance evaluation of short-term wind power prediction models”, Wind Engineering, V. 29, n° 6, (2005), 475-489.

[39] Sayigh, A., “Photovoltaics for Sustainable Electricity and Buildings”, Springer International Publishing, (2016).

[40] Paulescu, M., Paulescu, E., Gravila, P., and Badescu, V., “Weather Modeling and Forecasting of PV Systems Operation”, 1, Springer-Verlag London, England, United Kingdom, (2013).

[41] Hukseflux, “Radiation measurement sensors”, http://www.hukseflux.com/.

[42] WMO, “Guide to meteorological instruments and methods of observation”, 7th ed, World meteorological organization No. 8 Chapters 7 and 11, (2008).

[43] Kerr, A., and Tabony, R., “Comparison of sunshine recorded by Campbell–Stokes and automatic sensors”, Weather, V. 59, nº 4, (2004), 90–95.

[44] Badescu, V., “A new kind of cloudy sky model to compute instantaneous values of diffuse and global solar irradiance”, Theoretical and Applied Climatology, V. 72, nº 1, (2002), 127-136.

[45] WRDC, “World Radiation Data Center, Main Geophysical Observatory, St. Petersburg, Russia”, http://wrdc.mgo.rssi.ru/.

[46] GEWEX, “Global energy and water cycle experiment”, http://www.gewex.org/.

[47] WCRP, “World climate research programme”, (2017), https://www.wcrp-climate.org/.

[48] PVGIS, “PVGIS, Photovoltaic Geographical Information System”, (2017), http://re.jrc.ec.europa.eu/pvgis/download/download.htm.

[49] Satel-Light, “European database of daylight and solar radiation”, (2017), http://www.satel-light.com.

[50] SODA, “Solar radiation data”, (2017), http://www.soda-is.com/eng/index.html.

[51] HelioClim, “HelioClim server, Centre Energetique et Procedes of Ecole des Mines de Paris”, (2017), http://www.soda-pro.com/help/helioclim/helioclim-3-overview.

[52] SMSE, “NASA surface meteorology and solar energy”, (2017), http://eosweb.larc.nasa.gov/sse/.

[53] WEC, “Survey of energy resources, World Energy Council”, (2017), http://ny.whlib.ac.cn/pdf/Survey_of_Energy_Resources_2007.pdf.

[54] Isabella, O., Jäger, K., Smets, A., van Swaaij, R., and Zeman, M., “Solar Energy: The physics and engineering of photovoltaic conversion, technologies and systems”, UIT Cambridge Limited, (2016).

[55] Wenham, S.R., “Applied photovoltaics”, Routledge, (2012).

[56] Einstein, A., “Über einen die Erzeugung und Verwandlung des Lichtes betreffenden heuristischen Gesichtspunkt”, Annalen der physik, V. 322, n° 6, (1905), 132-148.

[57] Chapin, D.M., Fuller, C., and Pearson, G., “A new silicon p-n junction photocell for converting solar radiation into electrical power”, Journal of Applied Physics, V. 25, n° 5, (1954), 676-677.

[58] Reynolds, D., Leies, G., Antes, L., and Marburger, R., “Photovoltaic effect in cadmium sulfide”, Physical Review, V. 96, n° 2, (1954), 533.

[59] NASA, “International Space Station Imagery, ISS017-E-012652”, (2017), https://spaceflight.nasa.gov/gallery/images/station/crew-17/html/iss017e012652.html.

[60] Chowdhury, S., Sumita, U., Islam, A., and Bedja, I., “Importance of policy for energy system transformation: Diffusion of PV technology in Japan and Germany”, Energy Policy, V. 68, (2014), 285-293.

[61] Masson, G., Latour, M., Rekinger, M., Theologitis, I., and Papoutsi, M., “Global Market Outlook for Photovoltaics 2013–2017”, European Photovoltaic Industry Association, Brussels, Belgium, (2013), 12-32.

[62] Rekioua, D., and Matagne, E., “Optimization of photovoltaic power systems: modelization, simulation and control”, Springer Science & Business Media, (2012).

[63] NREL, "best research cell efficiency," November 2019, https://www.nrel.gov/pv/assets/pdfs/best-research-cell-efficiencies.20190802.pdf.

[64] Edoff, M., “Thin film solar cells: research in an industrial perspective”, Ambio, V. 41, n°. 2, (2012), 112-118.

[65] “Organic solar cells”, (2017), http://www.iapp.de/iapp/agruppen/osol/?research:organic_solar_cells:basics_of_osc.

[66] Schaefer, O., Willborn, S., Goeke, S., Toledo, J.A., Cassagne, V., and Roesch, A., “Self Consumption of PV Electricity”, EPIA, (2013).

[67] Sumathi, S., Kumar, L.A., and Surekha, P., “Solar PV and wind energy conversion systems: an introduction to theory, modeling with MATLAB/SIMULINK, and the role of soft computing techniques”, Springer, (2015).

[68] Muselli, M., Notton, G., and Louche, A., “Design of hybrid-photovoltaic power generator, with optimization of energy management”, Solar energy, V. 65, n°. 3, (1999), 143-157.

[69] Wies, R., Johnson, R., Agarwal, A., and Chubb, T., “Economic analysis and environmental impacts of a PV with diesel-battery system for remote villages”, IEEE Transactions on Power Systems, V. 20, nº 2, (2005), 692-700.

[70] Lena, G., “Rural Electrification with PV Hybrid Systems: Overview and Recommendations for Further Deployment”, International Energy Agency Photovoltaic Power Systems Programme and Club of African National Agencies and Structures In Charge Of Rural Electrification, (2013).

[71] Gergaud, O., Multon, B., and Ahmed, H.B., “Analysis and experimental validation of various photovoltaic system models”, In ELECTRIMACS, (2002), 6.

[72] Jones, C., “Underwood a modeling method for building-integrated PV systems,” Solar Energy, V. 70, n°. 4, 349.

[73] Patel, M., “Wind and solar power systems”, CRC Press LLC, (2005).

[74] Markvart, T., “Solar electricity”, John Wiley & Sons, (2000).

[75] Linden, D., “Handbook of batteries and fuel cells”, 3rd edn, Mcgraw-Hill, New York, (2002).

[76] Divya, K., and Østergaard, J., “Battery energy storage technology for power systems—An overview”, Electric Power Systems Research, V. 79, n° 4, (2009), 511-520.

[77] Achaibou, N., “Introduction to study storage system in a photovoltaic system”, J Renew Energy CDER, (1999), 1-6.

[78] Zoroofi, S., “Modelling and simulation of vehicular power systems”, Master’s thesis, Department of Energy and Environment Division of Electric Power Engineering, Chalmers University Of Technology, Göteborg, Sweden, (2008).

[79] Achaibou, N., Haddadi, M., and Malek, A., “Lead acid batteries simulation including experimental validation”, Journal of Power Sources, V. 185, n° 2, (2008),1484-1491.

[80] Lalouni, S., “Optimizing the quality of electrical energy in the case of a battery charger”, Master’s thesis, University of Bejaia, Bejaia, Algeria, (2005).

[81] Salameh, Z.M., Casacca, M.A., and Lynch, W.A., “A mathematical model for lead-acid batteries”, IEEE Transactions on Energy Conversion, V. 7, n° 1, (1992), 93-98.

[82] “Review of electrical energy storage technologies and systems and of their potential for the UK”, EA Technology, (2004), 34, http://www.wearemichigan.com/JobsAndEnergy/documents/file15185.pdf.

[83] Kosin, L., and Usach, F., “Electric characteristics of lead battery”, Russ J Appl Chem, V. 143, n° 3, (1995), 1-4.

[84] Labbé, J., “Electrolytic Hydrogen as a storage of electricity for Photovoltaic Systems Insulated”, PhD thesis, School of Mines Paris, Specialty Energetic (2006).

[85] Pantelimon, R.F., Adam, M., Andruşcă, M., and Pancu, C., “Aspects regarding solar battery charge controllers”, Advanced Topics in Electrical Engineering (ATEE), 8th International Symposium on IEEE, (2013). 1-6.

[86] Li, J., and Danzer, M.A., “Optimal charge control strategies for stationary photovoltaic battery systems”, Journal of Power Sources, V. 258, (2014), 365-373.

[87] Salas, V., Suponthana, W., and Salas, R., “Overview of the off-grid photovoltaic diesel batteries systems with AC loads”, Applied Energy, V. 157, (2015), 195-216.

[88] Salas, V., Olias, E., Barrado, A., and Lazaro, A., “Review of the maximum power point tracking algorithms for stand-alone photovoltaic systems”, Solar energy materials and solar cells, V. 90, n° 11, (2006), 1555-1578.

[89] Bruendlinger, R., Bletterie, B., Milde, M., and Oldenkamp, H., “Maximum power point tracking performance under partially shaded PV array conditions”, in Proc of 21st EUPVSEC, (2006), 2157-2160.

[90] Swingler, A., “Photovoltaic string inverters and shade-tolerant maximum power point tracking: Toward optimal harvest efficiency and maximum ROI”, Schneider Electric, (2010), 20.

[91] Tey, K.S., Mekhilef, S., Yang, H.-T., and Chuang, M.-K., “A differential evolution based MPPT method for photovoltaic modules under partial shading conditions”, International Journal of Photoenergy, V. 2014, (2014).

[92] Ozdemir, S., Altin, N., and Sefa, I., “Single stage three level grid interactive MPPT inverter for PV systems”, Energy Conversion and Management, V. 80, (2014), 561-572.

[93] Moix, P.O., “New trends in hybrid systems with battery inverter”, (2014), http://www.studer-innotec.com/media/document/0/new_trends_in_hybrid_systems_with_battery_inverter.pdf.

[94] Nayar, C., “Control and interfacing of bi-directional inverters for off-grid and weak grid photovoltaic power systems”, Power Engineering Society Summer Meeting IEEE, V. 2, (2000), 1280-1282.

[95] Trowler, D., and Whitaker, B., “Bi-directional inverter and energy storage system”, Texas Instruments, Arkansas, (2008), 1-29.

[96] Whitepaper on offgrid and back systems. Fronius International GmbH, (2014).

[97] Ozdemir, E., and Kavaslar, F., “A new multifunctional power converter for grid connected residential photovoltaic applications”, Energy Conversion Congress and Exposition, IEEE, (2009), 2650-2656

[98] Amirabadi, M., Toliyat, H.A., and Alexander, W.C., “A multiport AC link PV inverter with reduced size and weight for stand-alone application”, IEEE Transactions on Industry Applications, V. 49, n° 5, (2013), 2217-2228.

[99] Amirabadi, M., Toliyat, H.A., and Alexander, W.C., “Single-phase soft-switching AC-link buck-boost inverter”, Applied Power Electronics Conference and Exposition (APEC), 2014 Twenty-Ninth Annual IEEE, IEEE, (2014), 2192-2199.

[100] Schies, A., “Simulation of diesel savings of PV hybridized mini-grids, Brasil”, Fraunhofer Institute for Solar, Energy Systems ISE, Off Grid Power Forum Intersolar Europe, (June 6th, 2014).

[101] Siemens, “New transformerless solar inverters achieve 98 percent efficiency”, Press release.

[102] Khatib, T., and Elmenreich, W., “Modeling of Photovoltaic Systems Using MATLAB: Simplified Green Codes”, John Wiley & Sons, (2016).

[103] Dufo-López, R., and Bernal-Agustín, J.L., “Design and control strategies of PV-Diesel systems using genetic algorithms”, Solar energy, V. 79, n° 1, (2005), 33-46.

[104] Skarstein, Ø., and Uhlen, K., “Design considerations with respect to long-term diesel saving in wind/diesel plants”, Wind engineering, (1989), 72-87.

[105] Lambert, T., Gilman, P., and Lilienthal, P., “Chapter 15, Micropower system modeling with Homer , in Integration of Alternative Sources of Energy (eds F. A. Farret and M. G. Simões)”, Integration of Alternative Sources of Energy, 15, John Wiley & Sons, Inc, (5 April 2006), 379-418.

[106] Upadhyay, S., and Sharma, M.P., “A review on configurations, control and sizing methodologies of hybrid energy systems”, Renewable and Sustainable Energy Reviews, V. 38, (2014), 47-63.

[107] Sinha, S., and Chandel, S., “Review of recent trends in optimization techniques for solar photovoltaic–wind based hybrid energy systems”, Renewable and Sustainable Energy Reviews, V. 50, (2015), 755-769.

[108] Khatod, D.K., Pant, V., and Sharma, J., “Analytical approach for well-being assessment of small autonomous power systems with solar and wind energy sources”, IEEE Transactions on Energy Conversion, V. 25, n° 2, (2010), 535-545.

[109] Semanche, A., Hamidat, A., and Benchatti, A., “Impact study of the solar energy on the energy performances of the rural housing in Algeria”, International Journal of Heat and Technology, V. 33, n° 4, (2015), 229-236.

[110] Nacer, T., Hamidat, A., Nadjemi, O., and Bey, M., “Feasibility study of grid connected photovoltaic system in family farms for electricity generation in rural areas”, Renewable Energy, V. 96, (2016), 305-318.

[111] Rezzouk, H., and Mellit, A., “Feasibility study and sensitivity analysis of a stand-alone photovoltaic–diesel–battery hybrid energy system in the north of Algeria”, Renewable and Sustainable Energy Reviews, V. 43, (2015), 1134-1150.

[112] Missoum, M., Hamidat, A., Imessad, K., Bensalem, S., and Khoudja, A., “Impact of a grid-connected PV system application in a bioclimatic house toward the zero energy status in the north of Algeria”, Energy and Buildings, V. 128, (2016), 370-383.

[113] Abdelhak, B.J., Najib, E., Abdelaziz, H., Hnaien, F., and Yalaoui, F., “Optimum sizing of hybrid PV/wind/battery using Fuzzy-Adaptive Genetic Algorithm in real and average battery service life”, Power Electronics, Electrical Drives, Automation and Motion (SPEEDAM), 2014 International Symposium on IEEE, (2014), 871-876.

[114] Homer, “Webinar minigrid homer energy”, https://cleanenergysolutions.org/sites/default/files/documents/webinar-minigrid-homer-energy.pdf>.

[115] Adaramola, M.S., Agelin-Chaab, M., and Paul, S.S., “Analysis of hybrid energy systems for application in southern Ghana”, Energy Conversion and Management, V. 88, (2014), 284-295.

[116] Bhattacharjee, S., and Acharya, S., “PV–wind hybrid power option for a low wind topography”, Energy Conversion and Management, V. 89, (2015), 942-954.

[117] Ramli, M.A., Hiendro, A., and Al-Turki, Y.A., “Techno-economic energy analysis of wind/solar hybrid system: Case study for western coastal area of Saudi Arabia”, Renewable Energy, V. 91, (2016), 374-385.

[118] Zahboune, H., Zouggar, S., Krajacic, G., Varbanov, P.S., Elhafyani, M., and Ziani, E., “Optimal hybrid renewable energy design in autonomous system using Modified Electric System Cascade Analysis and Homer software”, Energy Conversion and Management, V. 126, (2016), 909-922.

[119] Retscreen, “Retscreen web page”, (2017), http://www.nrcan.gc.ca/energy/software-tools/7465.

[120] Sinha, S., and Chandel, S.S., “Review of software tools for hybrid renewable energy systems”, Renewable and Sustainable Energy Reviews, V. 32, (2014), 192-205.

[121] Rehman, S., “Prospects of wind farm development in Saudi Arabia”, Renewable energy, V. 30, n° 3, (2005), 447-463.

[122] Himri, Y., Rehman, S., Setiawan, A.A., and Himri, S., “Wind energy for rural areas of Algeria”, Renewable and Sustainable Energy Reviews, V. 16, n° 5, (2012), 2381-2385.

[123] Zandi, M., Bahrami, M., Eslami, S., Gavagsaz-Ghoachani, R., Payman, A., Phattanasak, M., Nahid-Mobarakeh, B., and Pierfederici, S., “Evaluation and comparison of economic policies to increase distributed generation capacity in the Iranian household consumption sector using photovoltaic systems and RETScreen software”, Renewable Energy, V. 107, (2017), 215-222.

[124] iHOGA, “Hybrid Optimization by Genetic Algorithms software”, (2017), http://personal.unizar.es/rdufo/.

[125] Chauhan, A., and Saini, R., “A review on integrated renewable energy system based power generation for stand-alone applications: configurations, storage options, sizing methodologies and control”, Renewable and Sustainable Energy Reviews, V. 38, (2014), 99-120.

[126] Dufo-López, R., Lujano-Rojas, J.M., and Bernal-Agustín, J.L., “Comparison of different lead–acid battery lifetime prediction models for use in simulation of stand-alone photovoltaic systems”, Applied Energy, V. 115, (2014), 242-253.

[127] Schiffer, J., Sauer, D.U., Bindner, H., Cronin, T., Lundsager, P., and Kaiser, R., “Model prediction for ranking lead-acid batteries according to expected lifetime in renewable energy systems and autonomous power-supply systems”, Journal of Power sources, V. 168, n° 1, (2007), 66-78.

[128] Erdinc, O., and Uzunoglu, M., “Optimum design of hybrid renewable energy systems: Overview of different approaches”, Renewable and Sustainable Energy Reviews, V. 16, n° 3, (2012), 1412-1425.

[129] Fadaee, M., and Radzi, M.A.M., “Multi-objective optimization of a stand-alone hybrid renewable energy system by using evolutionary algorithms: A review”, Renewable and Sustainable Energy Reviews, V. 16, n° 5, (2012), 3364-3369.

[130] Chicco, G., and Mancarella, P., “Distributed multi-generation: A comprehensive view,” Renewable and Sustainable Energy Reviews, V. 13, n° 3, (2009), 535-551.

[131] Nadjemi, O., Nacer, T., Hamidat, A., and Salhi, H., “Optimal hybrid PV/wind energy system sizing: Application of cuckoo search algorithm for Algerian dairy farms”, Renewable and Sustainable Energy Reviews, V. 70, (2017), 1352-1365.

[132] Gan, L.K., Shek, J.K.H., and Mueller, M.A., “Optimised operation of an off-grid hybrid wind-diesel-battery system using genetic algorithm”, Energy Conversion and Management, V. 126, (2016), 446-462.

[133] Al-Alawi, A., Al-Alawi, S.M., and Islam, S.M., “Predictive control of an integrated PV-diesel water and power supply system using an artificial neural network”, Renewable energy, V. 32, n° 8, (2007),1426-1439.

[134] Rashed, M., Elmitwally, A., and Kaddah, S., “New control approach for a PV-diesel autonomous power system”, Electric Power Systems Research, V. 78, n° 6, (2008), 949-956.

[135] Elmitwally, A., and Rashed, M., “Flexible operation strategy for an isolated PV-diesel microgrid without energy storage”, IEEE transactions on energy conversion, V. 26, n° 1, (2011), 235-244.

[136] Abdin, E., Osheiba, A., and Khater, M., “Modeling and optimal controllers design for a stand-alone photovoltaic-diesel generating unit”, IEEE Transactions on energy conversion, V. 14, n° 3, (1999), 560-565.

[137] Mohammed, A., Pasupuleti, J., Khatib, T., and Elmenreich, W., “A review of process and operational system control of hybrid photovoltaic/diesel generator systems”, Renewable and Sustainable Energy Reviews, V. 44, (2015), 436-446.

[138] Goncalves, J., Mendes, J., and Resende , M., “A genetic algorithm for the resource constrained multi-project scheduling problem”, European Journal of Operational Research, V. 189, nº 3, (2008), 1171-1190.

[139] Chen, S., and Huang, C., “A new approach to generate weighted fuzzy rules using genetic algorithms for estimating null values”, Expert Systems with Applications, V. 35, n° 3, (2008), 905-917.

[140] Holland, J., “Adaptation in natural and artificial systems”, Massachusetts, Cambridge: MIT Press, (1992).

[141] Dufo-López, R., and Bernal-Agustín, J.L., “Influence of mathematical models in design of PV-Diesel systems”, Energy Conversion and management, V. 49, n° 4, (2008), 820-831.

[142] Khare, A., and Rangnekar, S., “A review of particle swarm optimization and its applications in Solar Photovoltaic system”, Applied Soft Computing, V. 13, n° 5, (2013), 2997-3006.

[143] Kennedy, J., and Eberhart, R., “Particle swarm optimization”, Neural Networks, 1995 Proceedings, IEEE International Conference, V. 4, (1995),1942-1948

[144] Hakimi, S., and Moghaddas-Tafreshi, S., “Optimal sizing of a stand-alone hybrid power system via particle swarm optimization for Kahnouj area in south-east of Iran”, Renewable energy, V. 34, n° 7, (2009), 1855-1862.

[145] Suryoatmojo, H., “Artificial intelligence based optimal configuration of hybrid power generation system”, Phd thesis, Department of Computer Science and Electrical Engineering Graduate School of Science and Technology, Kumamoto University, Japan, (2010).

[146] Abdelaziz, A.Y., Mohammed, F., Mekhamer, S., and Badr, M., “Distribution systems reconfiguration using a modified particle swarm optimization algorithm”, Electric Power Systems Research, V. 79, n° 11, (2009), 1521-1530.

[147] Al-falahi, M.D., Jayasinghe, S., and Enshaei, H., “A review on recent size optimization methodologies for standalone solar and wind hybrid renewable energy system”, Energy Conversion and Management, V. 143, (2017), 252-274.

[148] Khalili-Damghani, K., Abtahi, A.-R., and Tavana, M., “A new multi-objective particle swarm optimization method for solving reliability redundancy allocation problems”, Reliability Engineering & System Safety, V. 111, (2013), 58-75.

[149] Carlos, A.C.C., Gary, B.L., and David, A.V.V., “Evolutionary Algorithms for Solving Multi-Objective Problems (Genetic and Evolutionary Computation)”, Springer-Verlag New York Inc, (2006).

[150] Dufo-López, R., and Bernal-Agustín, J.L., “Multi-objective design of PV–wind–diesel–hydrogen–battery systems” Renewable Energy, V. 33, n° 12, (2008), 2559-2572.

[151] Abedi, S., Alimardani, A., Gharehpetian, G.B., Riahy, G.H., and Hosseinian, S.H., “A comprehensive method for optimal power management and design of hybrid RES-based autonomous energy systems”, Renewable and Sustainable Energy Reviews, V. 16, n° 3, (2012), 1577-1587.

[152] Yang, H., Zhou, W., Lu, L., and Fang, Z., “Optimal sizing method for stand-alone hybrid solar–wind system with LPSP technology by using genetic algorithm”, Solar Energy, V. 82, n° 4, (2008), 354-367.

[153] Suryoatmojo, H., Elbaset, A.A., and Hiyama, T., “Economic and Reliability Evaluation of Wind-Diesel-Battery System for Isolated Island Considering CO_2 Emission”, IEEJ Transactions on Power and Energy, V. 129, n° 8, (2009), 1000-1008.

[154] Jhe, X., and Deyun, X., “New Metropolis coefficients of Particle Swarm Optimization”, Chinese Control and Decision Conference, (2008), 3518-3521.

[155] Zhou, W., Lou, C., Li, Z., Lu, L., and Yang, H., “Current status of research on optimum sizing of stand-alone hybrid solar–wind power generation systems”, Applied Energy, V. 87, n° 2, (2010), 380-389.

[156] Givler, T., and Lilienthal, P., “Using HOMER Software, NREL’s Micropower Optimization Model, to Explore the Role of Gen-sets in Small Solar Power Systems Case Study: Sri Lanka”, Technical Report, National Renewable Energy Laboratory, (May 2005).

[157] Afzal, A., Mohibullah, M., and Kumar Sharma, V., “Optimal hybrid renewable energy systems for energy security: a comparative study”, International Journal of Sustainable Energy, V. 29, n° 1, (2010), 48-58.

[158] Kamel, S., and Dahl, C., “The economics of hybrid power systems for sustainable desert agriculture in Egypt”, Energy, V. 30, n° 8, (2005), 1271-1281.

[159] Yang, H.X., Lu, L., and Burnett, J., “Weather data and probability analysis of hybrid photovoltaic–wind power generation systems in Hong Kong”, Renewable Energy, V. 28, n° 11, (2003), 1813-1824.

[160] Fodhil, F., Hamidat, A., and Nadjemi, O., “Optimal Sizing of Stand-Alone Hybrid PV-Diesel-Battery System Using PSO and the ε-Constraint Method”, I J C T A, International Science Press, V. 9, n° 38, (2016), 99-110.

[161] “Prix du panneau photovoltaïque en Algérie, Portail Algerien des ENERGIES RENOUVELABLES”, http://portail.cder.dz/spip.php?article3925.

[162] Solarbuzz, “Facts and figures homepage”, http://www.solarbuzz.com/facts-and-figures/

[163] “catalogue des kits solaires, Condor Electronics”, www.condor.dz/images/pdf/CatalogueDesKitsSolaires.pdf.

[164] Rodriguez, J., “levelised cost of storage: A better way to compare battery value on batteries & energy storage,useful solar tools and resources”, http://www.solarchoice.net.au/blog/levelised-cost-of-storage-compare-battery-value.

[165] Houghton, J.T., Ding, Y., Griggs, D.J., Noguer, M., Linden, P.J.V.d., Dai, X., et al., “Inter-Governmental panel on Climate Change 2001: The scientific Basis”, Cambridge University Press, Cambridge, United Kingdom and New York, NY, USA, (2001).